Design and Testing Novel Wearable Instrumentation for Assessing Pelvic Floor Function and Exploring Continence Mechanisms

by

Ali Attari

A dissertation submitted in partial fulfillment
of the requirements for the degree of
Doctor of Philosophy
(Mechanical Engineering)
in the University of Michigan
2020

Doctoral Committee:

Professor James A. Ashton-Miller, Chair
Professor John O. L. DeLancey
Associate Research Scientist Grant H. Kruger
Professor Alan S. Wineman

Ali Attari

attari@umich.edu

ORCID iD: 0000-0002-3987-6320

DEDICATION

To my family, for their unconditional love and endless support.

ACKNOWLEDGEMENTS

This work would not have been completed without the help of many extraordinary individuals. I am truly blessed to be supported by so many wonderful people, more than I can acknowledge in these pages.

In particular, I would like to express my sincere gratitude to my advisor, Professor James A. Ashton-Miller for his support, encouragement and guidance in all my years as a graduate student. I have always admired his patience, passion for research, and character. He truly is the epitome of a mentor. I would also like to thank Dr. John O. L. DeLancey, a surgeon but I think engineer at heart, who has acted as a second mentor to me. He generously spent many hours providing invaluable clinical insights and feedback that helped refine my work. I have been inspired by his dedication to conducting exceptionally high quality research. I want to thank them both for treating me kindly with all my many shortcomings.

I also want to thank the rest of my committee members: Professor Alan S. Wineman, for his enthusiasm and gift for explaining complicated modelling concepts simply, and Professor Grant H. Kruger, for his innovative solutions to improve the design of the Personal Uroflowmeter (PUF) device.

This work would not have been possible without the financial support from Procter & Gamble (P&G) and their FemCare Group, the National Institute of Diabetes and Digestive and Kidney Diseases, the Wallace H. Coulter Foundation and the Michigan Translational Research and Commercialization (MTRAC) program. I would also like to acknowledge a number of gifted individuals at P&G, in particular Tana Kirkbride and Alexzandra Ramachandran, for so ably leading our UM-P&G joint collaboration, and my other co-inventors on the PUF device. I also want to thank all the U-M ME Department staff for their assistance in smoothing my journey over the years.

I want to extend my thanks to the members of the U-M Pelvic Floor Research Group (PFRG) and particularly Dr. Carolyn Swenson for providing access to the MR scans that helped facilitate Chapter 2 of this dissertation. I also thank all the patients who participated in our studies with the hope that one day their contributions will provide a cure of others.

I want to acknowledge Dr. William D. Chey and (now Dr.) Jason Baker in his GI Physiology Laboratory in the U-M Division of Gastroenterology for their wonderful help and enthusiasm during the development and clinical testing of the Digital Manometry (DM) device. I also thank Professor Mark A. Burns and his group in Chemical Engineering for their generous technical assistance in developing the PUF sensors. In that regard, I especially thank Dr. Wen-chi Lin, Dr. Sara Mena, Mr. Brian Johnson and Ms. Alyse Krausz in that regard and particularly Ms. Anna Nelson who kindly helped me through the different sensor fabrication processes. I also want express my gratitude to all the staff at Lurie Nanofabrication Facility for their valuable technical help in the sensor fabrication processes.

I need to thank the former and current fellows and students of the U-M Biomechanics Research Lab for their fellowship and being such great colleagues. Many thanks to Payam Mirshams who shared his experience with me throughout these years. I also want to mention Sasha Kapshai, Mark Gordon, Youkeun Oh, Hogene Kim, Melanie Beaulieu, Paige Tracy, Dan Imaizumi Krieger, Mariana Masteling, Shuai Xiong, So Young Baek, Zizheng (Fred) Zhang, Yongsoo Shin, Kruthi Srinivasa Raju and Himanshu Saxena.

I owe sincere gratitude to my other colleagues at the University of Michigan, in particular Dr. Mahdi Sadeghi not only for his technical and scientific assistance, but also for his wonderful support and friendship over the past eight years; to me he is like the older brother I never had. I also want to acknowledge Mostafa Gh., Farzad Kh. and Ali D. for their technical insights on improving the instrumentation aspects of my devices. I also want to acknowledge Ali K. for his assistance on resolving some difficult fluid dynamic problems.

Thanks and love to all my friends in Ann Arbor who treated me sincerely; I am particularly grateful to Mahdi, Narges, Sina, Mahya, Mina Z., Abbas, Payam, Nina, Maryam Gh., Mohammad, Meysam, Nasrin, Tannaz, Elham, Negin, Ali A., Fatemeh, Vahnoud, Mina N., Shahab, Sulmaz, Farzad, Bahareh, Ali T., Maryam T. and Reza.

Coming to my family, words cannot express how deeply I owe thanks to my lovely parents who went through so many sacrifices for me to get to this point. I am grateful to Baba "Saeed" who always supported and encouraged me to do my best and taught me invaluable life lessons. To Maman "Hoory", who has always been there with her unconditional and endless love. To my adorable sister "Hana", who always believed in me and inspired me by her artistic work. To my aunt "Mary", who rooted in me the passion to help those in need. To all my in-laws for their support, and to the memory of my grandparents for their delightful anecdotes.

Finally, Mahsa, my love, and a rare jewel, how can I ever thank you enough? I owe my deepest gratitude to you for your exceptional companionship and unending understanding. You have patiently tolerated me working on my research day and night, and you have supported me through thick and thin. I am truly blessed to have you in my life and I could not have done this without you!

TABLE OF CONTENTS

CHAPTER

LIST OF FIGURES

LIST OF TABLES

LIST OF APPENDICES

APPENDIX

ABSTRACT

Urinary incontinence (UI) and fecal incontinence (FI) affect 20% of North Americans, with a higher prevalence in women and the elderly. The prevention and treatment of these conditions unfortunately leaves much to be desired, despite the $88B and $49B annual U.S. costs associated with managing UI and FI, respectively. Recent research suggests that the major problem lies with the sphincters themselves, rather than other structures. More needs to be learned about how age, injury and disease affect these sphincters. The literature is reviewed in Chapter 1, knowledge gaps are identified and testable hypotheses formulated.

In Chapter 2, we describe the first subject-specific, 3-D, biomechanics model of the urethra capable of contracting the three individual muscle layers along their lines of action. This was developed to better understand how the different layers contribute to urethral closure during activities of daily living. Exploratory studies of the vascular plexus suggest a role in affecting functional urethral length. While this model helps one to understand which muscles contribute to continence, it could not provide insights into the amount of urine leaked which, after all, is what bothers women the most.

In Chapter 3, we describe a novel approach for quantifying urine leakage both in and out of the clinic. While one can presently obtain micturition flowmetry in the seated posture in the clinic, this precludes the possibility of any information being gathered on leakage during activities of daily living (ADL). Instead, a patient must keep a leakage diary for several days, which unfortunately is prone to recall bias and other errors. Therefore, a novel wearable personal

uroflowmeter (PUF) was invented and developed to attach over the urethral meatus in women to collect urine flow rate and leakage data during ADL leakage episodes. This was connected with a waist-mounted inertial measurement unit (IMU) to provide data on the pose and ADL associated with the volume of each leakage episode.

Chapter 4 describes the first-in-human testing of the PUF in women in and outside the clinic, demonstrating the feasibility of wearable uroflowmetry. Moreover, theoretical studies of labia majora coaptation suggest that the labia can inadvertently form a potential reservoir for urine leakage during a sneeze or cough. This insight will help eliminate the confusion over the relationship between the ADL causing the passage of urine through the urethra (i.e., a cough) and that which later causes urine to leak from the labial reservoir (i.e., rising from a chair). A few incidents of this phenomenon were measured for the first time while testing the PUF in women.

In terms of anorectal function, Chapter 5 reports the design and development of a disposable point-of-service instrumented anorectal manometry glove (“digital manometry”, DM) for testing anal sphincter and anorectal function at an order of magnitude lower cost than the standard high resolution anorectal manometry (HR-ARM).

Chapter 6 reports first-in-human testing of the DM device in patients with and without FI and chronic constipation. Comparisons of the DM and HR-ARM results show reasonable agreement. In addition, the DM also provided myoelectric information useful for identifying paradoxical contraction of the anorectal muscle in patients with dyssynergic defecation.

In summary, the dissertation provides novel and inexpensive approaches for a clinician or researcher to better document and understand incontinence.

CHAPTER 1

Introduction

1.1. Motivation

The sphincters of the body play an often underappreciated role in maintaining quality of life. These include the upper and lower esophageal sphincters, the pyloric sphincter, the external and internal anorectal sphincters, and the urethral sphincter. The urethral and anal sphincters share anatomical similarities, for example, both having longitudinal muscle encircled by voluntarily controlled circular muscle in order to maintain continence and regulate the passage of fluid or solid waste, as needed. When their function is degraded by age, injury or disease effects the quality of the life of the patient can be seriously affected both physically and emotionally.

The most common type of urethral sphincter failure is urinary incontinence (UI). UI is more prevalent in women and affects more than 12 million individuals in North America with an annual cost of $88.2B [1]–[3]. Nevertheless, the success rate of the treating UI is not more than 48%-56% [4] depending on the definition of success. Clearly, this is not acceptable and it suggests that either 1) the underlying factors and function of the lower urinary tract (LUT) are not well understood, 2) the diagnostic tools are not yet effective enough, or 3) we may not have treatments to address all failures. According to the National Institute of Diabetes and Digestive and Kidney Diseases (NIDDK), investments on early UI diagnosis and management would decrease UI associated costs [3].

In terms of anorectal function, chronic constipation and fecal incontinence are two diseases associated with the anal sphincter. The gold standard equipment to correctly triage patients to the right treatment plan is expensive and limited to tertiary medical centers [5]. Therefore, many patients are deprived of the opportunity to be correctly diagnosed and are often treated with ineffective solutions [6].

This dissertation will address some of these shortcomings by proposing a 3-D novel multiphysics biomechanical computational model of the urethral sphincter to better understand how it works, and developing and testing two new devices for testing urethral and anal sphincter function in humans.

1.2. Literature Review

1.2.1. Existing Urethra Models

In early studies, the urethra was simply modeled as a straight tube [7]–[9]. In those cases, the Bernoulli principle was applied by using measured input and output pressures, and flow rate data to calculate the inner diameter of the urethra. Later, Griffith [10] modeled the urethra as a uniform elastic tube and used Hooke's law to find a relationship between pressure and radius of the urethra during micturition. However, the results were not realistic due to the oversimplified assumptions for the female urethrae [11].

In 1994, Kim [12] constructed a 2D finite element (FEM) model of the urethra and the pelvic floor complex using linear elements to investigate the continence mechanisms during stress events such as coughing, laughing or lifting a heavy object. He included a 7 French rigid catheter in his simulations to be able to correctly validate his findings with the literature data. The anatomical dimensions and material properties of his model were taken from the literature and adjusted to suit his model [13]. In order to simulate stress events, boundary conditions (BC) such as the intra-abdominal pressure were altered from the resting state to the extent that the resultant pressure distributions corroborated the experimental data. He concluded that active contraction of the urethral sphincter, especially in the distal regions of the urethra, significantly contributes to maintaining continence. Despite his reasonable assumptions and valuable findings, his model was incapable of simulating the anatomical intricacies of the three individual urethral sphincter muscles, mainly due to the limited computational power of that period.

Later, several other researchers modeled the organs, muscles, and ligaments of female pelvis in 3D space [14]–[18], but only a small number of them focused on modeling the urethra or stress urinary incontinence. A limitation was that most considered the urethral complex as a singular passive tissue without active contraction of its musculature layers.

Zhang et al. [19] developed an idealized pelvic floor FEM model and included urine as a "fluid-like media" and Eulerian elements to simulate urine leakage for the case of female athletes landing a jump. This is probably the only existing FEM model for which the simulation results have been validated using custom-made instrumented absorbent pads worn by subjects. However, there were several limitations associated with the model: 1) the use of elastic instead of hyperelastic properties, 2) simply modeling the urethra with shell elements and disregarding the urethral muscle layers, and 3) the absence of viscoelastic material models when a time dependent study of jump landing impact was being studied. In addition to their FEM model limitations, they did not clearly explain 1) how their wetness detector could measure a leakage amount of less than a droplet (0.05 ml), or 2) measure the leaked volume over the course of time without physically being capable of correctly measuring temporal flowmetry data. Meanwhile, to simulate urine leakage and explore factors causing incontinence, Spirka et al. [20]–[23]

developed a more realistic fluid-solid interactive model of the lower urinary tract system via an arbitrary Lagrangian-Eulerian (ALE) method. The fluid-solid interaction of the model was one-way coupled, meaning that instead of solving equations of tissue and fluid mechanics simultaneously, the solver at every time interval would first solve the fluid physics (for the urine), and then feed the corresponding pressure and deformation values to the solid-mechanics domain (for the surrounding tissues) via the shared boundaries. Although his model was also oversimplified in terms of the geometry, loads and boundary conditions, using existing clinical data he verified that the urethral stiffness, pressures, and support play an important role in maintaining continence.

1.2.2. Uroflowmetry and Leakage Measurement

Clinically, in order to assess the function of the lower urinary tract system and to diagnose various voiding dysfunctions (with even similar symptoms), several non-invasive tools such as uroflowmeters and voiding diaries are used [24]. Uroflowmeters can reveal information such as the mean and maximum urine flow rate, time to void and urine flowmetry curve during the micturition. For example, mean and maximum urine flow rate in stress incontinent women are 50% higher than those with pelvic organ prolapse [25]. Similarly, voiding diaries also reveal the voiding pattern and its frequency by providing objective information which can be used to identify improvements after treatment [24].

Leakage Diaries

Regardless of the cause of a patient's urinary incontinence, a standard clinical measure of urine leakage involves the patient being asked to keep a diary to self-report the frequency and make a subjective estimate of the severity of urine leakage episodes over 3 to 7 consecutive days of daily activities [26], [27]. However, the volume of urine leaked cannot reliably be estimated.

Even if it was possible, it is easy to forget to enter the episode in the diary. Finally, patients may not always feel or notice the episode because of distractions, or even be motivated to enter the episode [28], [29]. Hence, the self-report leakage diary has limitations that include recall bias, especially in the case of older or cognitively-impaired individuals. Lastly, leakage diaries cannot quantify urine leakage flow rate because no means is provided for the temporal recording of flow rate or volume over time. This last information may be needed by companies designing absorbent pads to be sure their pads can absorb high enough rates of urine loss.

Passive Leakage Volume Measurement

An objective measure for quantifying urine loss over a given time period includes the weighing of absorbent pads worn for certain time periods or during given daily activities, urine collection bags, or outlining minor leakage on a paper towel held under the perineum [30]. However, none of these methods can quantify the instantaneous flow rate, only the average flow rate over a certain time. In addition, they fail to measure the number of leakage episodes occurring during activities of daily living in an intact patient, a cognitively-impaired individual, or in a person who is unresponsive, for example. A physician may want to know how many leakage episodes there are in order to be able to interpret what a patient is telling her/him about how much the leakage bothers her.

Wetness Sensors

Numerous wetness detection sensors have been proposed to measure incontinence [31]–[39]. Most of these measure changes in electrical conductivity via set off electrodes embedded in the underwear or the incontinence pad. They are incapable of measuring instantaneous leakage flow rate or volume. A wetness measurement was used employed to validate results of a lower urinary tract FEM model of female athletes during a jump [19].

Uroflowmetry

Existing uroflowmeters are mostly stationary laboratory- or clinic-based instruments. These involve asking the patient to sit on a commode as he or she would on a toilet. A series of methods describe how to measure the micturition profile via toilet- or urinal-based uroflowmetry [40], [41] and are not useful in measuring incontinent episodes during daily life. Prior art includes instrumented toilets developed to collect and analyze urine specimens with minimal intervention during micturition, and urinal style uroflowmeter stations. In some instances, a semi-portable uroflowmeter consisting of a unisex urinal mounted on caster wheels has been used [42]. In addition, a uroflowmeter in the form of a handheld pitcher-like container that measures the weight of the urine collected via a scale integrated into its base has been used [43]. By deriving the weight change over a given time period, the voiding flow rate could be calculated. However, such devices can be inaccurate and noisy as, for example, when the container moves, scale readings are affected by the accelerations associated with those movements, etc. Additionally, the momentum of the urine stream on the scale may result in sudden fluctuations in the flow rate readouts. Another example of a uroflowmeter includes a sensor integrated in tubing attached to a collection funnel attached to the commode-style toilet or even the hospital [44]. However, such devices are still toilet based and stationary, and do not lend themselves to measurements during daily activities, in a cognitively-impaired individual, and/or in a person who is unresponsive, for example. In addition, such devices use conductivity of the urine to measure the flow rate and, thus, if the salinity of the urine changes due to body dehydration or other symptoms, then artifacts may be introduced into the measurements. None of these instruments are very practical leaving open the possibility to design something better.

1.2.3. High Resolution Anorectal Manometry

High resolution anorectal manometry (HR-ARM) has become the standard method for performing detailed evaluation of anorectal function [45]. HR-ARM provides information for the diagnosis of fecal incontinence (FI) and chronic constipation (CC) which affect up to 18% and 19%, respectively, of the adult population in North America [46]–[48]. More specifically, HR-ARM allows the identification of chronically constipated patients with dyssynergic defecation and FI patients with sphincter weakness, both of which are most effectively treated with physical therapy and biofeedback training rather than standard medical therapies like anti-diarrheals or laxatives. A major limitation is that HR-ARM technology is expensive so it is generally only available at tertiary care centers, restricting access to the modest number of patients who have access to such a center. Details of HR-ARM probe are discussed in Chapter 6, section 6.2.3.

1.3. Knowledge Gaps

1.3.1. KG1: What is the contribution of each urethral muscle layer to the urethral closure pressure?

Surprisingly, little is known about how the urethral sphincter, with its three muscle layers and vascular plexus, actually works or what goes wrong when it fails. Existing urethral sphincter models disregard the active function of individual urethral muscle and simply consider the urethral sphincter as a unibody structure in simulations. One of the few experimental studies in women estimated the contributions of the striated and smooth layers to each amount 33% of the closure pressure with the vascular plexus providing the remaining 33% [49]. From an engineering point of view, the fact that the circular smooth muscle and longitudinal smooth muscle have orthogonal contractile directions would suggest they do not have the same effect on the urethral closure pressure. However, their individual contribution have never been measured experimentally or even estimated theoretically. (Chapter 2)

1.3.2. KG2: Does the dorsal[1] passive portion of the striated circular layer affect the predicted urethral closure pressure?

As mentioned in the KG1, since most existing urethral models are not anatomically accurate. They are often portrayed as a straight tube, which may not be true, and in addition may be portrayed as axisymmetric, which is not true. So, the asymmetric shape of the urethra has often been neglected. Studies had shown the thickness of the dorsal portion of the female circular striated muscle decreases as the age increases [50], and the anterior and posterior urethral pressures are different, especially in incontinent patients [51]. Therefore, in the existing models, when viewing a transverse plane section, for example, the function of the dorsal passive portion of the STM has never been explored within the context of the active anterolateral “horseshoe portion”. (Chapter 2)

1.3.3. KG3: In an axisymmetric model of the vascular plexus, what determines the closure pressure and what factors affect the functional urethral length?

A few studies have simulated the mechanics of male urinary duct [52]–[58]. However, author is not aware of any FEM fluid-solid interactive models being used to study the role of the vascular plexus (inner) layer in female urethrae. (Chapter 2)

---

[1] We use ‘dorsal’ and ‘ventral’ as appropriate for the female urethra. Dorsal is the portion adjacent to the vaginal and ventral is the portion adjacent to the pubic bone. This differs from custom in the male urethra where the portion of the urethra closest to the sacrum is designated “ventral” because the anatomical position of the urethra is considered to be in the erect position.

1.3.4. KG4: How do muscle layers change closure pressure in a Kegel, Valsalva or during micturition relative to the resting state?

Since no existing FEM urethra models have considered the structure-function relationships suggested by the layered anatomy of the urethra or active contraction of each musculature layer, LUT activities have instead been simulated either by manipulating the periurethral structures, or by passive deformation of the single layer isotropic urethra model. Therefore, they cannot verify contradictory hypotheses for the roles of individual layers during different LUT scenarios. For example, some authors believe the LSM contributes to continence by forming a thick plug when contracting via the Poisson effect [59], [60]. As a result, to start micturition, LSM should relax. In contrast to this hypothesis, others have claimed that the contraction of LSM shortens the urethral length and begins the micturition process [61], [62]. Yet others have reported that the smooth muscle contributes to 33% of resting closure pressure [49]. Clearly, there is the need for a better theoretical understanding of structure-function relationships within the female urethra (Chapter 2).

1.3.5. KG5: Is it possible to design a wearable personal uroflowmeter (PUF), worn between the labia, to measure urine flow rate and leakage volume (flow rates from 1 droplet to 40 ml/s) during activities of daily living, or volume voided during micturition?

As reviewed above, existing diary-based measurements are subjective, inaccurate, and incapable of measuring urine flow rate. Moreover, the gold standard office-based uroflowmetry devices cannot assess urine leakage outside the lab during activities of daily living such as sleeping, rising from a chair, walking, running, or jumping because, in the aforementioned uroflowmetry devices, the posture of the patient is limited only to having the hips flexed at 90 degrees relative to an upright torso. In addition because it is in this dissertation hypothesized that the coapted labia in women can form a reservoir in the introitus to inadvertently store urine between them, especially with small volumes of leakage, none of the prior art offers direct measures of the leakage flow rate or volume from the urethral meatus itself. This represents an opportunity to improve leakage measurement methodology from the ambulatory relatively healthy patient to the seriously ill immobile patient in a step down unit (Chapters 3 and 4).

1.3.6. KG6: Is it possible to identify the physical activity of the uroflowmeter wearer and correlate the leakage with that activity during daily living?

Because they are not wearable, none of the existing uroflowmetry devices presents an accurate and reliable solution for measuring the instantaneous flow rate or volume of urine leakage episodes during daily activities of a cognitively-impaired individual, or with a person who is unresponsive, for example, using wearable instrumentation while also measuring the pose or activity of the wearer. There is therefore a need for such wearable instrumentation to better understand how activities of daily living contribute to urine leakage (Chapters 3 and 4).

1.3.7. KG7: Can measurements of anorectal pressures and the myoelectric activity of the anorectal complex simultaneously be made using an inexpensive, disposable, point-of-service, device to assess anorectal function and dysfunction?

High-resolution anorectal manometry is the gold standard for performing detailed evaluation anorectal function. However, it requires a relatively expensive system, an additional visit for the patient, and experienced staff to operate and interpret the results. Hence, HR-ARM is limited to tertiary care medical centers with the result that many patients are deprived of the opportunity to be properly diagnosed and triaged to appropriate therapy. There is a need for a simpler and less costly system which can provide the most salient information provided by HR-

ARM at the point of clinical service to better understand why anorectal dysfunction occurs in dyssynergic defecation and constipation (Chapters 5 and 6).

1.4. Systems Analyses Model

Figure 1 shows a simplified systems analysis model of the individual substructures of the urethral sphincter in the lower urinary tract (Chapter 2).

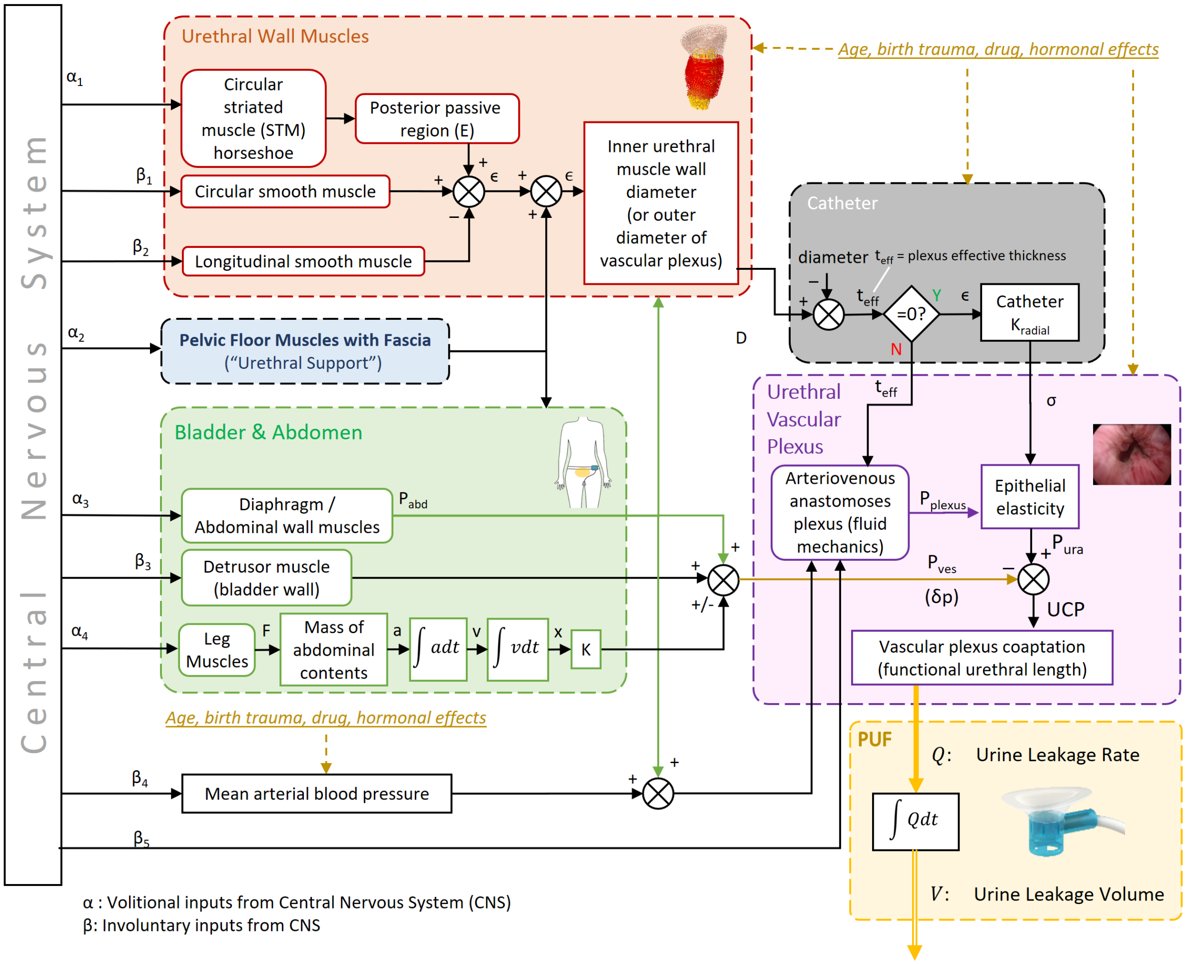

Figure 1. A simplified system diagram of the urethra and the related elements of the lower urinary tract system with efferent nerves from the central nervous system. This also shows an overall view of how the personal uroflowmeter (PUF) would be used to validate results from the urethra model. An equivalent diagram can be constructed for the anorectal complex (Chapters 5 and 6). In the catheter block t_{eff} is twice the width of the blood-filled wall of the plexus that remains surrounding the catheter.

The personal uroflowmeter (PUF) (Chapters 3 and 4) has a role in two main blocks: 1) to quantify the urine leakage (yellow box) and 2) measure the physical activity of the patient in different activities of daily living (green box). A similar diagram can be constructed for the anorectal sphincter complex (Chapters 5 and 6). One can imagine a larger scale diagram containing both systems with interconnection. One simplifying assumption is that the diagram and the corresponding model are one-way coupled; meaning that the blocks only affect the subsequently connected ones and not vice versa. In reality, usually there is a return path between most blocks e.g., the fluid-solid physics (urine-tissue) have a fully coupled interaction.

1.5. Working Hypotheses

To address the existing knowledge gaps following hypotheses are made and addressed each corresponding chapter:

Overarching Hypothesis:

It is possible to design better tools for measuring and understanding pelvic floor sphincter function and dysfunction than are available today. So, in this dissertation, Chapter 2 offers a theoretical model to explore urethral function, Chapters 3 and 4 provide a new tool for measuring urine leakage during activities of daily living, and Chapters 5 and 6 provide an inexpensive alternative for measuring anorectal function.

Chapter 2

H2.1: Maximum contraction of the urethral circular striated muscle contributes as much as urethral smooth muscle does to the increase in UCP [49].

H2.2: Maximum contraction of the urethral longitudinal smooth muscle has no effect on UCP.

H2.3: The effective vascular pressure between the arterial and venous pressures in vascular plexus layer, relative to intravesical pressure, contributes to functional urethral length.

Chapter 3

H3.1: It is possible to design personal uroflowmeter (PUF) fitting between the labia and to measure urine flow rate and leakage or void volume (flow rates from 1 droplet to 40 ml/s)

H3.2: It is possible to record and identify the physical activity of the wearer and correlate the leakage with that activity during daily living.

Chapter 4

H4.1: The experimental PUF flowmetry data is within 10% of that measured via a gold standard reference (i.e., scale or the AI pads weight difference)

H4.2: There is face validity in that a waist-mounted wearable activity sensor output correlates with the volunteer's subjectively recorded physical activity.

H4.3: The PUF-measured urine leakage significantly correlates with a given physical activity recognized by the waist-mounted wearable determining unit.

Chapter 5

H5.1: It is possible to design and build a disposable wearable point-of-service device to measure pressures of the anorectal sphincter at an order of magnitude cheaper expense than the gold standard HR-ARM.

Chapter 6

H6.1: DM pressure readings are equivalent to those measured with a HR-ARM in a sample of healthy subjects, fecal incontinent (FI), and chronic constipation (CC) patients.

H6.2: It is possible to measure the myoelectric activity of the puborectal and the external anal sphincter muscles using electrodes mounted on the above probe.

H6.3: There is no difference in subjective ratings of comfort reported by individuals undergoing DM and HR-ARM.

CHAPTER 2

A Theoretical Exploration of Structure-Function Relationships in the Female Urethra: Anatomy, Subject-Specific Modeling, Function, and Validation

Parts of this chapter have been presented at the *American Urogynecologic Society* and the *International Urogynecological Association* (AUGS/IUGA) joint scientific meeting (2019)

2.1. Introduction

To examine the proposed hypotheses for this chapter, modeling of the urethra is implemented in two separate sections:

1) A 3-D subject-specific asymmetric tissue mechanics model of the urethral musculature layers
2) A simple axisymmetric fluid-solid interactive model to begin to explore the function of the urethral vascular plexus layer

In the first section, the goals were to construct a 3D subject-specific finite element model from MRI scan with individual muscle layers that can contract, relax, apply pressure, and deform urethral and other connected tissues. In the second part, the goal was to construct a simple exploratory axisymmetric fluid-solid interactive model of the proximal portion of vascular plexus layer in the urethra to explore the effect of the arterial and venous pressures in maintaining functional urethral length – a factor contributing to the urinary continence.

2.1.1. Anatomy of the Urethral Sphincter

In this dissertation, the urethra will be represented by six structures: bladder neck region, trigonal ring, striated circular muscle, circular smooth muscle, longitudinal smooth muscle and the vascular plexus (Figure 2 and Figure 3).

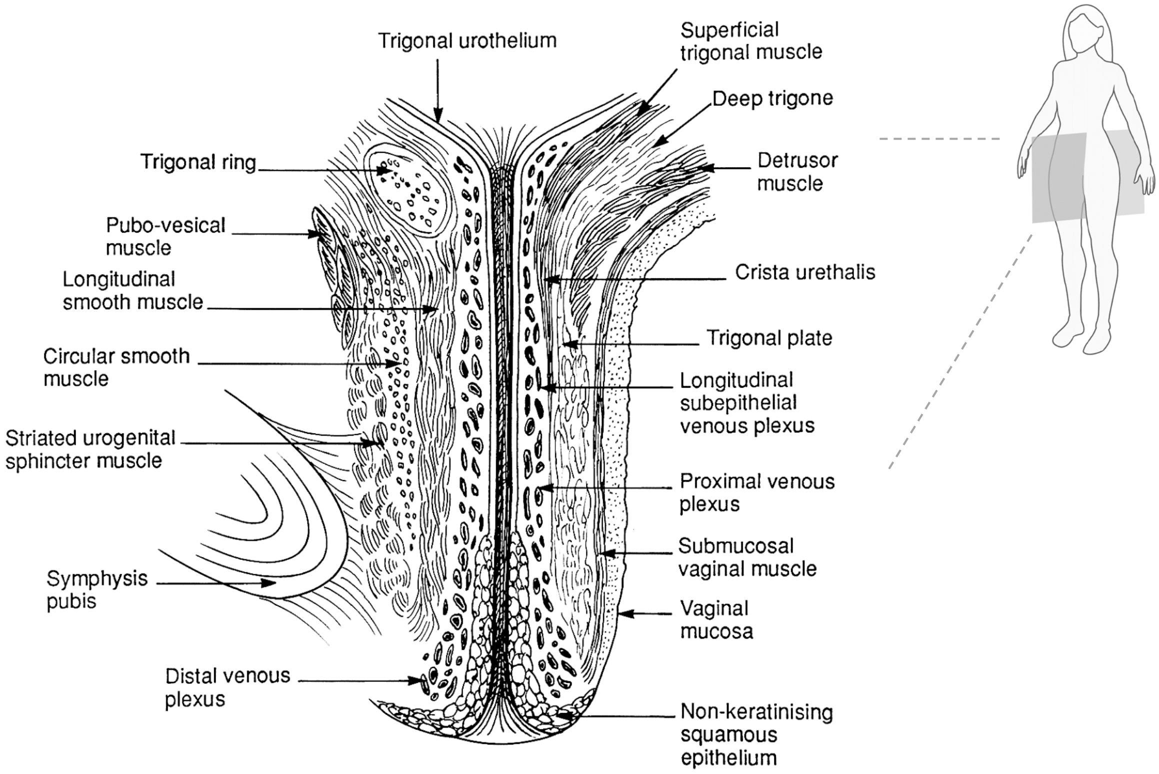

Figure 2. Left view of an illustration of a mid-sagittal section through of a female urethra (Ashton-Miller et al. 2001),

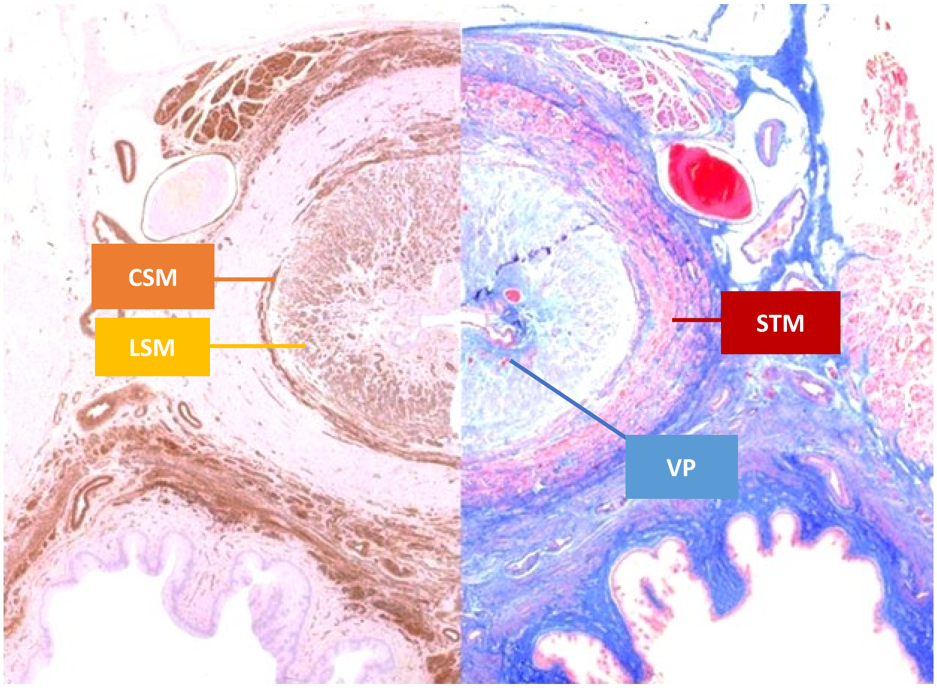

Figure 3. An alpha-actin smooth muscle stain (left) and a trichrome stained (right) transverse cross-section sections of the mid urethra (Strobehn 1997). STM denotes striated circumferential muscle, CSM: circumferential smooth muscle, LSM: longitudinal smooth muscle, and VP: vascular plexus.

2.1.2. Urethral Closure Pressure

An important factor in maintaining urinary continence is the urethral closure pressure (UCP). The UCP is defined as the difference between the urethral pressure and the intravesical pressure. The UCP reaches a maximum near mid-urethral length. The maximum urethral closure pressure (MUCP) is considered as the single most important factor for maintaining continence [63].

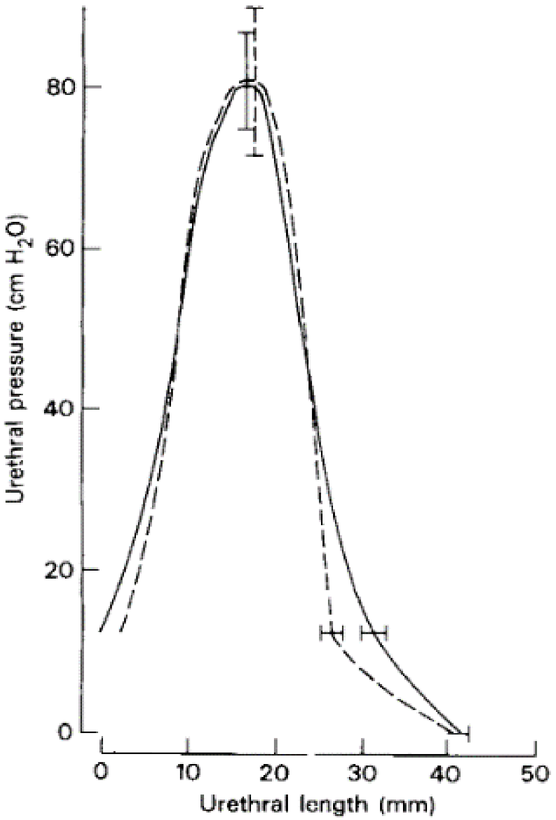

Figure 4. Average resting (solid) and stress (dashed) pressure profile in symptom-free female urethrae (Hilton 1983). On the x-axis '0 corresponds to the bladder neck and '40 mm' to the urethral meatus. The peak value is the maximum urethral pressure (MUP). The UCP at '0' is non-zero because it represents the pressure at the bladder neck due to the hydrostatic pressure there formed by the column of abdominal contents whose height reaches the underside of the abdominal muscles in the supine posture in which this patient was examined. The "urethral closure pressure" (UCP) is defined as the urethral pressure minus the bladder pressure. The maximum UCP (MUCP) is that value at maximum urethral pressure. Bar markers represents the range for the standard error for functional urethral length (horizontal bars) and the maximum urethral closure pressure (vertical bars).

Figure 4 shows a classic example of the UCP profile along the urethra [64]. The lower the MUCP, the more likely the patient is to leak. This effect was explored as the 'continence margin' by Kim et al. in 1997. As shown in Figure 5B, in a healthy individual during activities which suddenly raise intra-abdominal pressure (coughing in this example), the intraurethral pressure also increases and stays higher than the intravesical pressure to maintain continence (Figure 5B). Therefore, the plot of the vesico-urethral pressuregram never crosses the continence margin (dotted line of y = x). However, in an incontinent patient (Figure 5A) when the vesical pressure rises, the incompetency of the intraurethral pressure was translated in the pressuregram crossing the continence margin, thereby showing leakage of urine to that measurement point in the urethra.

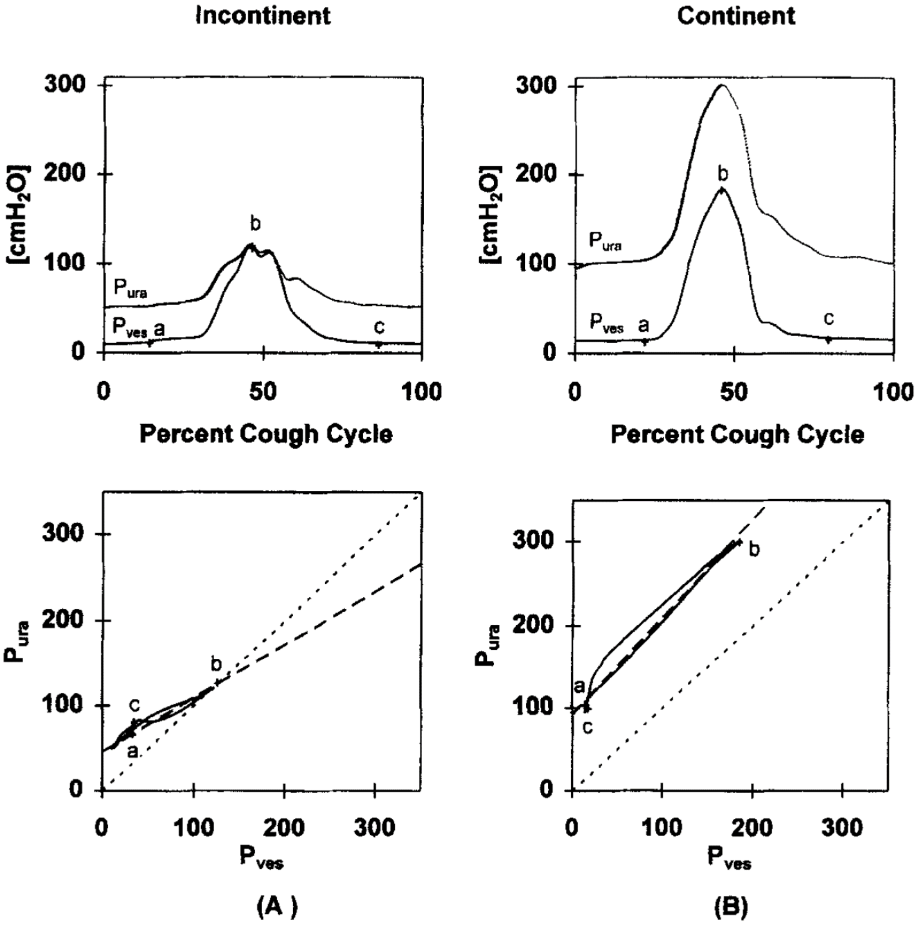

Figure 5. The vesical (P_{ves}) and urethral (P_{ura}) pressures during a single cough at the midurethral location (top figures) and the corresponding vesico-urethral pressuregram analysis (bottom figures) from Kim et al. (1997). (**A**) a woman (45 yr, 2 children) with stress urinary incontince, and (**B**) a continent woman (29 yr, 0 children). **a**: at rest, **b**: peak cough pressure and **c**: leak point. P_{ura} and P_{ves} have units of cmH_2O.

2.1.3. Submucosal Vascular Plexus Layer and Lumen

The urethral lumen lines the opening of the inner urethra. The musculature layers of the urethra do not constrict the urethral lumen to zero diameter. Instead, it is the role of the innermost, submucosal, layer of the female urethra, called vascular plexus (VP) to seal the urethra and stop urine from leaking via vascular pressure acting on the outer layer of the lumen. The VP aids coaptation of opposing surfaces of the inner surface of the lumen throughout the entire functional length of the urethra, aided by the transverse pressure from the VP.

The VP consists mainly of arterio-venous anastomoses (AVA) under an epithelial layer. The arteries deliver blood to the venous plexus. Huisman suggested that the blood flow through the VP may be controlled by simple constriction and dilation of the arterioles [61].

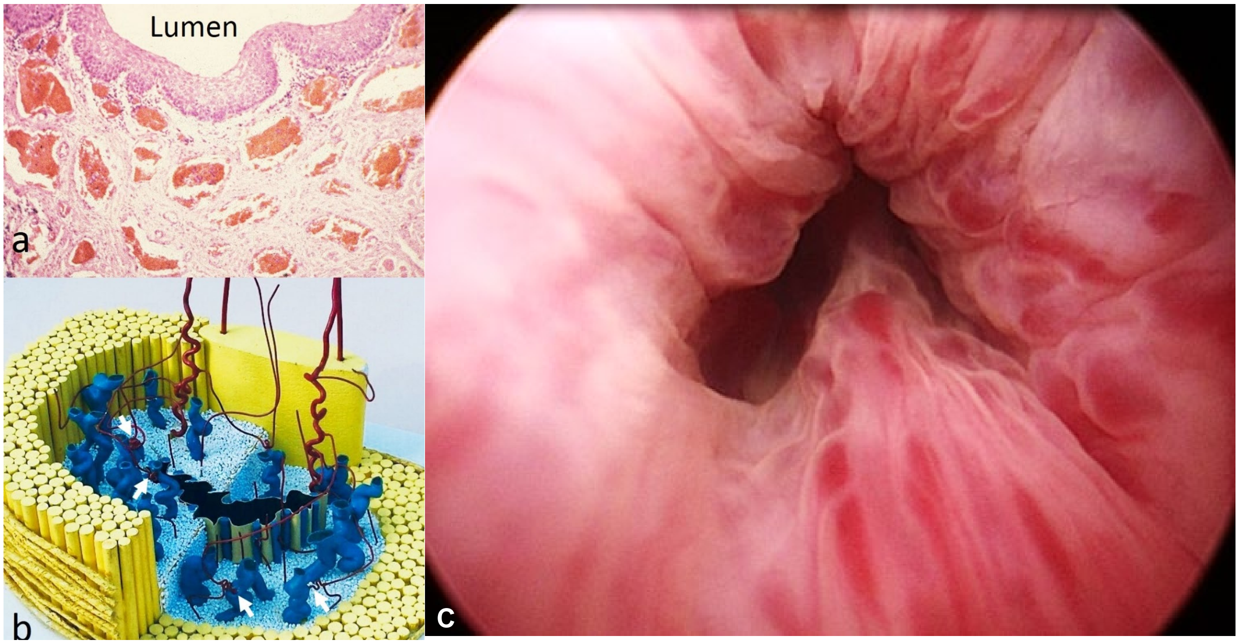

Figure 6. (a) An axial view of a transverse histological slice through the VP layer (©DeLancey). (b) 3D physical model of the proximal vascular plexus (image from a personal communication from A.B. Huisman to J.O.L DeLancey) showing the tortuous veins directed along the urethral length. White arrows show the arterioles controlling the blood supply for the arteriovenous anastomoses. (c) Visible blood vessels (dark red) in a cystoscopic image inside the female midurethral lumen (viewed proximally) as it is held open by the constant flow of isotonic saline (not visible) being pumped through into the bladder in order to enable this image; note the soft and high flexible lumen, more stellate than circular in cross-section, collapses to form a hermetic seal (©DeLancey).

2.1.4. Age-related Dysfunction

A failure in the function of any of the individual elements mentioned above may result in a reduction of the UCP and consequently loss of continence. It is known that aging can also result in a progressive reduction in the number of striated urethral muscle fibers [50], [65] as well as smooth muscle cells [66].

Aging also reduces the maximum closure pressure (Figure 7) causing incontinence [65]. Increasing age does not usually significantly affect clinical measures of pelvic organ support, urethral support or levator function [67]. Finally, Huisman [61] has shown that with increasing age, the distal non-keratinizing squamous lining of the VP moves proximally.

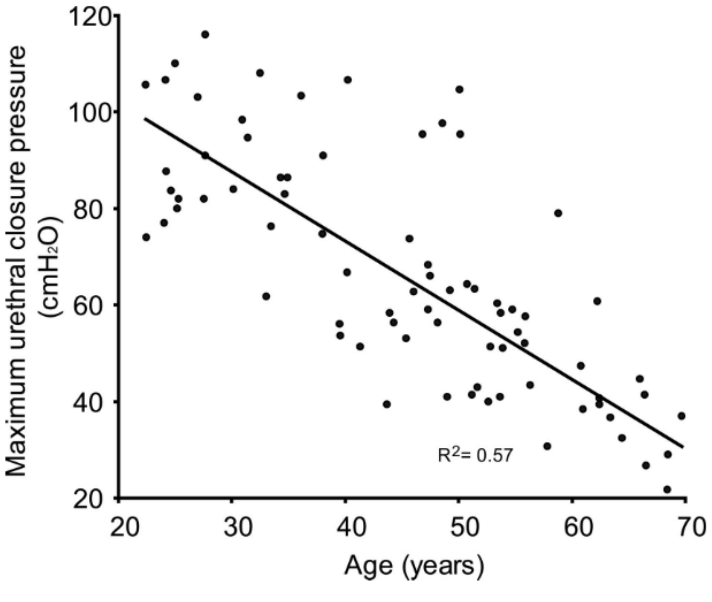

Figure 7. Reduction of MUCP in nulliparous women with age (Trowbridge 2007).

<u>Three Types of Urinary Incontinence</u>

A "complaint of any involuntary leakage of urine" is defined as urinary incontinence (UI) [68]. UI is categorized into different types. Three common types of UI are stress (SUI), urge (UUI) and "mixed" UI. SUI is defined as "involuntary leakage with effort or physical exertion, sneezing, or coughing"[69]. In UUI, the detrusor muscle of the bladder activates too often even before the urine completely fills up the bladder. A patient with urge urinary incontinence often experiences sudden involuntary loss of the entire contents of her bladder. The mixed type is the combination of both UUI and SUI.

Stress Urinary Incontinence

About 50% of women who have stress urinary incontinence suffer from a weak urethral sphincter [63]. In order to maintain continence, the urethral sphincter muscle must provide higher closure pressure compared to the bladder pressure. In events such as coughing, exercising, or lifting heavy objects, during which the intra-abdominal pressure rises abruptly, if the urethral sphincter fails to increase tension and maintain the closure pressure above the threshold for leakage [70], then the woman experiences urine loss. Patients frequently complain of not leaking on a first cough. This is because the first cough may drive the urine partway down into the urethra, seconds later the next cough drives it further down, and the next cough or coughs may expel it from the urethra.

2.2. Methods (I) – Urethral Musculature Sphincter

2.2.1. 3D Geometry Construction from MR Scans

The urethra is comprised of six different structures: the bladder neck region, trigonal ring, vascular plexus, STM, CSM, and the LSM. The overall 3D geometry of the urethra was captured using 3-Tesla Ingenia MRI scanner (Philips Medical Systems, Best, Netherlands) of a 23 year-old nulliparous healthy adult female. The 3D Slicer software platform [71] was used to process the DICOM files and create early 3D domains. The model was then refined in SolidWorks® (Figure 8).

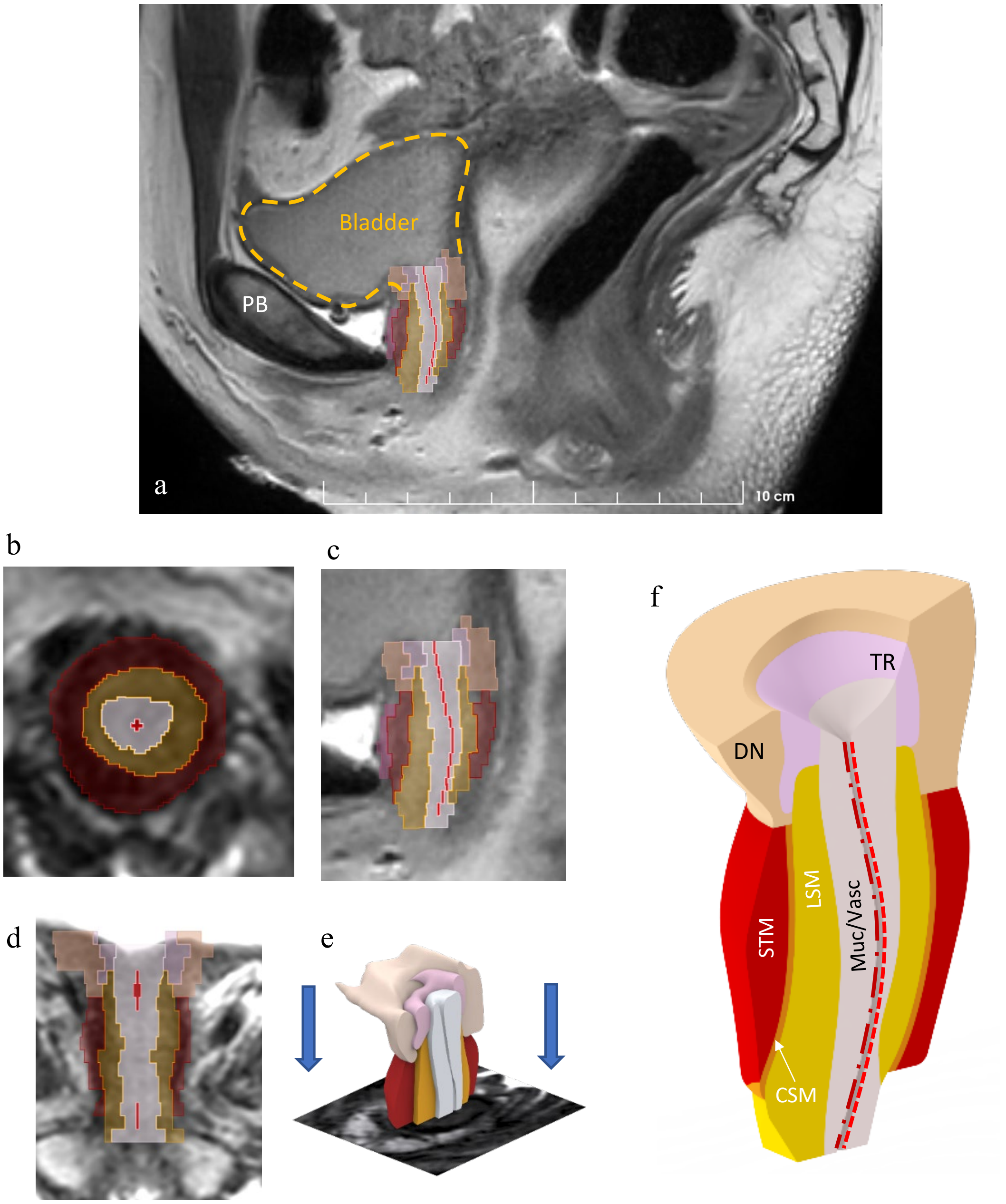

Figure 8. Creating a 3D model of the urethra using 3D slicer and MR scans; a) mid-sagittal view of a 23 years old healthy female. Bladder outline is shown by yellow dashed spline. b) axial view c) mid-sagittal view, and d) the coronal view of the urethral sphincter. Each muscle layer was segmented separately axially for the entire length of the urethra. A 3D model was constructed by lofting axial segmented slices (e). The final refined 3D model is shown in (e), the compressor urethrae is not shown in the 3D model and it is excluded from the simulations. **STM**: circular striated muscle, **CSM**: circular smooth muscle, **LSM**: longitudinal smooth muscle, **Muc/Vasc**: Vascular plexus and submucosa **DN**: Detrusor Neck, **TR**: Trigonal Ring.

2.2.2. Curvilinear Coordinate System

COMSOL® Multiphysics (Burlington, MA, USA) [72] was used for meshing and solving the FEA equations. The muscles and their lines of action were created using domain-specific curvilinear coordinate systems (Figure 9) via the diffusion method to match histological data. This method is a scalar "potential method" resulting in an incompressible vector field and is useful for geometries that are smooth but leads to concentrations at sharp corners. The coordinate system of each individual element was locally selected such that eigenvectors of the local coordinate system matched the mathematical vector field. The first eigenvector aligning to the line of action is what is called the line of action of each muscle layer (i.e., fiber direction for striated muscle).

This method is similar to solving the conduction heat transfer problem of finding the temperature gradient from an inlet boundary to the outlet when there is a temperature difference. This way, the heat flow field represents the first basis vector (e_1).

One can define an orthogonal curvilinear coordinate system using following equations:

$$\boldsymbol{e}_1 = \frac{\boldsymbol{v}}{|\boldsymbol{v}|} \qquad \text{Equation 1}$$

$$\boldsymbol{e}_2 = \frac{\boldsymbol{y} - (\boldsymbol{y}.\boldsymbol{e}_1)\boldsymbol{e}_1}{|\boldsymbol{y} - (\boldsymbol{y}.\boldsymbol{e}_1)\boldsymbol{e}_1|} \qquad \text{Equation 2}$$

$$\boldsymbol{e}_3 = \boldsymbol{e}_1 \times \boldsymbol{e}_2 \qquad \text{Equation 3}$$

For every layer except the longitudinal smooth muscle layer, the $\boldsymbol{y}$ axis is considered as the second basis vector ($\boldsymbol{e_2}$) which is selected manually according to the global Cartesian coordinate system (e.g., the green vectors in Figure 9).

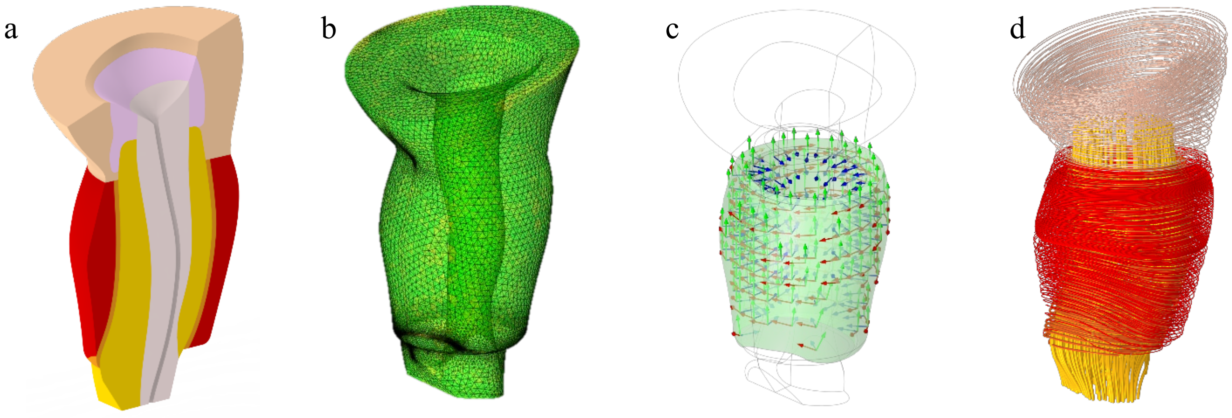

Figure 9. Steps in FEM modeling of the 3-D subject-specific female urethra: a) refined 3D model (SolidWORKS®), b) meshing of the urethral 3D volume, c) example of creating curvilinear coordinate system for the STM layer, d) creation of muscle fibers (striated muscle) or line of action (smooth muscle) for each muscle domain.

The construction of the curvilinear coordinate system in the LSM was done in two steps. The purpose was to have the first component ($\boldsymbol{e_1}$) of local coordinate systems along fiber direction (STM) or line of action (smooth muscle) in each domain, and the third component ($\boldsymbol{e_3}$) to align to the quasi-radial direction. Therefore, first, an initial helper coordinate system was created similar to the other circular layers. This generated a quasi-cylindrical coordinate system deformed to the asymmetric shape of the LSM with the first basis vector ($\boldsymbol{e_1}$) rotating around the longitudinal mid-urethral spline. Afterwards, the main coordinate system for the LSM was formed with the first basis ($\boldsymbol{e_1}$) along the line of action of the LSM domain and the second basis ($\boldsymbol{e_2}$) aligning with the previously generated vector field ($\boldsymbol{e_1}$) around the longitudinal mid-urethral spline.

As a result, for all layers, contraction can be simply made by applying external strains on the first basis of each layer, while the results are validated by measuring stresses or corresponding pressures in the quasi-radial direction i.e., translated pressure on an inserted catheter.

The equations below were used to define the curvilinear coordinate system using the diffusion method:

$$\nabla.(\nabla U) = 0 \qquad \text{Equation 4}$$

$$\boldsymbol{v} = -\frac{\nabla U}{|-\nabla U|} \qquad \text{Equation 5}$$

And for the wall boundary condition:

$$-\boldsymbol{n}.\nabla U = 0 \qquad \text{Equation 6}$$

Respectively for the inlet and outlet boundaries (both ends of the LSM):

$$-\boldsymbol{n}.\nabla U = 1 \qquad \text{Equation 7}$$

$$U = 0 \qquad \text{Equation 8}$$

In order to define a closed-loop circular vector field (e.g., CSM and STM), the jump boundary condition was defined at mid sagittal transverse plane:

$$U_{up} = 1 \qquad \text{Equation 9}$$

$$U_{down} = 0 \qquad \text{Equation 10}$$

2.2.3. Muscle Contraction

As is shown above, two types of muscle, striated and smooth, are found in the female urethral sphincter. The functional unit of fibers in striated muscle are sarcomeres in which the contraction happens at the cellular level. These visible contractile filaments repeat in cylindrical bundles called myofibrils [73].

Smooth muscle is different from striated muscle in several aspects. Structurally, smooth muscle lacks the striations and alternatively has a fusiform shape. Functionally, in contrast to the striated muscle which can be contracted voluntarily, its contraction is controlled involuntarily by the nervous system via autonomic regulation of a calcium-calmodulin interaction and its behavior can be altered with hormones, neurotransmitters, and other receptors [74].

Striated muscle can contract up to 60% of its slack length and develop an active contraction stress of 274 kPa (2.8 kgf/sq.cm) [75], [76]. Depending on the smooth muscle, the maximum contractility would be different, however it can maximally shorten up to 60% of its length under no load [77]. The maximum contractile stress reported for the arterial muscle strips, which is assumed to be similar to urethral smooth muscle with 60% smooth muscle cells, is 220 kPA. This translates into 370 kPa for the pure smooth muscle component (hog carotid artery)[78], [79]. However, as Clobes et al found, the urethral smooth muscle layers contain a substantial volume of connective tissue so they do consist of pure smooth muscle [66]. Finally, smooth muscle contracts more slowly but its contractions lasts longer than skeletal muscle [80].

To model muscle contraction, the contraction stretch ratio (λ_c) was defined as the ratio of the contracted length L_c to slack length L_s i.e., when the muscle is stimulated but unstressed [81] (e.g., free boundary condition at one or both ends):

$$\lambda_c = \frac{L_c}{L_s} \quad , \qquad 0 < \lambda_c \leq 1$$

Equation 11

In the tissue mechanics FEM simulation, this would be the input to the problem in the form of external strain along the fiber direction or line of action. The total stretch ratio λ in tissue would then be the resultant of contraction (λ_c) and mechanical (λ_m) stretch ratios, or the ratio of the current length to the slack length:

$$\lambda = \lambda_m \lambda_c = \frac{l}{L_s} \qquad \text{Equation 12}$$

Therefore the mechanical stretch ratio (λ_m) is the passive deformation from the contracted state to the current state associated with the applied stress.

Convention:

From this point, to unify the muscle contraction terminology, it is defined as:

*"**the percentage of the shortened length of the stimulated but unstressed muscle to its resting length**".*

$$\textit{Muscle contraction (\%)} = (1 - \lambda_c) \times 100 = \frac{L_s - L_c}{L_s} \times 100.$$

Therefore λ_c was defined as an input parameter for each muscle, and the resulting total stretch ratio λ for all muscle, including the contracted muscle, were then calculated as an output.

2.2.4. Tissue Models and Material Properties

Obtaining the true material properties of the human urethra and consequently choosing the suitable constitutive model for the urethra was found to be challenging. One could obtain urethral material properties from human cadavers [82], however, one can argue that there is a significant difference between material properties of the tissue *in vivo* and *in vitro*. In fact, muscle tone is absent after the death and therefore *in vitro* properties are not suitable for our simulations. Other techniques such as reflectometry [83] can only report the resultant elastance of the entire urethral sphincter complex but it is incapable of distinguishing properties of the individual layers.

A 9-parameter Mooney-Rivlin hyperelastic constitutive model was adopted. Here the corresponding strain energy density function is:

$$\begin{aligned} W_s = {} & C_{10}(\bar{I}_1 - 3) + C_{01}(\bar{I}_2 - 3) + C_{20}(\bar{I}_1 - 3)^2 + C_{02}(\bar{I}_2 - 3)^2 + C_{11}(\bar{I}_1 - 3)(\bar{I}_2 - 3) \\ & + C_{30}(\bar{I}_1 - 3)^3 + C_{03}(\bar{I}_2 - 3)^3 + C_{21}(\bar{I}_1 - 3)^2(\bar{I}_2 - 3) \\ & + C_{12}(\bar{I}_1 - 3)(\bar{I}_2 - 3)^2 + \frac{1}{2}\kappa(J_{el} - 1)^2 \end{aligned} \qquad \text{Equation 13}$$

Since the urethral tissues are very similar to the arteries, the material properties of the femoral artery were used from the literature [84]. The constants in the energy density function (Equation 13) are directly provided by the same literature.

2.2.5. Urethral FEM problem setup

The following equations were used in solving the tissue mechanics problem by the COMSOL® solver:

$$0 = \nabla.(FS)^T + \boldsymbol{F}v \qquad \text{Equation 14}$$

$$F = I + \nabla\mathbf{u} \qquad \text{Equation 15}$$

$$S = S_{ext} + \frac{\partial W_s}{\partial \epsilon} \qquad \text{Equation 16}$$

$$\sigma = J^{-1}FSF^T \qquad \text{Equation 17}$$

$$J = \det(F) \qquad \text{Equation 18}$$

$$\epsilon = \frac{1}{2}(F^TF - I) \qquad \text{Equation 19}$$

Boundary Conditions

Since the muscle layers are attached together at internal boundaries, a union (or tie) boundary condition was defined for the shared interfaces. In addition, the anterior distal end of the LSM was chosen as a fixed boundary condition representing its attachment to the pubic bone (Equation 20). To consider the effect of periurethral tissues, the outside surface of the urethral wall was considered as a passive linear elastic foundation (Equation 21) with the total stiffness of mesentery tissues [79].

$$\boldsymbol{u} = 0 \qquad \text{Equation 20}$$

$$\boldsymbol{F_A} = \frac{k_{tot}}{A}(\boldsymbol{u} - \boldsymbol{u_0}) \qquad \text{Equation 21}$$

In this section, the vascular plexus can be excluded by the assumption of using a rigid 7 French catheter (~2.3 mm diameter) inserted into the lumen, completely expelling blood from the vascular plexus, and measuring the UCP during urodynamic exams. Therefore, in the simulations resulting in the constriction of the urethra, an elemental roller boundary condition (Equation 22) was defined for the internal surface of the LSM. In the case of simulating the contraction of the LSM – where dilation happens – a free boundary condition was chosen instead. Therefore, simulation results could also be validated using the existing literature.

$$\boldsymbol{u}.\boldsymbol{n} = 0 \qquad \text{Equation 22}$$

Solver

For the example urethra shown earlier, a total of 50,000 tetrahedral quadratic serendipity elements were found to suffice to capture enough geometric detail without over-refining the mesh. In these simulations, it was assumed that the contraction happened in quasi-static form. Therefore, a stationary parametric study was performed instead of a time-dependent analysis.

This significantly reduced the processing time. The FEM model was simulated using a parallel direct solver algorithm (PARDISO) [85] in COMSOL®.

Through the parametric sweep of active contraction stretch ratio (λ_c) in the direction that muscle fibers or line of actions are oriented, muscle contraction was simulated. In other words, an external strain in the form of contraction stretch ratio (λ_c) along the curvilinear principal directions was applied to obtain corresponding stresses or pressure distributions in tissues.

The only exception was the dorsal 70° segment of the STM which consists of passive tissues incapable of contracting [50]. Therefore, the external strain was only applied to the lateral and ventral regions (a 'horseshoe' shape in a transverse plane section) in the simulation. The simulation result considering this assumption was compared with the case where the entire STM was actively contracting in order to elucidate the effect of the passive tissue presence.

2.3. Methods (II) – Vascular Plexus

2.3.1. Axisymmetric VP Geometry for an Exploratory Simulation

The plexus layer was modeled as a fluid domain filled with blood. It was assumed to have inlet and outlet boundaries representing the arterial and venous pressures. The plexus domain is separated from either the bladder neck or intra-lumen fluid domain filled with urine, by a thin ultra-elastic epithelial layer. It is the interaction between those physics that will be explored here.

A $1.5\ mm \times 1.5\ mm$ window from the proximal portion of the vascular plexus, immediately inferior to the bladder neck, where plexus, urine, and epithelium domains exist was studied (Figure 10). The width of the window was chosen from the values provided by the literature for the plexus layer [50]. The height of the window of interest was only a portion of the total plexus length. This would not change the result but reduced the computational time.

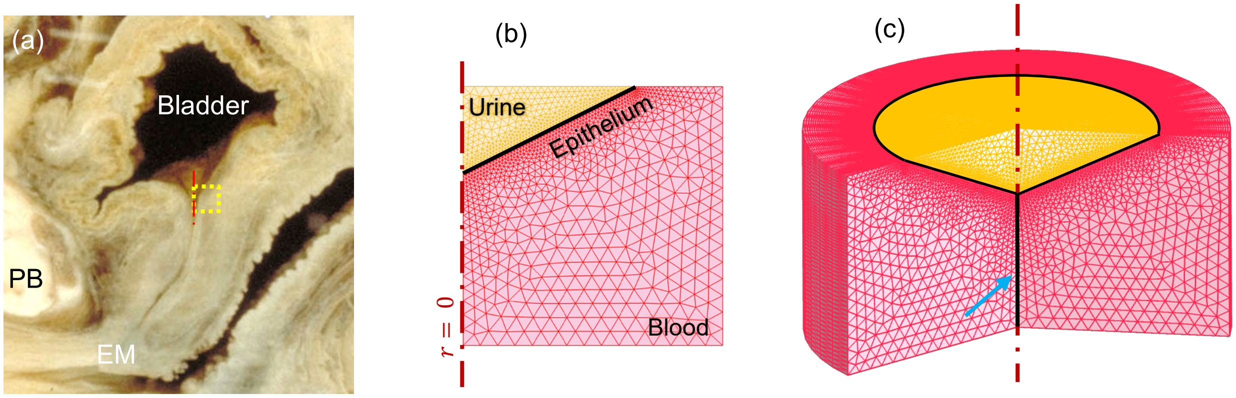

Figure 10. (a) Left lateral view of a mid-sagittal section of a cadaveric female lower urinary tract (©DeLancey). The dotted square represents the region of interest in the proximal urethra immediately inferior to the bladder neck. PB represents pubic bone and EM represents external meatus. (b) axisymmetric meshed window (in the region of interest) of the proximal vascular plexus filled with blood, the epithelium separating the plexus from the urine in the proximal urethra. Axisymmetric meshed domain partially revolved showing the 1.5 mm thick annular shape of the proximal urethra and its vascular plexus. The closed lumen is shown by the blue arrow.

The symmetry axis was placed on the left edge of the window. The urine fluid domain was represented by the triangular shape in the upper left corner of the window. The rest of the window was considered the plexus domain, and the epithelium layer separated both fluid domains (solid black line in Figure 10b). The thickness of the epithelial layer in the model was 100 μm in this model.

Overall, this window was meshed with about 2300 triangular elements. The density of mesh elements were higher close to the epithelial internal boundary (wall).

2.3.2. Fluid-Solid Interactive Physics and the Moving Mesh

The epithelial layer was modeled with quadratic elastic shell elements. The fluid dynamics physics of both the urine and blood-filled plexus domains was solved using the time dependent Navier-Stokes equations. Since deformation of this interactive model was fairly large, the Arbitrary Lagrangian and Eulerian (ALE) moving mesh scheme was adopted (see CFD, Structural Mechanics, and Moving Mesh sections of the COMSOL® user's manual [72]). For the sake of simplicity, the intrinsic viscous damping of the plexus layer tissue was neglected in these simulations.

The boundary conditions of the ends of the epithelial shell were defined as 'rollers' along each edge (points a and b in Figure 11). The top segment of the urine domain was set as an open boundary with a bladder pressure (P_u). The right segment of the top edge of the plexus domain was set to be the inlet with the arterial pressure (P_a), while the bottom edge was defined as the outlet with venous pressure (P_v). Both of the inlet and outlet boundaries were chosen as one-way boundaries so as to suppress backflow in the plexus boundary. In the FEM study, these three pressures were altered around the equilibrium state to see how they would deform and move the epithelial boundary. If the epithelial boundary rolls caudally, because of increased vesical pressure or decreased effective plexus pressure, this reflects the urine intruding into the lumen thereby temporarily shortening the functional length of the urethra. More specifically, if the point b in Figure 11 moves proximally the functional urethral length is lengthened improving the continence margin, while if it moved distally the vesical length would open and the functional urethral length would be reduced, reducing the continence margin. To avoid the complexities of dealing with topology changes and self-contact mechanics, the simulations were halted once the epithelial layer stably moved in either direction and reached the other boundaries.

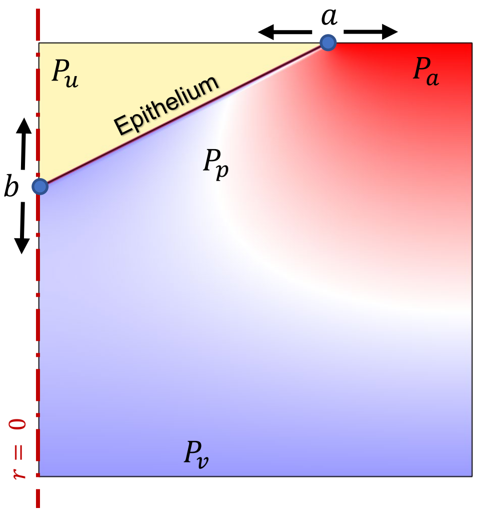

Figure 11. Arterial, venous and vesical pressures are variables that were systematically changed in the FEM simulation to explore their effect on the closure pressure and the functional length of the urethra.

In setting up the wall boundary types in the fluid dynamics physics, the “slip” condition was chosen for the right wall, and “no slip” boundary condition was chosen for the internal wall i.e., the epithelium. The “no-slip” boundary condition on the epithelial edge (or wall) means that the fluid velocity relative to the boundary was set to zero.

Finally, in defining the moving mesh, both fluidic domains were chosen as deforming domains. The top and the symmetry edge (r = 0) – on which the epithelial shell ends are rolling - were defined to have sliding mesh.

2.3.3. Material Properties

Table 1 shows the material properties taken from the literature [13], [86]–[89] for this simulation.

Table 1. Material properties of the epithelial layer, blood and urine used in the fluid-solid interactive physics of the vascular plexus layer.

Epithelium	Young's Modules	14 kPa	Yamada (1970)
	Density	1190 kg/m^3	
	Poisson's ratio	0.45	
Blood	Dynamic Viscosity	3.5×10^{-3} Pa.s	Gustafson (1980)
	Density	1060 kg/m^3	
Urine	Dynamic Viscosity	7×10-4 Pa.s	Kim (2017), Oppliger (2005)
	Density	1023 kg/m^3	

2.4. Results

2.4.1. Contribution of each urethral muscle

The computations (Table 2) showed that when STM contracted in length by 3%, the UCP increased up to 35 cmH2O (Figure 12), whereas when the CSM contracted 3%, the UCP increased up to 12 cmH_2O (Figure 13 and Figure 14). The lower UCP change in this case could be a result of a lower CSM thickness compared to the STM. However, when the LSM contracted even up to 20%, the UCP did not significantly increase, but it shortened the urethra (Figure 15). When all three muscles contracted simultaneously by 3%, the UCP reached 30 cmH_2O in the mid urethra, because the LSM counteracted the effect of the STM.

Table 2. Change in the maximum UCP from rest when each individual muscle layer was contracted (3%).

Muscle Layer	State (λ_c)	**Change** in the MUCP Pressure (cmH_2O) from rest
At Rest	1	0
Circular Striated Muscle	0.97	**35**
Circular Smooth Muscle	0.97	12
Longitudinal Smooth	0.97	0
All three	0.97	30

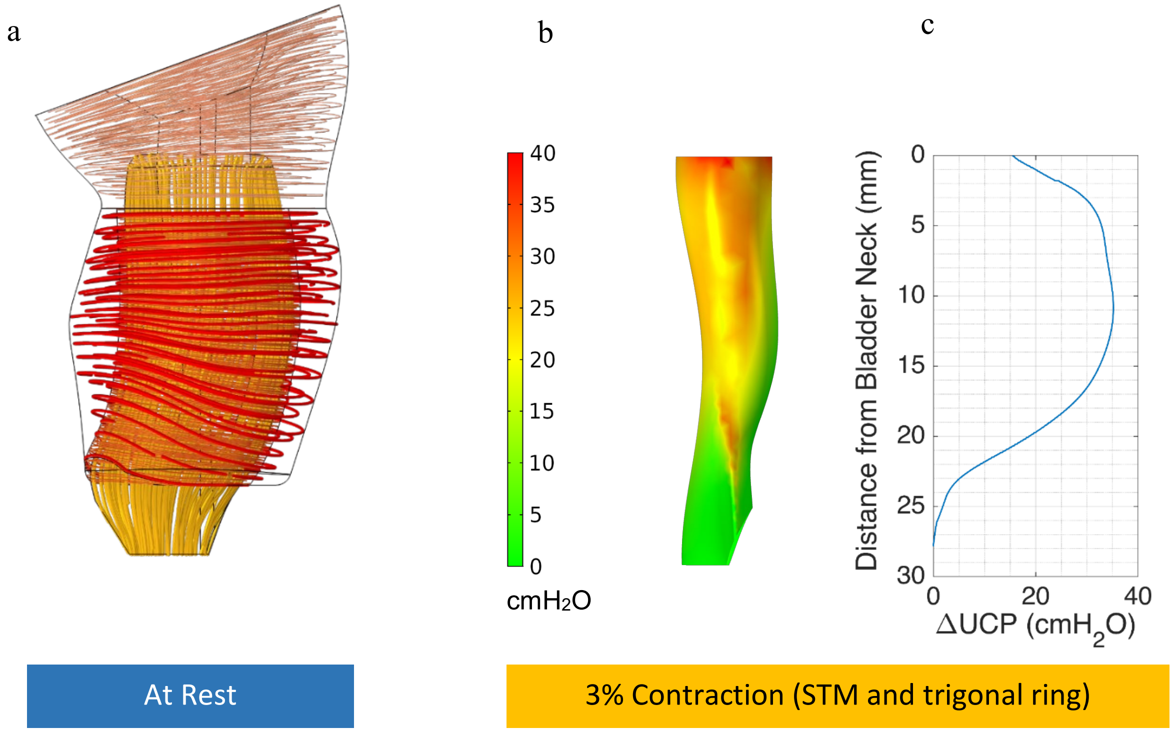

Figure 12. a) Urethra muscle fibers at rest, b) urethral closure pressure distribution on the surface between plexus and LSM layer when the STM fibers contracted by 3% from the resting state, and c) change of the average pressure distribution along the urethra for the same STM contraction.

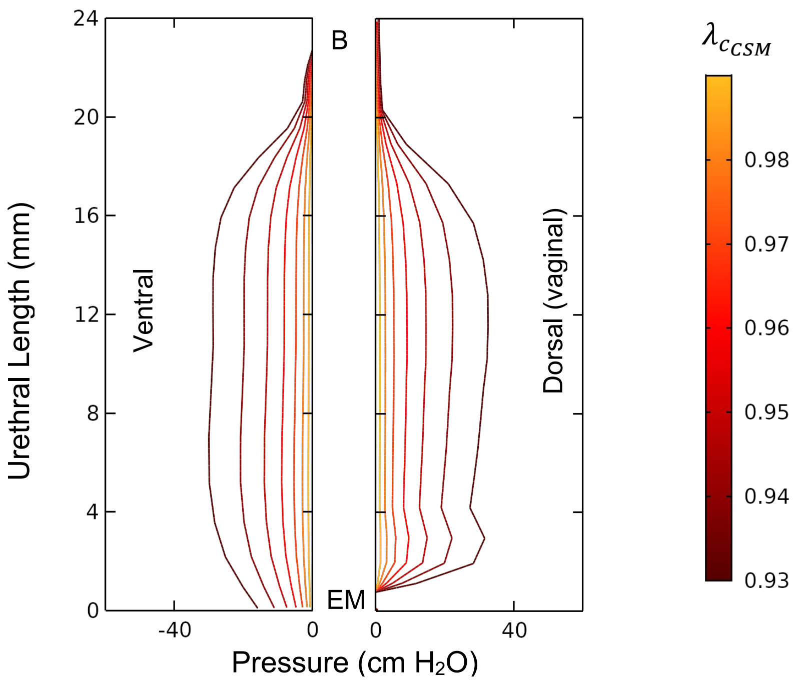

Figure 13. Pressure distribution on the catheter when only the CSM layer contracted up to 7% ($\lambda_{c_{CSM}} = 0.93$). CSM contributed three times less UCP than STM when contracted by the same contraction stretch ratio. **BN**: bladder Neck, **EM**: external meatus, and **PB**: pubic bone

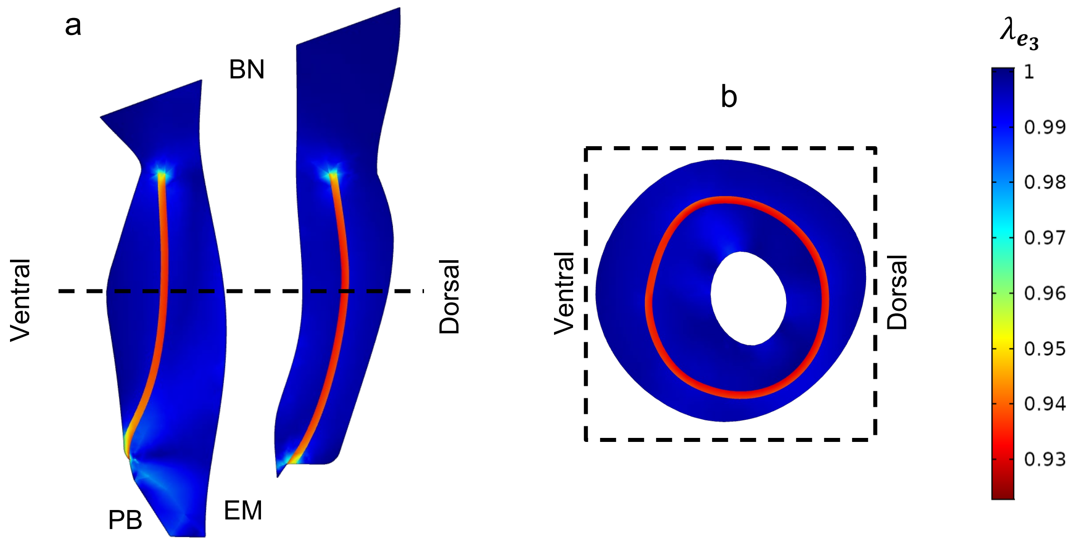

Figure 14. (a) Mid-sagittal and (b) mid-axial cross-section of the urethral musculature tissues showing the quasi-radial principal stretch ratio λ_{e_3} when CSM is contracted 7%. **BN**: bladder Neck, **EM**: external meatus, and **PB**: pubic bone

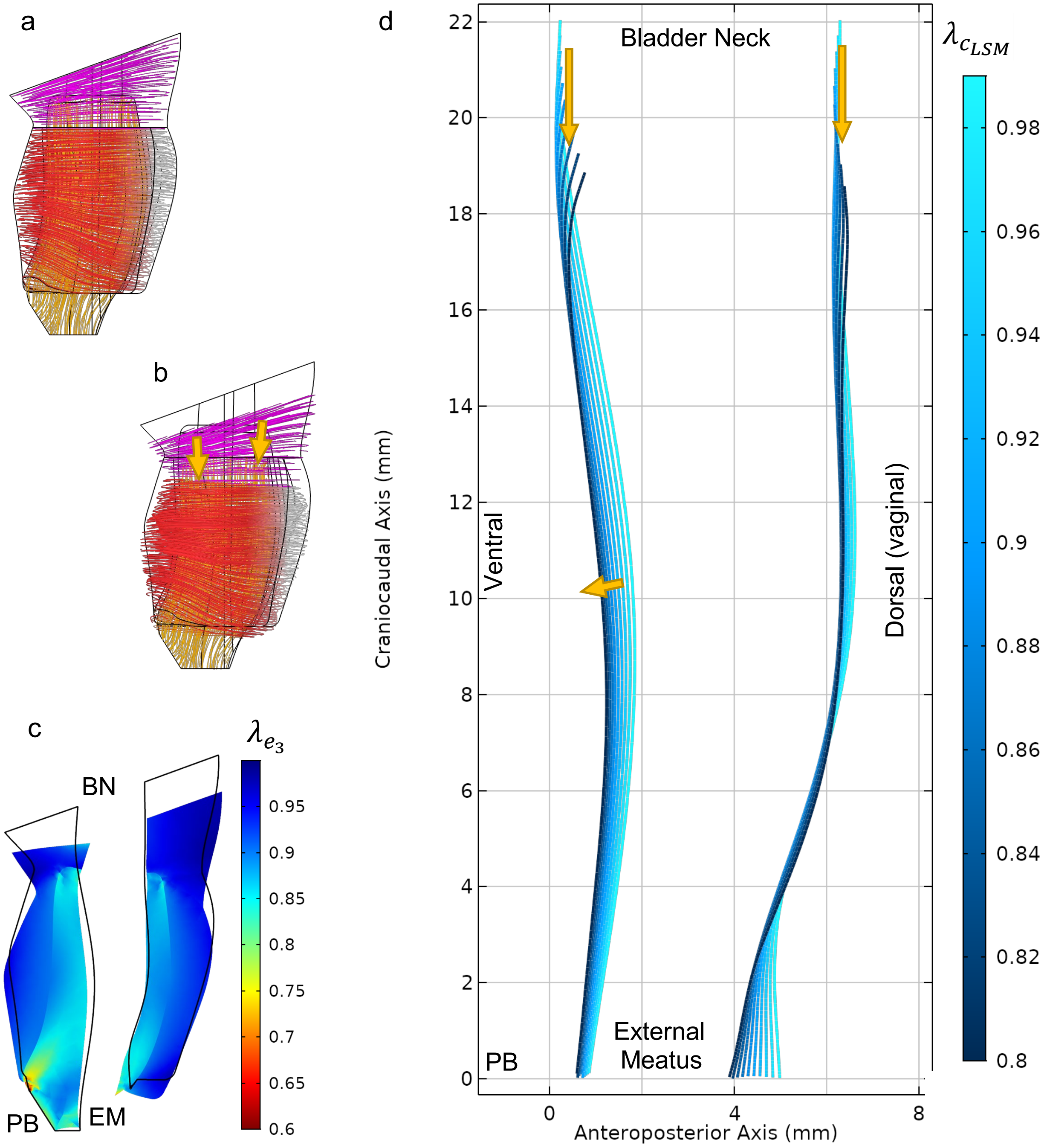

Figure 15. (a) Lateral view of the urethra muscle fibers at rest, and (b) when LSM contracts 20%. (c) The overall deformed midsagittal cross section of the urethra when LSM contracts 20%. The black outline represents the resting state. The color distribution represents the overall stretch ratio (resultant of active and mechanical) along the quasi-radial direction ($\boldsymbol{e_3}$). **BN**: bladder Neck, **EM**: external meatus, and **PB**: pubic bone. (d) the dorsal and ventral loci of the intersection of the inner surface of the LSM and mid-sagittal plane shows that the urethra is shortened and moved downward when LSM contracts to 20% of the rest state. The ventral mid-urethral region of the LSM did not constrict but stretched out the outer STM instead.

2.4.2. Effect of the dorsal passive portion of the STM

When STM was contracted, regardless of the dorsal passive portion, urethral pressure distribution dorsally was similar to the ventral one (Figure 16). When the dorsal portion was turned into a passive tissue in the simulations, and was only stretched by the horseshoe-shaped STM, the urethral pressure levels were reduced by 26% ventrally and 83% dorsally (Figure 17).

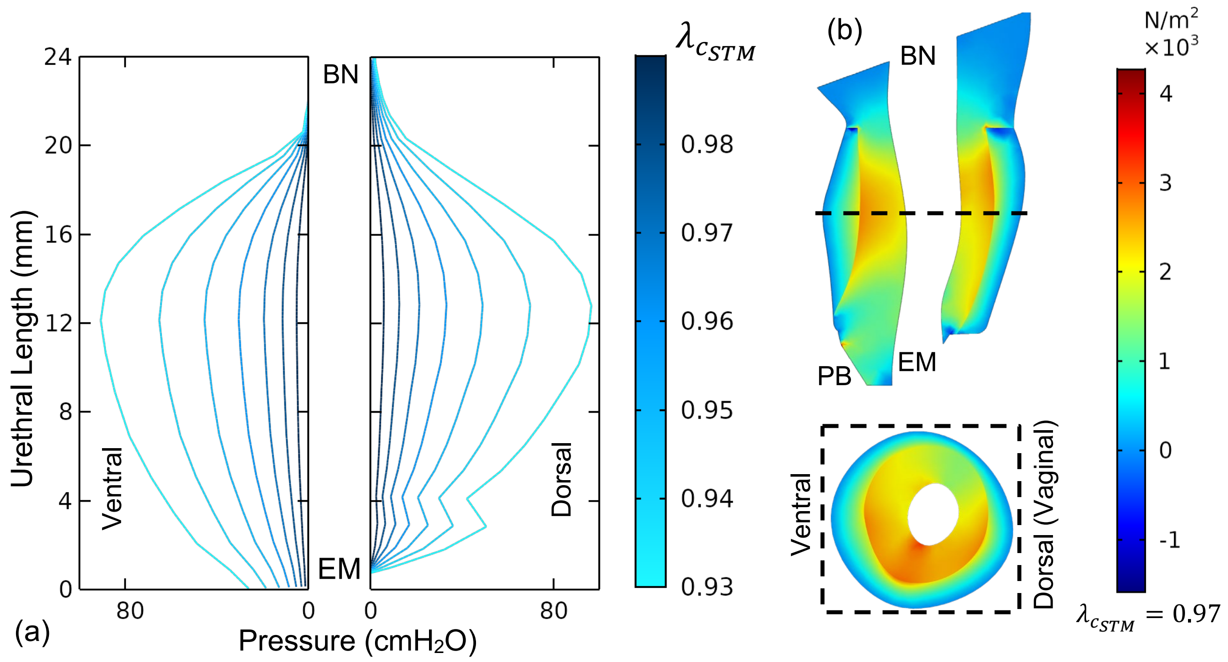

Figure 16. (a) Urethral pressure distribution when STM layer was comprised wholly of contractile fibers contracting up to 7%. **BN**: bladder Neck, **EM**: external meatus, and **PB**: pubic bone. (b) mid-sagittal mid-axial (dashed line) cross section of the urethra muscles showing the principal stress distribution along inward quasi-radial direction when STM contracts 3%.

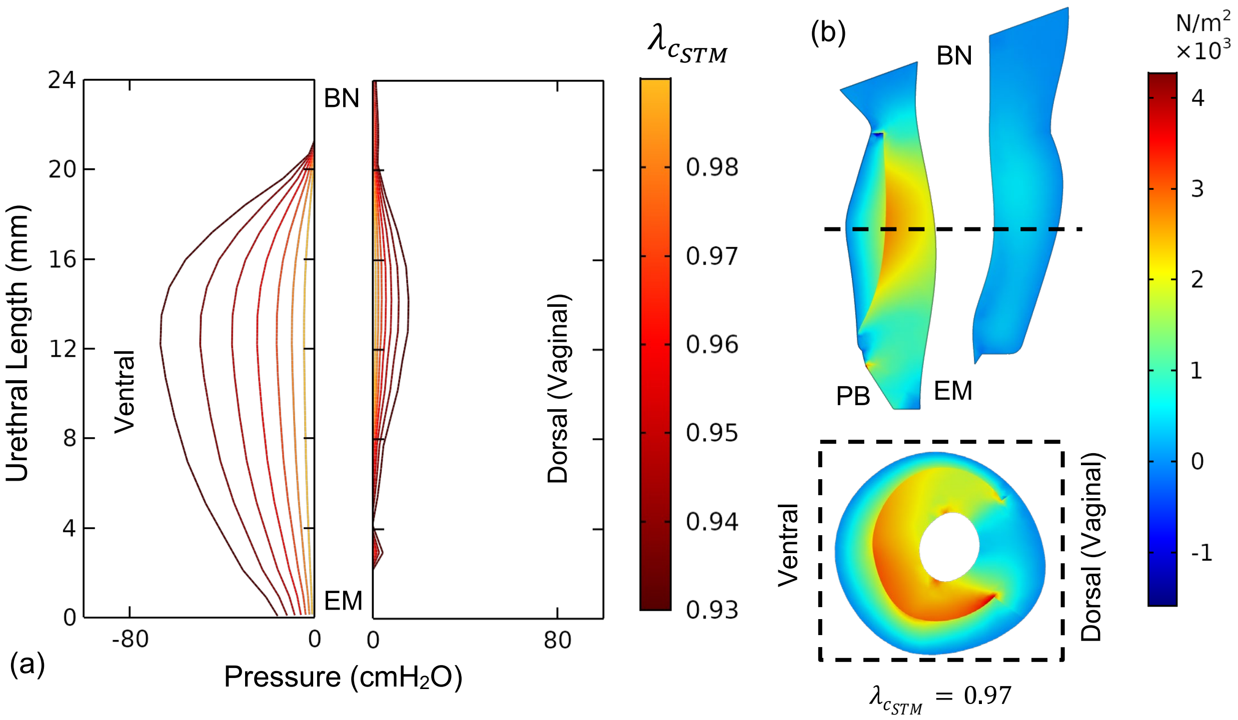

Figure 17. Urethral pressure distribution when the horseshoe of STM contracted up to 7%. The dorsal region of the STM was modeled as a passive tissue without actively contracting. **BN**: bladder Neck, **EM**: external meatus, and **PB**: pubic bone. (b) mid-axial and mid-sagittal cross section of the urethra muscles showing the principal stress distribution along inward quasi-radial direction when STM contracts 3%.

In addition, Figure 18 shows total displacement of the urethral muscles when pressure was applied on the inner surface of the LSM in order to simulate the expansion of an inserted intraurethral balloon catheter. The total distension of the vaginal side of the urethral wall was higher than the rest of the urethral musculature horseshoe as has indeed been observed in patients (personal communication with J. O. L. DeLancey on 6/19/2020).

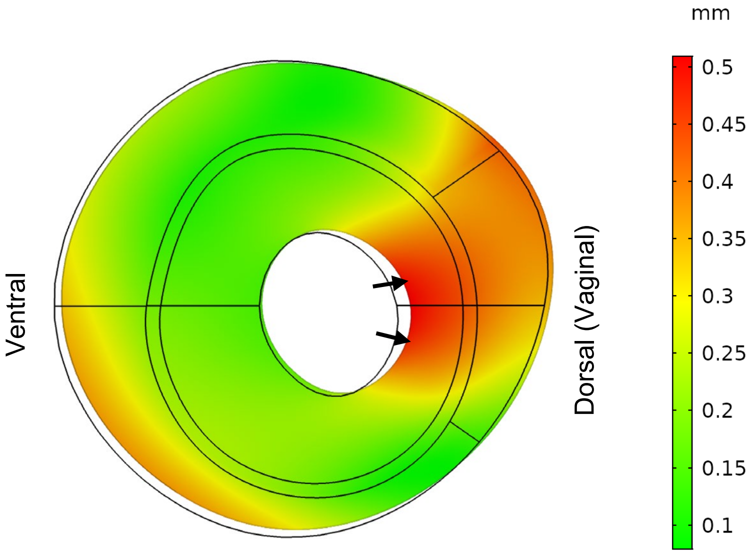

Figure 18. Displacement field of the mid-axial cross section of the urethral muscles when the intraurethral pressure was increased to simulate expansion of the exerted balloon. The STM horseshoe portion was contracted by 10%. The vaginal side of the STM simulated as a passive tissue presumably due to aging related contractile fiber loss. The black lines show boundary of each muscle domain at the initial state. The vaginal portion of the STM expanded more compared to the rest of the STM.

2.4.3. Vascular Plexus

To examine the role of the vascular plexus layer "at rest", the initial vesical pressure (P_u) was set at 15 mmHg (or 20.4 cmH_2O). The initial inlet (P_a) and outlet (P_v) pressures of the plexus domain were also set equal to the vesical pressure. Afterwards, a series of time dependent studies were ran and plexus pressures increased via a ramp function to reach a desired pressure based on the scenario being studied. The outlet pressure (P_v) was set to be a fraction of the inlet pressure through iterations to resemble the pressure drop across the vascular plexus [90].

$$P_v = P_a \times \alpha \qquad \text{Equation 23}$$

Results of this simulation showed that the epithelial border slides proximally and increases the functional urethral length. In other words, it helps keep the hermetic seal of the urethra (Figure 19).

In a parametric sweep study over the parameter α, a new insight was revealed in that for this simplified model of the plexus, it was the effective plexus pressure (P_p) between the inlet and outlet pressures that determines the closure pressure. However, P_p is not exactly the mean of the inlet and outlet pressures and depends upon factors including the true topology and state of the plexus. Therefore, P_p might vary between different urethrae and the state of the surrounding musculature tissues deforming the plexus in different scenarios.

In summary, a positive difference between the effective plexus pressure (P_p) and the vesical pressure (P_u) helps to maintain continence. Given the material properties of this problem, there is also a minor hysteresis pressure ($P_h \approx 2\ cmH_2O$) which depends on the stiffness of the epithelial layer. Therefore, in a non-accelerating frame:

$$P_p - P_u - P_h \begin{cases} \geq 0 & continence \\ < 0 & reduction\ in\ functional\ urethral\ length \end{cases}$$

In which $P_h \ll P_u$

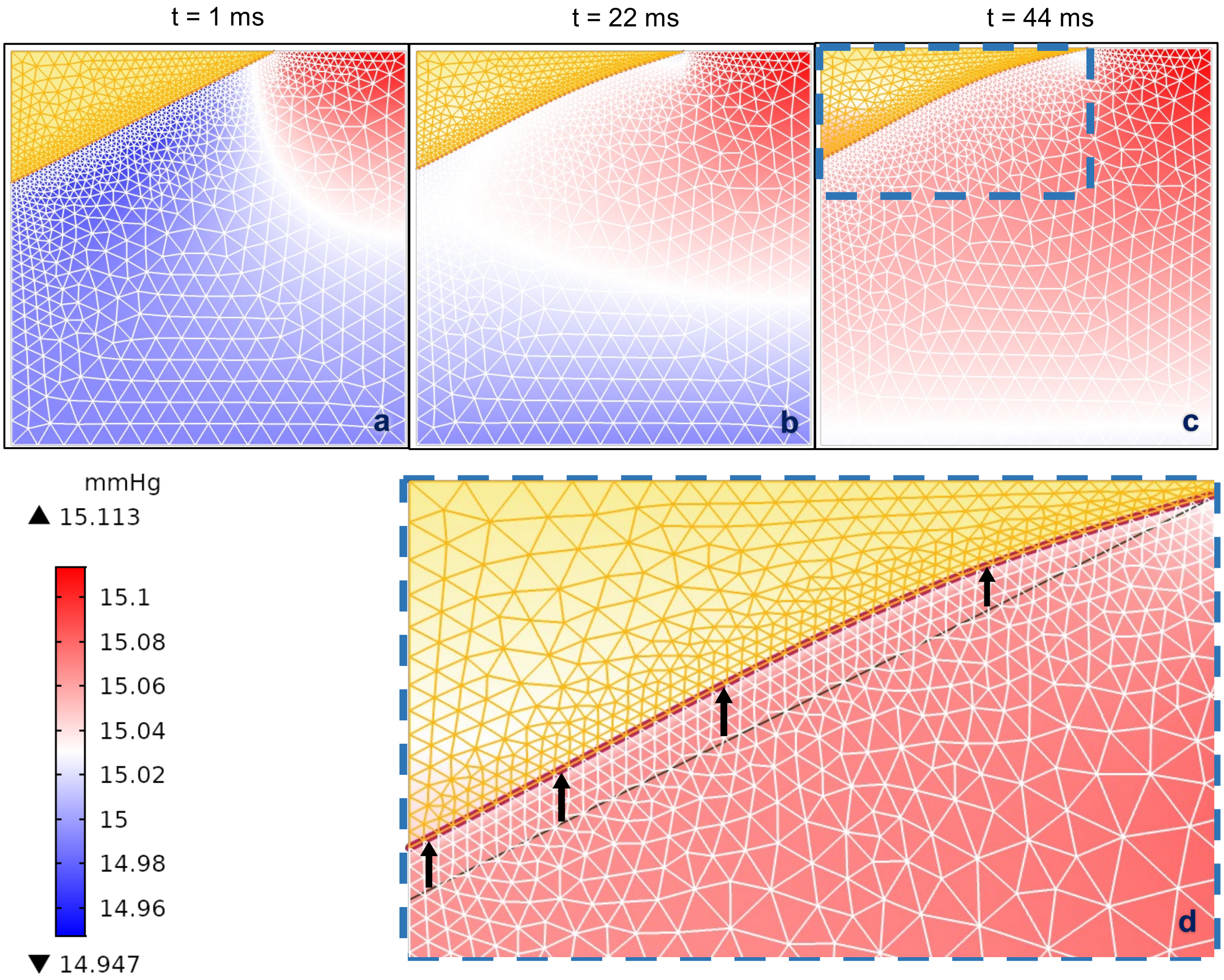

Figure 19. The pressure distribution at different time intervals across the 1.5 mm x 1.5 mm window of the proximal urethra where the vascular plexus (VP) layer starts. Results reveals that the higher blood pressure distribution in the VP compared to the vesical pressure can increase the functional urethral length and promote a hermetic seal. (a) Urine inside the bladder is shown by the yellow triangular region at top left corner. At t = 0 s the arterial pressure of the vascular plexus (inlet) is increased from the initial value equal to the vesical pressure (b) (t = 22ms) pressure distribution continues to increase across the VP and the epithelial boundary slides proximally (up). (c and d) further increase in VP inlet and respectively outlet pressures increases the functional urethral length.

Results of the second simulation (Figure 20) in which the intra-abdominal pressure (IAP) was increased quickly also verified the stated pressure equilibrium. In that simulation, the effect of IAP rise was modelled by increasing three pressures in all domains. In the first phase of this simulation (Figure 20b), the arterial pressure could compensate for the increased vesical pressure and therefore maintain the continence. However, in the absence of further increase in vesical pressure an incompetency of the intermediate vascular plexus pressure (P_p) caused the epithelial layer to deform and move distally. In so doing, it reduced the functional urethral length.

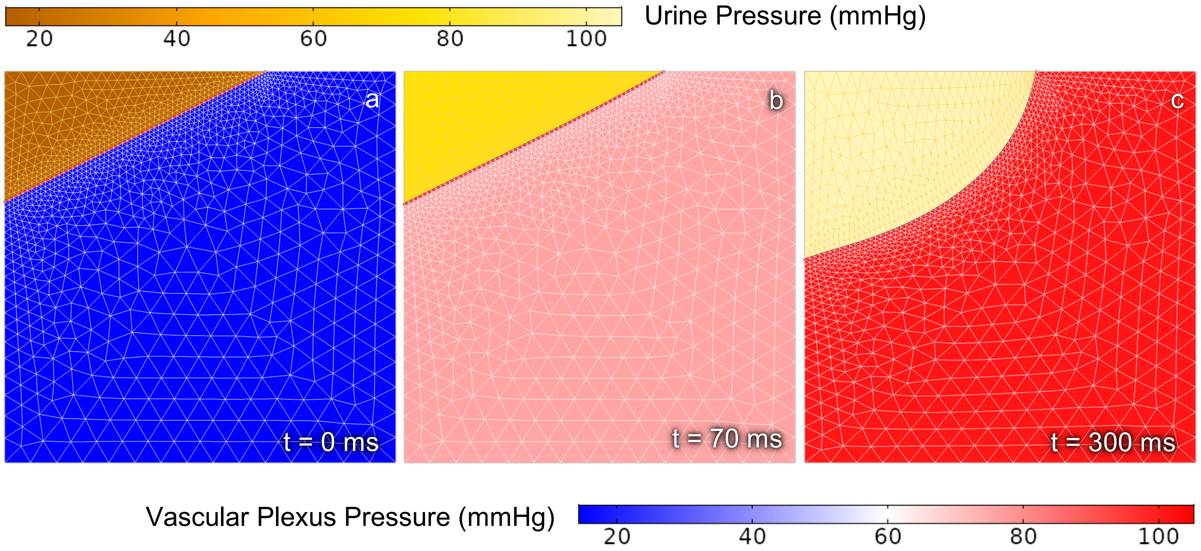

Figure 20. Pressure distribution across the vascular plexus layer and vesical domains filled with blood and urine, respectively, when intra-abdominal pressure suddenly rises during stress events such as cough or lifting a heavy object. (a) (t = 0 ms) at rest with pressure equilibrium (b) (t = 70 ms) intra-abdominal pressure rise increases vesical and arteriovenous pressures. The functional urethral length does not reduce as far as the average arteriovenous pressure also increases. c) (t = 300 ms) If the average pressure across the plexus layer fails to overcome the increased vesical pressure in a stress incontinent patient, the functional urethral length is reduced i.e., the epithelial layer expands and is pushed distally. This could initiate a leakage episode.

A similar result was obtained when the intermediate vascular plexus pressure was reduced from the equilibrium state simulating the start of the micturition process in which arterioles shut off the arterial pressure to the vascular plexus layer.

2.4.4. Contribution of urethral muscles in each activity

Results of contracting individual muscle layers (section 2.4.1) revealed that the longitudinal muscle shortens the urethral length in contrast to the circular muscles, which increases the urethral closure pressure via constriction. Each urethral kinematic scenario, such as a Kegel contraction or a micturition event, is a combination of active contraction and relaxation of those muscles.

According to the pressuregram analyses [70], in order to maintain continence, the maximum urethral pressure should be higher than the vesical pressure. Therefore, according to these simulations, since STM contributes to the urethral closure pressure, it suggests that at rest, STM can partially be activated to maintain the urethral pressure. During Kegel, to further increase the closure pressure, contraction of STM would further constrict the urethra via voluntary contraction. One might also speculate that the CSM may also be activated, but then it would have a significantly lower contribution to the closure pressure.

At rest, since contraction of the longitudinal muscle counteracts the pressure rise in the lumen caused by the circular muscles, simulations suggests that LSM is possibly deactivated. Then, the simulations also suggest that LSM should contract to reduce the urethral pressure and possibly initiate the micturition by pulling down and opening the bladder neck. Furthermore, the STM and circular fibers of the bladder neck should relax to facilitate the passage of urine.

2.5. Discussion

2.5.1. Strengths

To address the **first** knowledge gap, this chapter proposed the first 3-D subject-specific model capable of contracting individual urethral muscle layers. The consideration of the “fiber” direction (for striated muscle) and contraction line of action (for smooth muscle) has never been considered before in any urethra model. These two factors help in assessing the contribution of each muscle toward maintaining UCP.

Results from simulating STM contraction, corroborated earlier findings that have shown that women can voluntarily increase the maximum urethral closure pressure between 13 to 23 cmH_2O [91], [92] from the resting state, indicating how much a maximum contraction of the striated muscle can increase UCP *in vivo*.

Perhaps the most important of all the findings was the role of LSM in shortening the urethra but not increasing the UCP. In fact, while contraction of the circular muscles increased the UCP, LSM counteracted and reduced the elevated UCP. This finding contrasts with the existing literature where the "smooth" muscles of the urethra were held responsible for one third of the UCP [49] (although which of the two smooth muscles was envisioned was never elucidated).

This result also is inconsistent with the hypothesis that the LSM would contribute to the UCP by contracting and forming a thick plug via the Poisson effect [59], [60]. A careful examination of results revealed that the contraction of the LSM distends the STM, but did not constrict the lumen. This unique behavior was the consequence of the asymmetrical shape of the urethra and the fact that STM does not fully contract in the resting state. LSM contractions up to 20% straightened the curvature of the urethra (mostly ventrally) rather than forming a thick plug, further contraction of LSM produced irrational stress levels in the simulations.

Finally, these simulations indicate that the CSM layer is less effective in contributing to the UCP compared to the STM. It has been suggested that the CSM is incapable of significantly constricting the urethra due to its minimal layer thickness [61].

In addressing the **second** knowledge gap, it is known that aging affects the width of the dorsal active STM [50] even in the nulliparous women – excluding the possible nerve damage inflicted by pressure of the fetal head during vaginal delivery. Therefore, when the dorsal 70° arc of the STM was made a passive tissue, UCP was found to be less (dorsally in particular) compared to a fully contractile STM. A similar pressure profile [93] has been found in incontinent women. Therefore, this model provides a possible explanation of how and why aging can adversely affect continence and why stress incontinence is more prevalent in older women .

In addressing the **third** knowledge gap, an effective vascular plexus pressure (P_v) was defined. This was an intermediate pressure between the arterial and venous pressures, and it depends on the resistance of the arteriovenous anastomoses against the blood flow. The result of the axisymmetric vascular plexus model suggested that it is the difference of the effective vasculature pressure (P_p) and the vesical pressure (P_u) at the proximal bladder neck that determines the closure pressure. This pressure difference directly affects the functional urethral length and hermetic seal of the plexus layer.

Any structural change in the vasculature can alter the vascular resistance in the plexus layer and the effective vascular plexus pressure (P_v), thereby changing the continence thresholds. This could become critical in activities that intra-abdominal pressure increases. The model suggests that the failure in providing a high enough arteriovenous vasculature pressure reduces the functional urethral length and could lead to a leakage episode. Similarly, to initiate micturition, arteriole muscles can constrict and impede the blood supply to the VP, thereby reducing the effective vascular pressure in the plexus.

One might speculate that atherosclerosis could adversely affect the arterial pressure supplying the VP and might be one reason that SUI is more common in older women. Nevertheless, since blood pressure increases with age [94], while the urethral closure pressure declines, among many other possibilities [95], [96], it implies either there are structural changes in the vasculature [97] that prevents an effective vascular plexus pressure rise, or simply there is not enough support from the muscles in the urethral wall.

The Young's modulus of the epithelial boundary of the plexus layer in these simulations was low enough to have minimal hysteresis effect on the pressure equilibrium ($P_h \approx 2\ cmH_2O$). Nevertheless, aging and diseases can alter the type of epithelial cells of the lumen [61]. This in turn can affect the mechanical properties and possibly lower thresholds for continence.

Finally, this urethra model enabled the study of many different muscle contraction scenarios, some of which are impossible to test *in vivo*. It is hoped that this model eventually will help researchers to better understand the effects of aging and disease effects as well as to explore novel treatment strategies.

2.5.2. Limitations

The major limitation in this model was the absence of a detailed 3D model of the remarkable vascular plexus fully-coupled with the developed musculature layers to identify the effective vasculature pressure (P_v). Modeling both vasculature and musculature layers together could provide more realistic results.

Although the geometry of the urethra was constructed from serial high-resolution MR scans, not all urethral details could be captured. Therefore, the final geometry was refined with a help of histology slices that have much better resolution. Similarly, the fiber directions and line of actions were artificially made to match those observed in histology slices but, may deviate from the actual directions in the muscles. As an example, in reality the proximal and distal ends of the LSM are morphed into other layers, whereas in the present model the LSM fibers were mainly oriented longitudinally and unified with the circular fibers orthogonally only at the ends.

Several assumptions were made to simplify the physics, and these could introduce errors and make results deviate from reality:

1. Exclusion of the self-contact mechanics of the urethral lumen and the contact mechanics of the lumen with the inserted catheter.
2. Choice of quasi-static analyses instead of a time-dependent one in simulating the urethral musculature layers
3. Disregarding the viscoelasticity of urethral muscles and vascular plexus
4. Modeling the periurethral tissues with a simple elastic foundation rather than the actual organ and tissue particularly at the bladder neck

Another major limitation was the lack of material properties for the urethra; making it necessary to take them from femoral arteries. Although similar, they have differences and these could result in errors.

In the vascular plexus model, the effect of the gravity and activity-related accelerations on the domains were neglected; in practice these could lead to leakage through activities like jumping, running, coughing or sneezing.

Finally, more simulations on various urethral shapes are needed to fully confirm current results. The validation in this dissertation is done mainly using the catheter pressure measurements in the literature; however, those measurements were made using large diameter catheters which force the blood out of the plexus layer. Therefore, micro-catheters, novel imaging and other measurement techniques are required to further validate this model in live subjects during different pelvic floor maneuvers.

2.6. Conclusions

In this model:

- The STM contributed the most to the UCP and at least three times more than the CSM.
- The LSM made no contribution to the UCP only shortening the urethra, but without forming a thick plug described in the literature.
- The dorsal passive portion of the striated circular layer reduced the overall predicted urethral closure pressure with a significant 83% reduction in the dorsal region.
- The difference of the effective vascular plexus and vesical pressures determined the closure pressure and directly contributed to the functional urethral length.
- LSM role was determined to initiate micturition, while it was the STM that increased UCP in Kegel.

CHAPTER 3

Design of the Personal Uroflowmeter (PUF) Device

Parts of this chapter have been published in US provisional patent app 62/925309 on October 24th 2019 and accepted for the presentation in the *American Urogynecologic Society* (AUGS) virtual *Pelvic Floor Disorders* Week (2020).

3.1. Introduction

In the clinic, commode-style uroflowmeters are used to measure maximum urine flow rate and bladder emptying capacity as a baseline measurement for bladder storage and voiding functions. However, such tools are not suitable for measuring when and how much urine leaks during activities of daily living (e.g., walking, stretching, lifting, laughing, jogging, sports, an unexpected sneeze, and during times of urinary urgency). These methods do not lend themselves for assessing urine output or leakage patterns in a cognitively-impaired individual and/or in a very ill person in hospital who is unresponsive.

To address the above shortcomings, a wearable uroflowmetry system was therefore invented. The goal was to design a personal uroflowmeter (PUF) to measure and record the urine flow rates and volumes when leakage episodes occur during daily activities. The PUF would also be able to be used in hospital settings such as intensive care units to measure urine output in unconscious individuals to avoid the use of in-dwelling catheters.

The design, development, and initial testing of the wearable PUF device is described in two main phases:

1) This chapter describes the testing of the fit of the PUF funnel housing on the body, the attachment methods of the passive PUF device (without addition of the sensory instruments) over the urethral meatus and the calibration and testing of the flow rate sensor in a benchtop setup.
2) Testing the fully instrumented PUF and its flowmetry and activity recognition capabilities in women (Chapter 4).

3.2. Methods (I) – Passive Housing Design

The flow rate measurement unit of the PUF is comprised of a flexible funnel shaped housing which attaches over the urethral meatus and between the labia in order to capture urine excreted by the woman (Figure 21). The housing has a measurement channel formed to guide and quantify the flow rate of urine passing through the channel as well as the temperature of that urine.

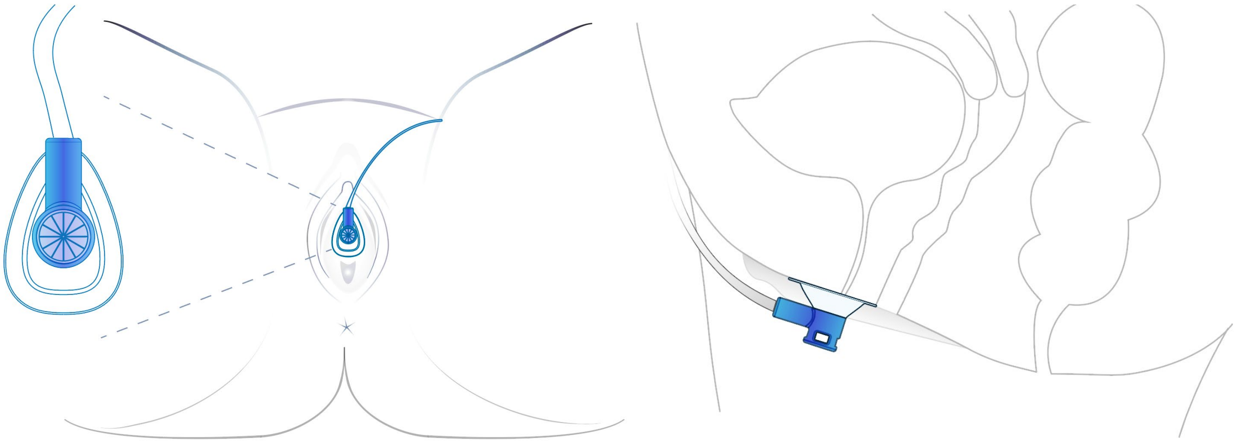

Figure 21. (a) An illustration showing the positioning of the wearable uroflowmeter located over the urethral meatus of a female in the lithotomy position. (b) A left lateral schematic representation of the PUF placement over the female urethral meatus.

The PUF housing is coupled to a wearable determining unit worn on the waist which has an embedded inertial measurement unit designed to record body movement data (Figure 22).

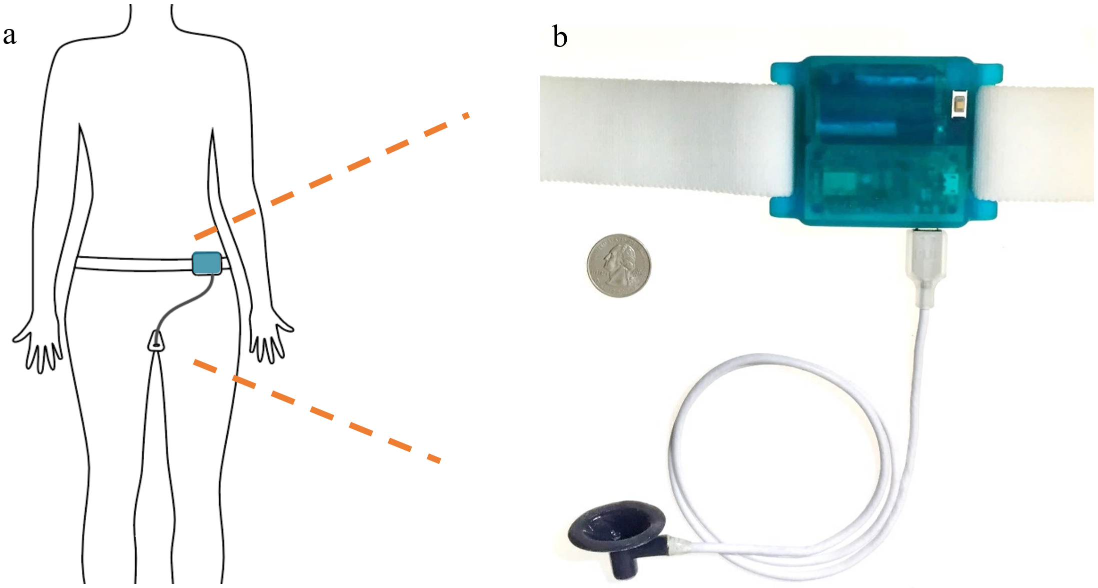

Figure 22. Schematic of the entire PUF apparatus. a) The overall apparatus to be worn by the subject, b) The waist determining unit performs signal processing of the flow rate and temperature signals. The results are either logged or transmitted to a receiver. In addition, a 9 degree of freedom inertial measurement unit (IMU) is installed to monitor the changes in the pelvis dynamics during activities of daily living. In that way the urine leakage rate and volume can be correlated in time with activity of the daily living that is associated with the measured leakage episode.

3.2.1. PUF Sensor Housing

The PUF sensor housing (Figure 23) is comprised of a flexible funnel portion held against the body to capture urine excreted by the person, a fluid passage with a rigid measurement portion, and an outlet to direct the captured urine away from the body. The measuring portion has a sensor in the rigid fluid channel configured to collect instantaneous urine flow rate and temperature.

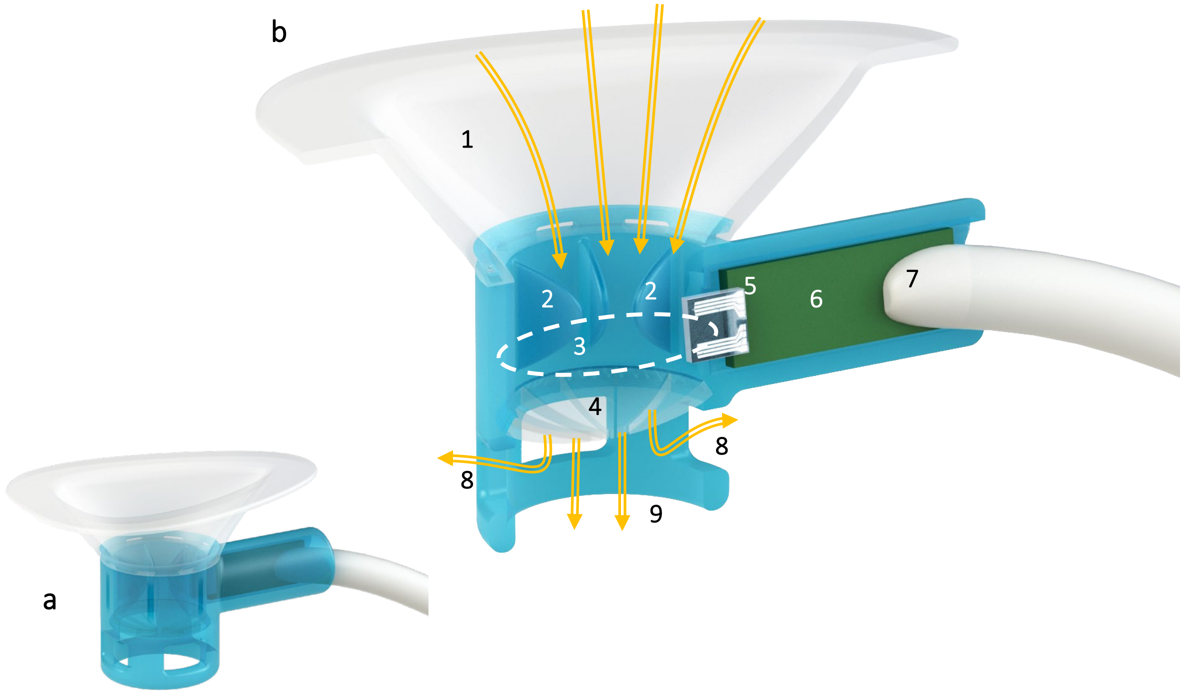

Figure 23. (a) PUF (V17) flowrate sensor housing and (b) cross sectional view of the PUF showing urine (yellow arrows) captured by the biocompatible flexible silicone funnel (with flange) (1) and passing through the guide vanes (2), sensor aperture (dotted line) (3) and the post sensor convex flexible buffer membrane (4) of the measurement channel. The glass substrate of the flow rate sensor (5) is protruded into the measurement channel to measure the instantaneous flow rate of the urine passing through the aperture. This substrate is mounted (wirebonded and encapsulated) onto a custom made printed circuit board (6) which itself is soldered to a premium grade cable (7). Lateral bypass windows (8) are designed to allow urine to flow in the case the main outlet (9) is obstructed by an incontinence pad.

Since the embedded flow rate sensor in the PUF housing is a fluid velocity sensor, the sensor aperture shown in Figure 23 had to have a constant aperture at a known location in order for the device to accurately measure flow rate at that location. Therefore, a urine channel of known circular cross-sectional shape was rapid-prototyped using a Form 2 3D printer (Formlabs, Somerville, MA, USA) – a resin based SLA 3D printer. Since the magnitude of fluid velocity changes radially in the urine channel, the location of the sensor filament had to be fixed radially at a given location. In order to provide a comfortable fit to different labial shapes, the funnel portion was over-molded onto the rigid channel with a flexible medical grade silicone elastomer

MED2-4220 (Nusil Technology LLC, Carpinteria, CA, USA). Several features shown in the Figure 23 were added after iterating on the design over a number of trials (see section 3.5.4).

3.2.2. PUF Sensor Housing Design Iterations

The final PUF housing design was developed mainly by analogic thinking [98] and morphological analytic [99] approaches. The original design of the housing (Figure 24) began with the punching of a hole through a commercial adult anti-incontinence patch made from foam and hydrogel adhesive called Finess® (Soft Health Technologies LLC, Aliso Viejo, CA, USA). (The patch was sold to be stuck over the urethral meatus by the user in order to completely block the passage of urine for a temporary period, as for example during a tennis match). Then a smaller version of the rapid prototyped funnel and housing shown earlier in the previous chapter was passed through the punched hole and integrated with the patch.

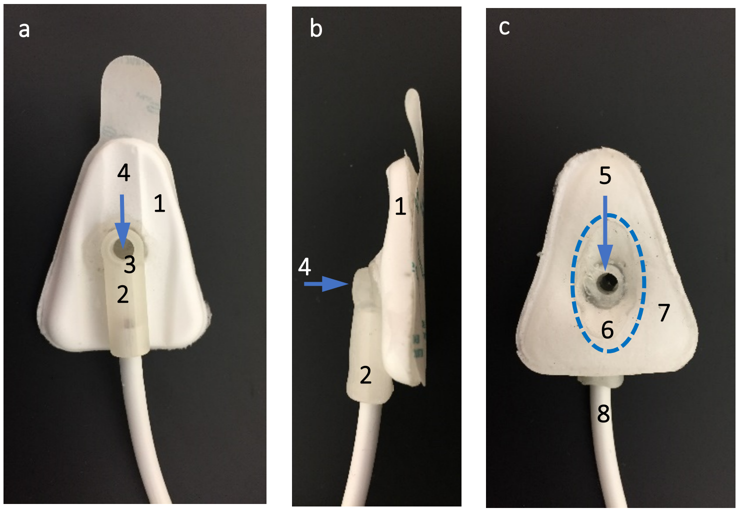

Figure 24. a) Distal, b) lateral and c) proximal views of the first PUF sensor housing design. 1) Flexible formed polymer foam sheet. 2) Rigid electronics housing for the sensor(s). 3) Flow sensor protruding to the urine channel. 4) Distal end of the urine channel. 5) Proximal end of the hole. 6) Silicone funnel attached to the rigid housing and passed through the hole (dashed ellipse). 7) Adhesive applied to the proximal surface to fasten to the labia surrounding the distal meatus. 8) Silicone cable.

Geometrical Shape

Early fit testing on female volunteers showed that the bulky patch was not comfortable for this application. Moreover, the hydrogel adhesive of the patch was not strong enough to resist the urine pressure rise inside the collecting funnel of the PUF so bypass leakage resulted. Eventually through multiple iterations, the urine channel was increased from 4 mm to 10 mm diameter and a flexible boat-shaped funnel was added, along with a rigid sensor aperture (Figure 25a). The sensor cable was originally passed posteriorly to the determining unit, but a design change was made to pass it anteriorly around the clitoris so that the user could freely defecate while wearing the device (also Figure 25a). These features helped to enhance the comfort level of the PUF.

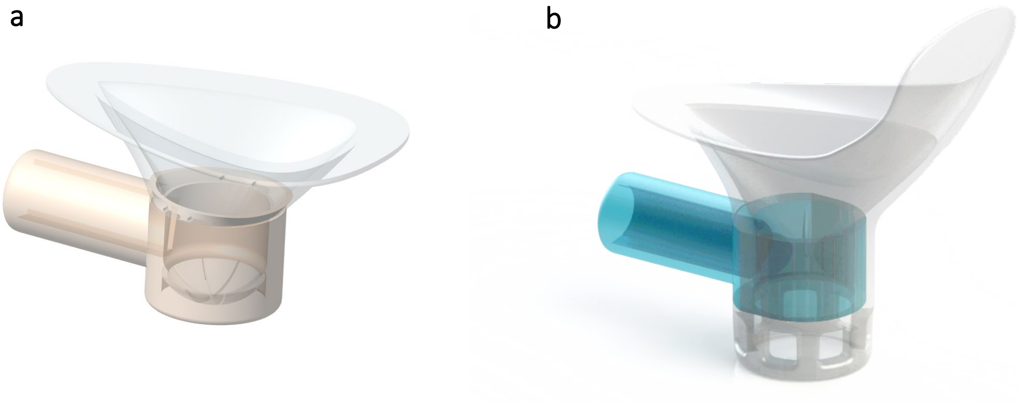

Figure 25. Two of the penultimate PUF housing designs that were tested before reaching the final version: (a) V14.4 with the flexible silicone boat-shaped funnel, and (b) V16.1 design with an added intra vaginal introitus flap and post-sensor side vents. The latter acted as a secondary pathway for urine to be discharged in case the main lower outlet was obstructed by the wearing of an incontinence pad.

A few subjects tried a different version of the PUF fitted with an extended vaginal flap (Figure 25b). The idea was to help thwart bypass leakage on the vaginal side by providing a better support. It proved, however, to be uncomfortable and was also not effective in sealing the urethral meatus on its posterior side mainly because the flap would twist inside the vagina during activities of daily living.

Hydrodynamic Improvements

Modifications to improve the urine hydrodynamics inside the channel included:

1) The addition of guide vanes
2) The addition of a flexible post-sensor buffer membrane
3) A change in the angle of attack of the sensor
4) The addition of the flange
5) The addition of side vents

The guide vanes were added to minimize the swirl of the urine as it passes over the sensor in order to reduce perturbations in the flow rate measurement.

A second important feature added through the development process was the addition of the post sensor ultra-flexible membrane to buffer the urine flow through the channel. Without this membrane, in low urine flow rates, only a portion of the urine channel would be filled and it would result in inaccurate flow rate measurements (note: recall that it is a velocity sensor). Therefore, this membrane ensured that the sensor aperture was always primed with urine in the low flow rate regime and it opens as the urine flow rate increased.

A third feature was the addition of side vents in the distal wall of the urine channel, post-sensor, in case an incontinence pad physically obstructed the main outlet of the housing. These vents help urine to escape the housing when the main caudal outlet is obstructed.

The fourth feature was the addition of the flange to the edge of the funnel in order to provide better support. In addition, an overlay adhesive sheet (e.g., wound dressing) was found to better help adhere the entire housing when fixing the PUF between the labia, due to a larger adhesive surface area. Through various iterations, the size of the flange was gradually increased to the maximum value that was comfortable for most women. The elliptical opening of the flange also was reduced close to the clitoris to form a boat shaped opening in order to provide a better comfort level, fit and seal.

Finally, it was proved that a small sensor attack angle was necessary in order to prevent fluid separation on the side of sensor die where the filaments are deposited (Figure 26). Otherwise, without this inclination angle the eddy currents that formed over the filament caused a reduction in the measured flow velocity value due to inconsistent values.

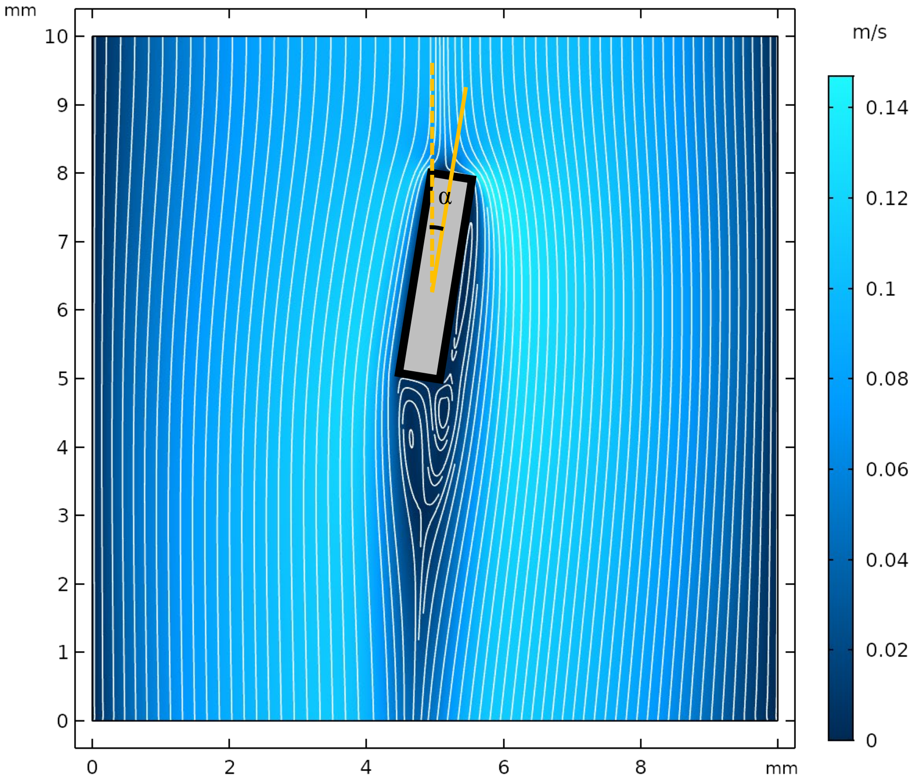

Figure 26. Introducing an attack angle (α) of the sensor relative to the direction of urine flow ensured that the left side of the sensor die, where the platinum filaments are deposited, does not experience the vorticity or eddy currents seen on the right side. This small inclination angle ensures that the flow separation always happens on the contralateral side. Results are from a computer simulation conducted using COMSOL Multiphysics®.

Materials and Fabrications Methods

A variety of different materials were experimented with in optimizing the PUF housing design. The goal was to achieve an optimal flexibility that makes the PUF comfortable to wear for subjects while still having enough elasticity to maintain its opening during different ADLs. For example, although 3D polyjet printers like J750 (Stratasys, Rehovot, Israel) can print a uniform object with multiple stiffness levels, the elasticity of the printed objects was not adequate and funnel and flange could lose their shape during ADL. On the other hand, although the elasticity of the housing printed completely in Flexible resin by Form 2 SLA printer (Formlabs, Somerville, MA) was good enough, some subjects could feel the semi-rigid edges (Figure 27).

The final housing design had a hybrid stiffness; a medical grade silicone MED2-4220 (Nusil Technology LLC, Carpinteria, CA) was used to mold the funnel portion on the rigid printed urine channel. The stiffness of the final funnel portion using that material would resemble auricular cartilage.

Figure 27. Examples of rapid prototyped PUF housings; the first PUF housing (V1) designed to be integrated with a modified incontinence patch. Blue and pink PUF housings in the upper left box were 3D printed from multiple stiffness materials in a single printing process. b) PUF housings (V9.x-V12.x) made from Flexible SLA resin (Formlabs®); the stiffness of the walls can be controlled by adjusting the thickness. PUF V14.x were made with 3D printed housings and soft over-molded biocompatible silicones. A dispersion silicone was used to cover typical printed parts to ensure biocompatibility.

PUF Attachment methods

A variety of different adhesives were used to try to attach and secure the PUF housing over the external urethral meatus. The mucosal skin surface between labia made this the attachment process challenging. While hydrogel adhesives were found initially to be effective on dry skin, they were ineffective once wet. Denture creams such as Fixodent (Procter & Gamble Cincinnati, OH, USA) were not effective in sealing the gap between the funnel flange and the mucosa either. However, hydrocolloid adhesive patches (e.g., McKesson, Irving, TX, USA) were found to be a reasonably effective medium for holding the housing to this mucosal region. Wound dressings such as IV3000 (Smith & Nephew®, London, United Kingdom) or Tegaderm (3M, Saint Paul, MN, USA) were also used successfully to cover the entire housing and further securing the housing to the body and help seal the attachment. The permeability of the wound dressings helped the labial skin stay dry longer.

Dry adhesive, replicated from [100], [101] through micro- and soft-lithography processes, unfortunately failed to provide a minimum level of required adhesion. Dry adhesives consist of an array of micro suction cups made from semi-soft silicone or PDMS material mimicking the suction organs of octopus tentacles (Figure 28).

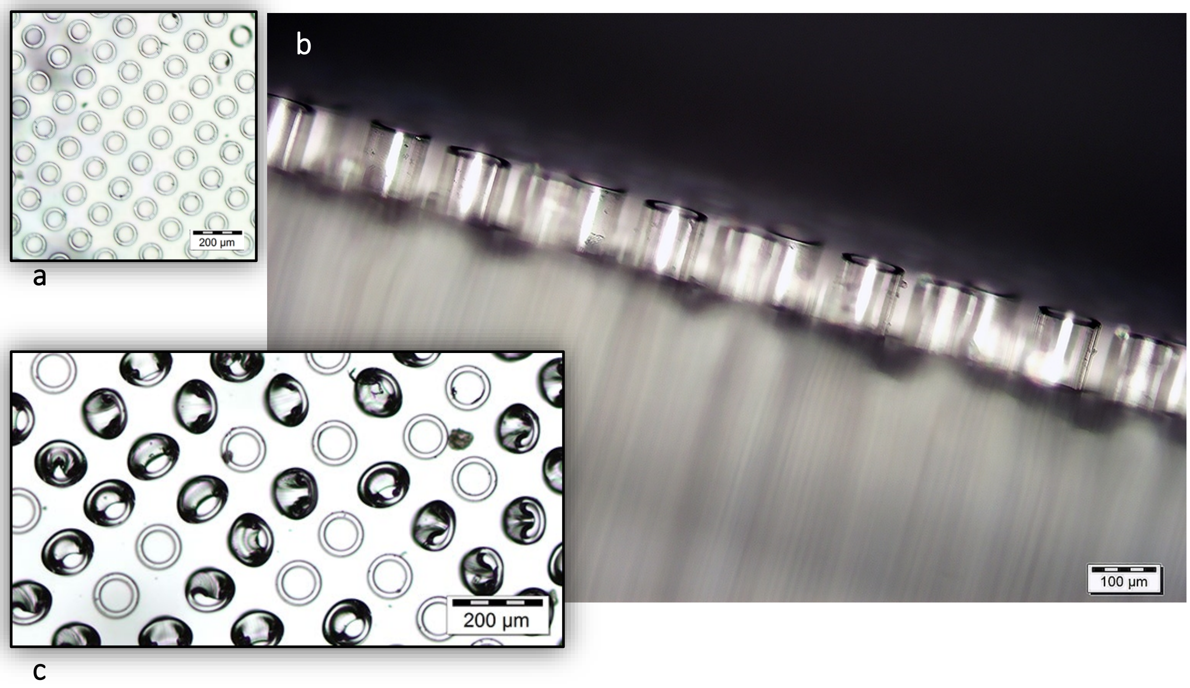

Figure 28. PDMS dry adhesive patches made by the soft-lithography processes at Lurie Nano Fabrication facility (University of Michigan, Ann Arbor, MI, USA). a) Top magnified view of a 1 mm x 1 mm dry adhesive patch. The dark uniform ring array is the top edges of the micro suction cups, b) 3D view of the dry adhesive patch magnified under microscope. c) Dry adhesive patch after being pressed against a flat surface. It did not provided the reported adhesion and after re-examining the patch, it revealed that most suction cups had collapsed into themselves.

Finally, biocompatible pressure-sensitive adhesives (e.g., MED-1356, Nusil, Carpinteria, CA, USA), used for male incontinence products, provided a reasonable attachment between individual PUF hydrocolloid and dressing patches, and could be easily removed at the end of the experiment.

3.2.1. Experiment Setup – Passive Housing

To test the comfort level, fit, and seal of the selected designs of the passive PUF housings, UM institutional review board approval was obtained (HUM00127026, an exemption). The human studies were carried out in one of the FemCare research facilities at a Procter & Gamble (Cincinnati, OH, USA) facility. This chapter reports the results from eight women who were recruited with a mean (± standard deviation) age of 50 (±24) years and BMI of 29.6 (±10) kg/m^2. All subjects signed a consent form before the study. Subjects were asked to drink two glasses of water and to not urinate two hours prior to their study visit. A registered nurse first placed the correct size PUF housing (if there were more than one associated with each design). Except for the first design (V1) which had a foam patch with a hydrogel adhesive on the back, some of the PUF housings were secured with a second layer of hydrocolloid adhesive layer because it provided better adhesion to the mucosal and wet surface. Finally, a thin wound dressing layer was also added for better support.

Each participant was asked to report on the comfort levels of the device in different postures, for example sitting, standing, lying etc., and during simple ADLs such as walking in place, walking to a commode, raising a leg, etc. Following the fit and comfort test, in a private room, subjects were then asked to sit on a commode setup and urinate into a container while wearing the device. One or two video cameras positioned under the subject simultaneously recorded the micturition to track any leakage or detachment of the housing from the body. After the micturition, the nurse examined the housing and its attachment to the body for possible leakage and then removed the PUF housing. Afterwards, the subject reported on the comfort level associated with each of these steps and any bypass leakage.

3.3. Methods (II) – Flowmetry Instrumentation

3.3.1. Low Power Flow Rate Sensor

The PUF flow rate and temperature sensor functions on the principle of hotwire anemometry, widely used in industrial applications. More specifically, it is a modified version of the flow rate sensor developed by Lin et al [102] and designed to measure a desired dynamic range from 1 droplet to 40 ml/s.

Hot-wire anemometers operate by sensing the convective heat transfer from a heated filament to the fluid over it. Normally, the power generated in the sensor filament (P) is dissipated in two ways: 1) convection to the fluid passing over the sensor (Q_f) and 2) conduction to the glass substrate of the sensor (Q_s). Q_f and Q_s are defined as:

$$Q_f = hA_s\Delta T$$ Equation 24

$$Q_s = \frac{\Delta T}{R_s}$$ Equation 25

in which h is the heat transfer coefficient, A_s is the area of the sensor filament and R_s is the "thermal" resistance of the substrate. ΔT is the temperature difference between the filament and fluid passing over the filament of the sensors. ΔT can be obtained by rearranging the above equations:

$$\Delta T = \frac{P}{\frac{1}{R_s} + hA_s}$$ Equation 26

In order to measure fluid flow rate, convection flux must dominate the conduction flux, i.e., $Q_f \gg Q_s$ [103]. Therefore the R_s must be high enough to reduce the conduction heat flux to the substrate. This was achieved through three steps: 1) choosing glass as the sensor substrate with a high thermal resistance, 2) reducing the filament area, and 3) reducing substrate thickness. Therefore, with a constant power provided by the filament, given that h is dependent on the fluid velocity, ΔT would be a direct measure of the fluid velocity. Since h also depends on the fluid temperature, knowledge of the fluid temperature is also required. Lin [104] has shown that the sensitivity of the flow rate sensor depends on the input power, and as the input power was reduced below a certain threshold, the filament is only sensitive to temperature and not the flow rate. Therefore, a second filament can be used to measure the fluid temperature and correct the fluid flow rate values.

3.3.2. Micro-fabrication of the PUF Sensor

Flow and temperature filaments of the PUF sensors (Figure 30) were deposited on 1 mm thick glass wafer with 300/1000 Å thick titanium/platinum using physical vapor deposition (PVD) technology in the Lurie Nanofabrication Facility (University of Michigan, Ann Arbor, MI, USA). The titanium layer works as a medium bonding the platinum filaments over the glass substrate. The filaments were covered by 1 μm and 40 nm silicone dioxide and nitride films, respectively, using a plasma-enhanced chemical vapor deposition technique (PEVCD), leaving only the terminals exposed for the wirebonding process.

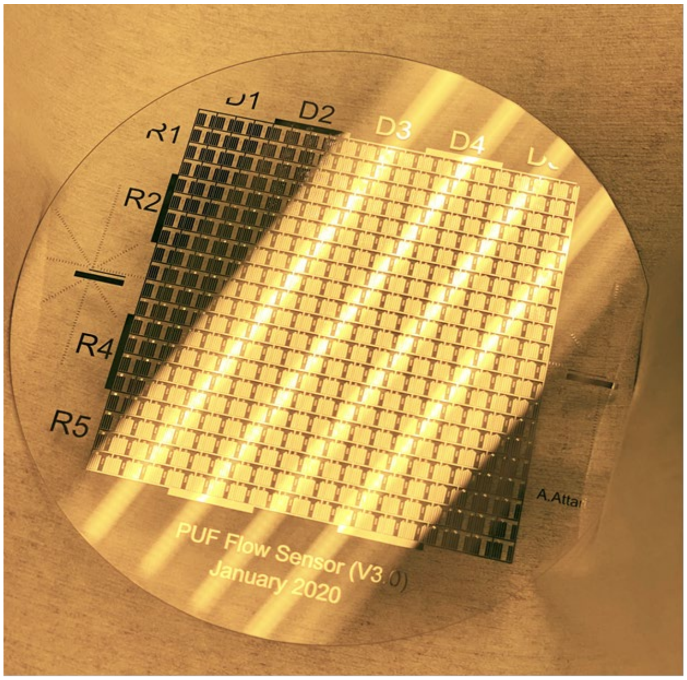

Figure 29. A 4” glass wafer (600 μm thick) with platinum- and titanium-deposited filament form the 400 PUF sensors before getting diced into individual 3 mm x 3 mm dies.

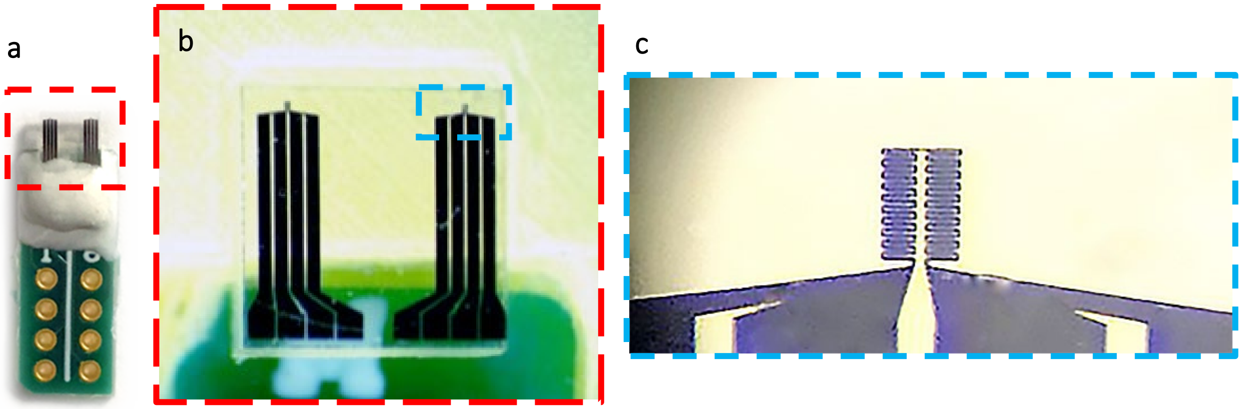

Figure 30. Example of a flow rate and temperature sensor die used in the PUF device. a) sensor die mounted on a PCB with encapsulation over the wirebondings, b) sensor die (without wirebonding and encapsulation), and c) magnified image of one of the anemometry filaments deposited on a 3 mm x 3 mm glass substrate.

3.3.3. Hotwire Anemometry Modes of Operation

The sensor circuitry can be implemented in two ways: 1) constant temperature anemometry (CTA) in which the temperature of the filament is kept constant by a feedback loop, and 2) constant current anemometry (CCA) in which a constant current is fed through the filament, and the resistance of the filament represents the speed of the fluid flow. Therefore, by measuring the voltage variations one can find the speed of the fluid flow or its temperature (depending on the current level) [105].

Although tuning hotwire filaments operating in the CCA mode is more difficult, it provides a higher bandwidth compared to the CTA mode [106]. In addition, keeping the filament excited in the CTA mode in a stable fashion in this application, where two different phases, air and urine, pass over the sensor is nearly impossible. Therefore, the CCA mode of operation was adopted.

3.3.4. PUF Instrumentation Circuitry

The circuitry inside the PUF determining unit consisted of five main sections: 1) power regulation and constant current sources, 2) amplifier section, 3) micro-controller, 4) inertial measurement unit, and 5) SD memory or Bluetooth transceiver unit. The microcontroller unit controlled individual attributes of the amplifier section, such as the gain and baseline, digitally using the I^2C protocol. The IMU components also communicated with the microcontroller using the same protocol.

Constant current sources were key components of the circuitry. Two current levels of 5 mA and 500 µA were dedicated for the flow rate and temperature filaments, respectively. The design of both filaments on each sensor die was identical, and both filaments were linearly sensitive to the temperature of the fluid passing over the sensor. However, the temperature-sensing filament using the lower current level was not sensitive to the fluid velocity (see section 3.3.1). Therefore, after calibrating the flow rate filament at different temperatures, the system could accurately report the temperature and flow rate of the fluid passing over the sensor. The circuit schematic of the latest tested determining unit is provided in Appendix II.

3.3.5. PUF Calibration Setup

In order to calibrate the PUF sensors, a two-gallon, temperature-controlled, water bath (PolyScience, Niles, IL, USA) was used. A centrifugal pump was submerged and secured in the water bath to pump heated water through a thermally-insulated tubing to a fixture rigidly holding the PUF sensor housing (Figure 31). The outlet of the PUF housing was located above a large beaker placed on a precision scale (Sartorius ENTRIS6202-1S, Göttingen, Germany). The resolution of the scale was 0.01 gram and it was connected to a computer to continuously record the instantaneous weight of the beaker filling with water. The data acquisition program on the computer differentiated the weight data to calculate the instantaneous flow rate. Simultaneously, it also captured the PUF sensor flow rate and temperature signals at 25 Hz. It was assumed that the density of the water passing through the system was constant. Distilled water was used in the calibration setup, and 40 droplets of algaecide solution (PolyScience, IL, Nile, USA) were added to avoid formation of algae. The average urine density of 1.02 gr/ml [89] was used for the mass-volume conversions. Finally, a third order, low pass, zero-phase digital filter was applied with cut-off frequency of 1.8 Hz.

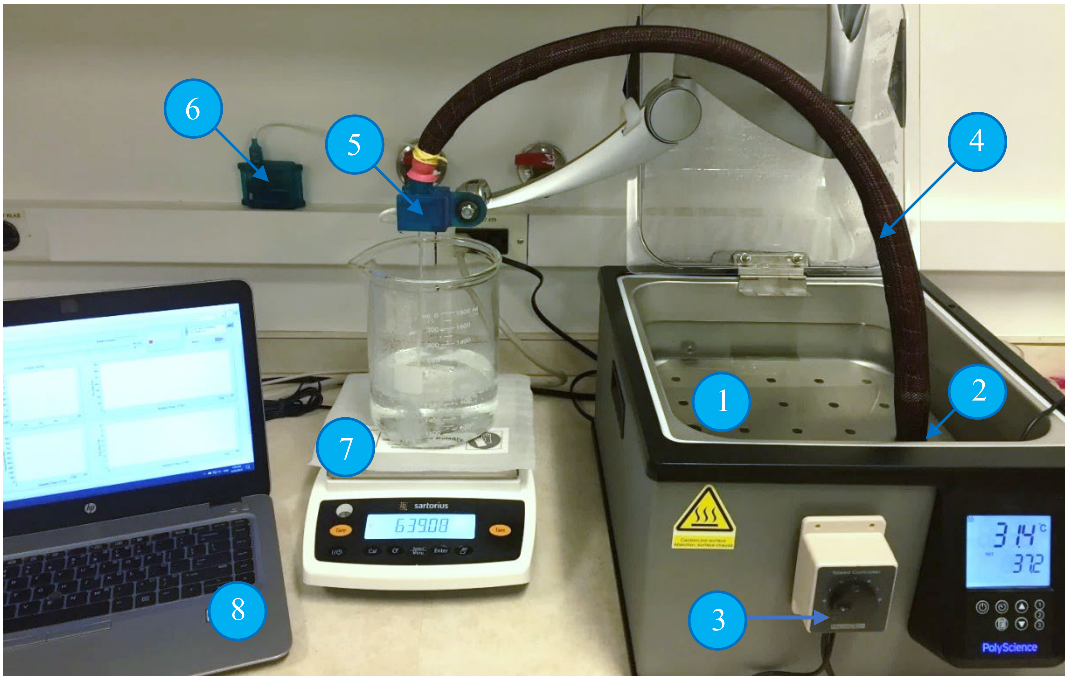

Figure 31. The PUF flow and temperature calibration setup: 1) temperature controlled water bath, 2) submerged centrifugal pump, 3) pump speed controller (PWM generator), 4) heat insulated tubing, 5) PUF sensor holder, 6) wireless determining unit, 7) precision scale as a gold standard reference flowmeter device, and 8) PC simultaneously recording the signals from determining unit and the precision scale.

To calibrate each sensor accurately, the tubing was first primed. This was a critical step to prevent trapped air bubbles passing though the sensor aperture during the calibration process and introducing inaccuracies into the calibration. To prime the tubing, the pump speed and therefore pressure was increased above a certain limit and then carefully reduced to about 25 cmH_2O over atmospheric pressure to keep the tubing primed and ensure that air would not flow back to the tubing from the sensor outlet.

After the priming step, the flow rate was increased from 0 ml/s to 40 ml/s in 2-6 ml/s increments. The sensor sensitivity was higher at lower flow rates, therefore smaller increments were used to calibrate sensor at low flow rates. Finally, pump speed was reduced to the minimum possible speed, passing just a few droplets per second. All PUF and scale data were recorded continuously throughout the session.

In calibrating each sensor, it was important to record sensor output voltage in the three different phases: 1) before priming the housing (with water), 2) after priming when housing was filled with water, but there was no water flow, and 3) when water flow rate was incremented. Each of these three phases had distinct voltage levels due to different heat fluxes, i.e., conduction heat transfer to the air, conduction heat transfer to the water and convection heat transfer to the water respectively. When testing the PUF sensor on human subjects, these voltage thresholds revealed when urine droplets leaked, were trapped or escaped from the housing during different ADL. This calibration process was repeated from two degrees below the body temperature to two degrees above it. Outputs of temperature and flow rate filaments of the PUF sensor were then used together to form a calibration function or model, so that the PUF could correctly report flowmetry and leakage data.

3.4. Methods (III) - Activity Recognition

As mentioned in the Chapter 1 knowledge gaps, existing uroflowmeters are stationary and therefore incapable of measuring activity-associated leakage data. To address this shortcoming, the PUF incorporated a 3-axis accelerometer and magnetometer FXOS8700 and a

3-axis gyroscope FXAS21002 (both from NXP, Eindhoven, Netherlands) to form a 9 degrees of freedom (9DoF) inertial measurement unit (IMU) to record subjects' body posture and movement simultaneously with the leakage and flowmetry data. These sensors were mounted in the determining unit worn on the waist. They provided data to the microcontroller via the I^2C protocol at a 40 Hz sampling rate. The accelerometer signals were filtered using a 10th order Butterworth lowpass filter with a corner frequency of 8 Hz during the post processing.

Different machine learning techniques have been proposed to identify the physical activity of a person from wearable data. One method has been to extract features from 9 DoF IMU signals during different ADLs and compare them with the existing classified patterns (e.g., sitting, standing, walking, etc.). However, a fully trained model was required to classify each individual wearer. Since this was a feasibility study and the number of subjects were limited, forming a comprehensive training data set was not possible. As a result, an alternative method of interpreting several data sets and extracting the key features was adopted.

Therefore, at the phase of testing of the comfort and fit of the PUF housing, subjects were also asked to wear the determining unit on their waist and perform certain ADLs including standing, sitting, lying , walking, jogging on a treadmill, and lifting a two 1 gallon containers of water. The IMU signals from these postures and activities were then collected from the determining unit, filtered, and post-processed to obtain secondary key information unique to each type of activity. This information was used to identify activity of the subjects in the subsequent flowmetry experiments. Although many factors including age and BMI can affect the range of motion and body accelerations, the overall scheme of each activity was consistent. This method has also been adopted recently to simplify the machine learning process [107].

3.5. Results

3.5.1. Comfort, Fit and Seal

In general, subjects reported little to no discomfort while wearing the latest PUF housing designs. Table 3 shows the mean reported comfort level associated with wearing the passive PUF housing for each posture or activity in the selected designs.

Table 3. Overall comfort levels of the PUF housing in three different designs (V1, V9.x and V10.x) reported. The comfort level is on a scale from 0 to 10, with 0 representing unbearable and 10 being the totally comfortable.

	PUF Housing Version *(see Figure 27)*		
Activity / Posture	V1 (N=8)	V9.x (N=5)	V10.x (N=4)
Lying on the exam table	8.6	8.2	9.5
Moving and rotating leg in all directions	9.1	9.0	9.5
Sitting on the exam table	7.9	7.8	8.3
Standing feet together	8.8	9.2	9.5
Standing feet apart	9.1	10.0	9.8
Standing on one leg and lifting other knee	9.1	9.8	9.8
Walking in place	8.8	9.2	9.0
Walking to commode	8.6	8.6	8.3
PUF removal	9.4	8.2	9.0
Mean comfort level	**8.8**	**8.9**	**9.2**

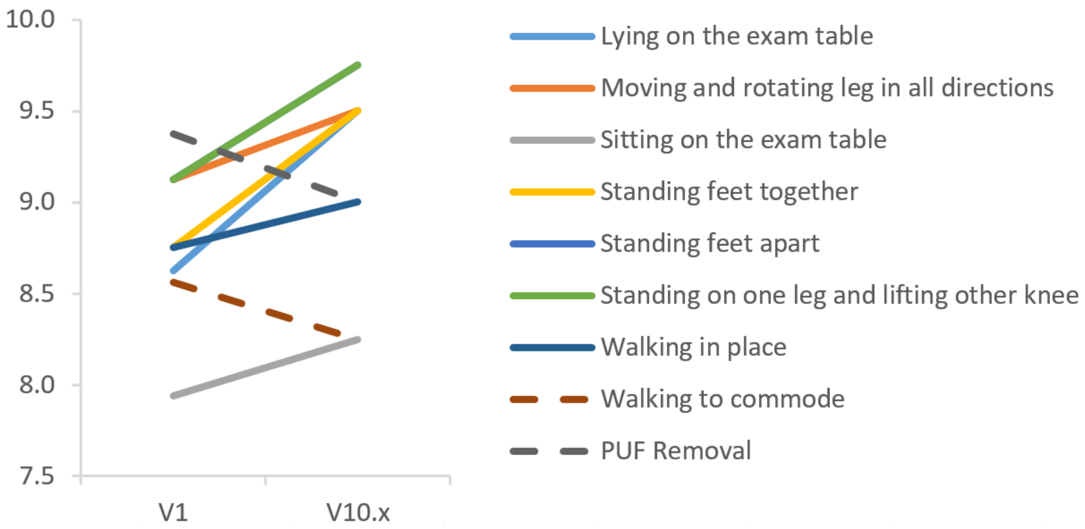

Figure 32. Improvement in the comfort levels of the PUF housing, from design V1 to V10.x. The scale is from 0 to 10 with 0 being "very uncomfortable" and 10 "very comfortable". Comfort level in every activity and posture improved except "walking to the commode" and "PUF removal" (dashed); both are mainly due to the wide elliptic funnel opening or the semi rigid edges of the rapid prototyped funnel, which would have stretched and irritated the mucosal inner surface of the labia. These issues were addressed in designs V14 and above by replacing the funnel material with a medical grade soft silicone and adopting a new boat-shaped funnel opening.

With normalized ratings, there was a 34% enhancement in the reported comfort levels from design V1 to V10.x. Overall, sitting on a chair was found to be the least comfortable posture. A few subjects in the follow up studies wearing the instrumented housings (V14) reported that sitting, while driving a car, was associated with the highest discomfort level. However, all subjects believed they could wear the device for at least three hours (see Table 4). Subject also reported minimal to no resistance during micturition while wearing the device. Overall, five performance indices were defined to summarize each factor contributing to the overall desirability of each design.

Table 4. Improvement in usability and performance indices defined for each housing design.

	PUF Housing Version *(see Figure 27)*		
Performance indices	**V1**	**V9.x**	**V10.x**
Comfortable to wear for 3 hours	80%	80%	100%
Comfortable micturition	40%	80%	100%
Normal micturition length	30%	60%	75%
Maintained attachment	90%	100%	100%
Felt no leakage	90%	100%	100%
Overall performance index	**66%**	**84%**	**95%**

Figure 33. A visual representation of performance indices associated with the selected PUF designs (see Figure 27). A larger polygon area represents a more desirable design.

3.5.2. Flow Rate Sensor

Figure 34 shows amplified voltage output of the flow sensor and the actual flow rate measured by the reference precision scale recorded in an example calibration process. The flow rate sensor could measure up to a 40 ml/s flow rate and distinguish a minimum flow rate of a single droplet (once the channel was primed). With the stated filter settings (3.3.5), the signal-to-noise ratio was found to be 20 dB, and it was found that the noise level increased with the actual flow rate especially after 15 ml/s.

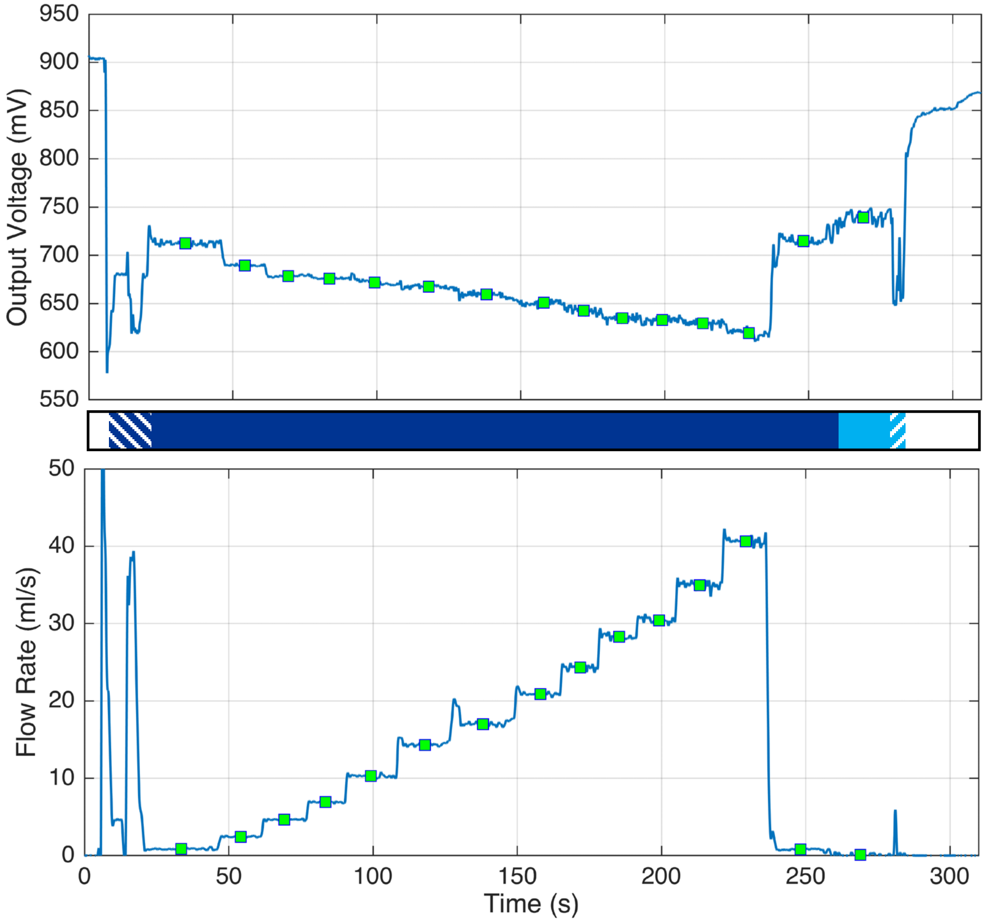

Figure 34. a) The PUF amplified and recorded the voltage output of the fluid sensor during a calibration process at 37˚C, b) Simultaneously, the precision scale recorded fluid flow rate passed through the sensor aperture and collected by the beaker that was on the precision scale. The green squares on both plots show the average measurement in each flowrate increment. The color bar shows individual phases during the calibration: when the housing is free from liquid (white), when the fluid is flowing through the aperture (dark blue), when the aperture is filled with fluid but there is no flow (light blue). The hashed areas show the transition with the left being the priming duration, and the right showing the tubing depletion.

The sensor calibration curve for the example shown was obtained as shown in Figure 35. The root mean square error (RMSE) of the fit found was 1.1 ml/s and the resolution of the measurement system was 0.05 ml or one droplet.

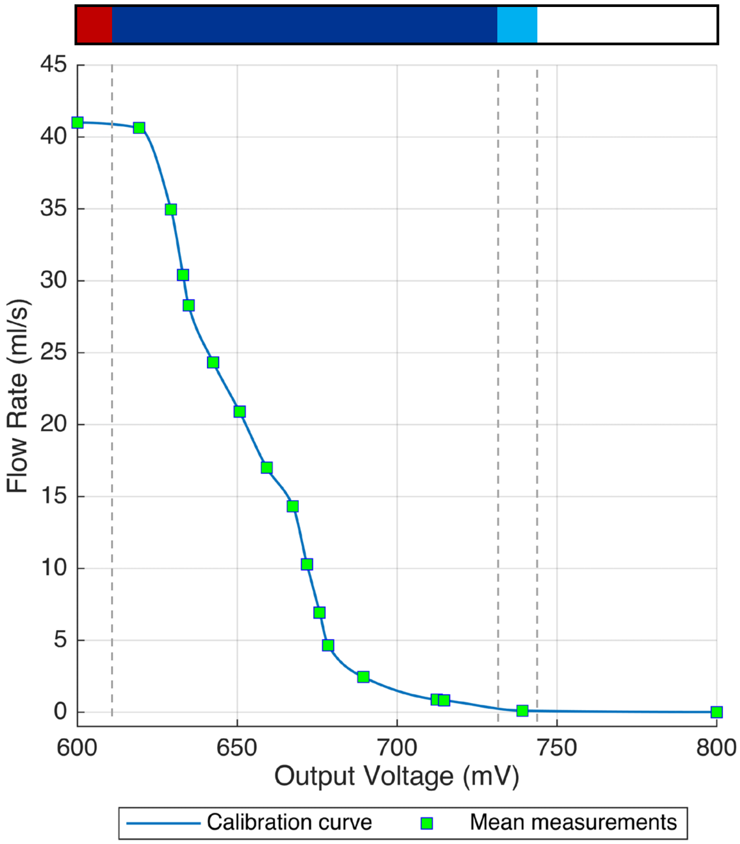

Figure 35. Sample calibration curve prepared to fit the amplified output voltage of the flow rate sensor to the measured (reference) flow rate in the calibration set up. The dark blue horizontal bar represents when the fluid passes through the sensor aperture. The PUF sensor can also detect urine presence in the fluid aperture even if there was no fluid flow (light blue bar). When the channel was depleted of fluid so no fluid passed over the sensor, the output voltage was higher than specific threshold (white bar). Above a threshold flow rate, the sensor saturates and the output voltage cannot reduce any further (red bar).

The voltage output of the sensor would then be saturated after a certain flow rate and the temperature of the sensor filament cannot reduce any further (V < 610 mV in Figure 35). Finally, the output voltage of the flow rate sensor became linearly dependent on the fluid temperature and corroborated findings of Lin et al. [102].

Figure 36 shows the transient response of the flow rate sensor of the PUF. The time constant (τ) was found to be about 200 ms.

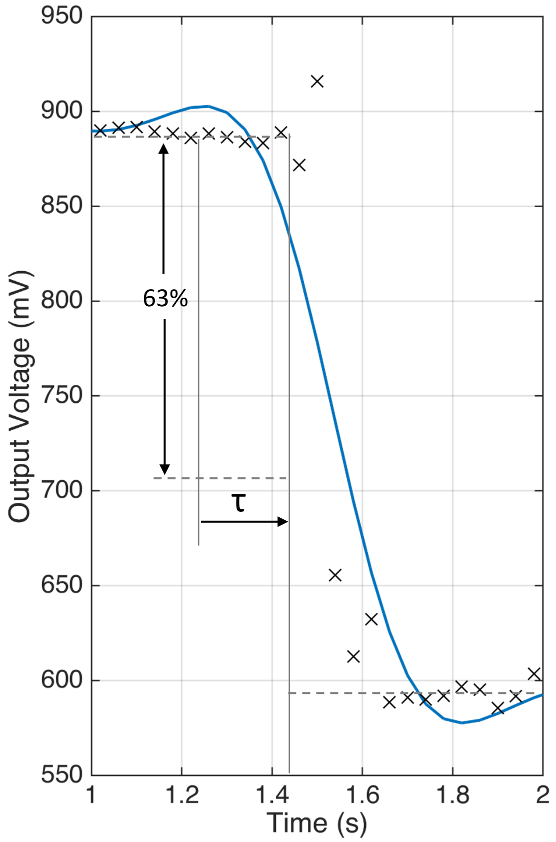

Figure 36. Transient response of the flow rate sensor to a step change. The time constant (τ = 200 ms) of the flow rate sensor (with a filament resistance of 600 Ω) measured by the transition time between the baseline and 63% of the final value.

3.5.3. ADL Activity recognition

Postures

Accelerations along each axis were the most helpful components among the other IMU signals for identifying the posture and the activity type. The projection of the gravity vector on each axis was mainly used to identify the posture. Figure 37 shows an example of results from one subject sitting on a mattress and then lying on her sides and back.

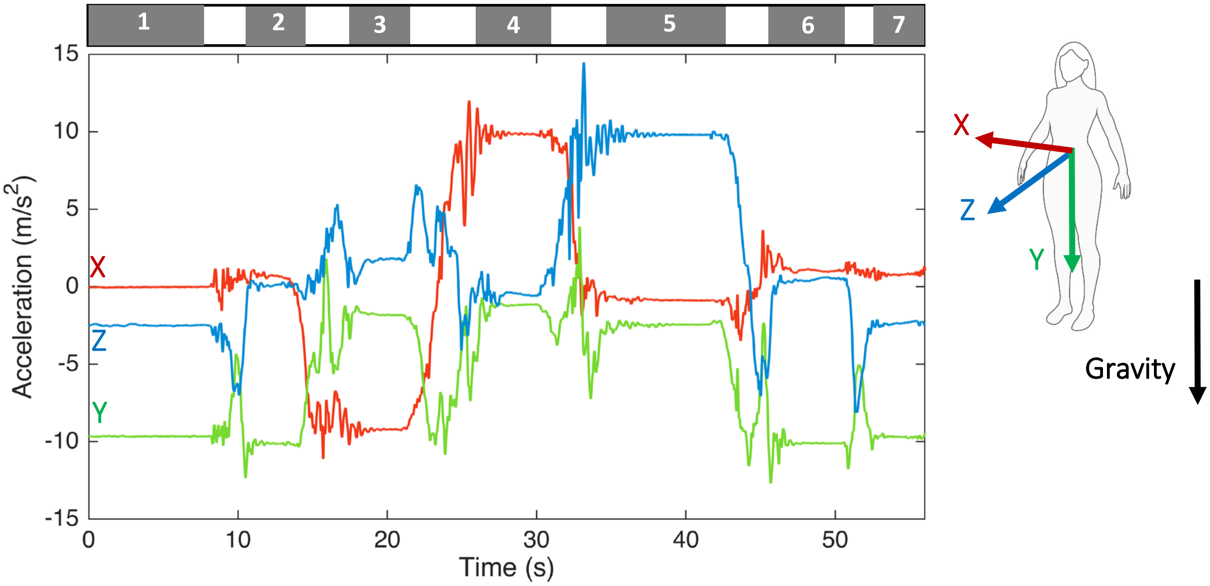

Figure 37. Acceleration components of the IMU signals when a subject wore the determining unit over her sacrum and changed her posture. Projection of the downward gravity vector on each axis is different depending on the posture. Top bar shows the measurement phases of standing (1), sitting on a mattress (2), lying to the right side (3), left side (4), back (5), sitting again (6), and standing again (7). The axes orientations are depicted with respect to the subject. “X” axis points the right side (red), “Y” axis points downward (green), and “Z” forward with respect to the subject.

While standing in place, there was no significant fluctuation in body acceleration and rotations and the effect of the gravity vector appeared as negative acceleration primarily on the "Y" axis (Figure 37-1) and a negative component on the “Z” axis due to minor rotation of the determining around the lateral axis “X” when mounted on the waist. When sitting, the lower back rotated sagittally (around the lateral axis “X”) and therefore a projection of the gravity vector appeared as a positive component on the longitudinal axis “Z” (Figure 37-2). This minor tilt angle does not necessarily exists in all subjects and depends on the general sitting posture of the subject, where exactly the determining unit was mounted on the waist, whether the subject was reclining in the seat, etc. Therefore, distinguishing sitting and standing postures without checking the activity transitions is sometimes impossible.

When the subject lay on her right and left side, the magnitude of the gravity vector appeared along lateral direction ("X" axis) in the negative and positive directions respectively (Figure 37-3 and 4). Similarly, when the subject lay on her back, gravity acted mainly along the "Z" axis (Figure 37-5).

One of the activities that caused leakage in one of the subjects was bending in order to lift a heavy object due to a presumed increase in intraabdominal pressure. Therefore knowing when a subject was bending was important. Similar to the case where subjects sat and lay on a mattress, changes in the orientation of the body changed the acceleration components of the acceleration between vertical and longitudinal directions (Figure 38), i.e., one increases and the other decreases, and vice versa. Therefore for any given time window, the mean of each acceleration signal was a characteristic feature of the associated posture or activity during that time window.

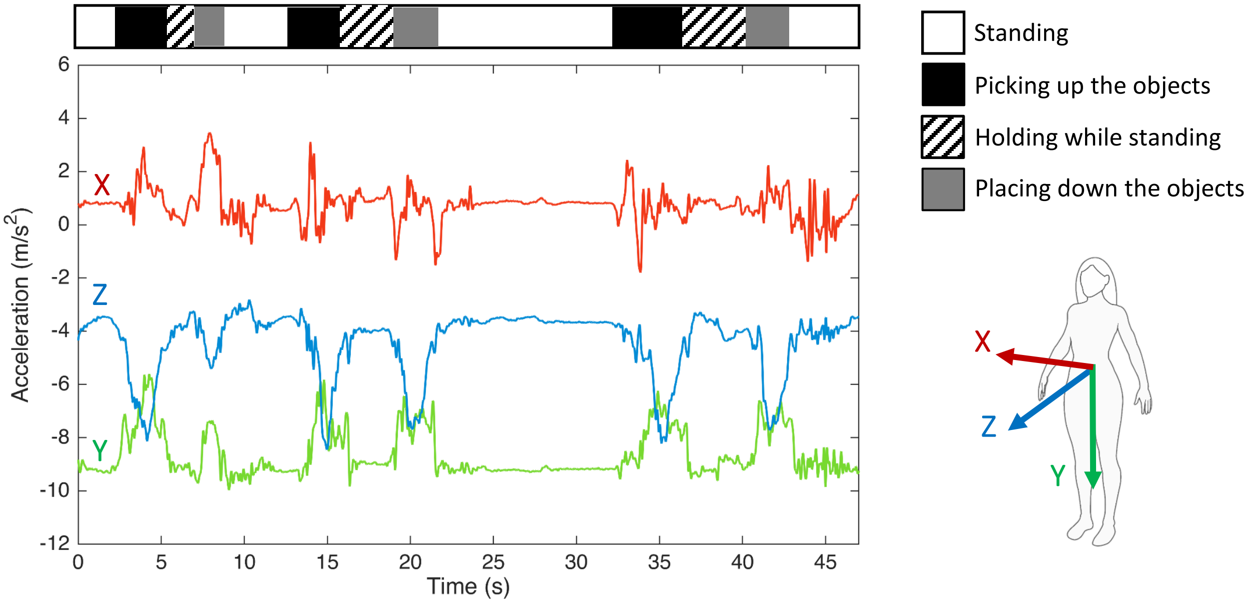

Figure 38. Acceleration signals when a subject bent over to lift two gallons of water (one in each hand), held them for 2-3 seconds, bent over again to place them back on the ground and repeated this process twice afterwards. Acceleration peaks in the lateral direction show that the subject had bent asymmetrically in the coronal plane when picking up and placing down the weights.

Physical Activities

In contrast to the body postures, physical activities such as walking and running were identified mainly by the periodic oscillation of the vertical and longitudinal accelerations. Key information in distinguishing different activity was the frequency of the dominant frequency in the power spectral density plots. For example, as shown in the Figure 39, the dominant frequency of the vertical acceleration of the determining unit worn by a subject who was running on a treadmill was 2.1 Hz. whereas her walking pace resulted in a lower dominant frequency of 1.3 Hz. Similar to the posture identification, other signals of the IMU also changed and oscillated in along with the vertical acceleration.

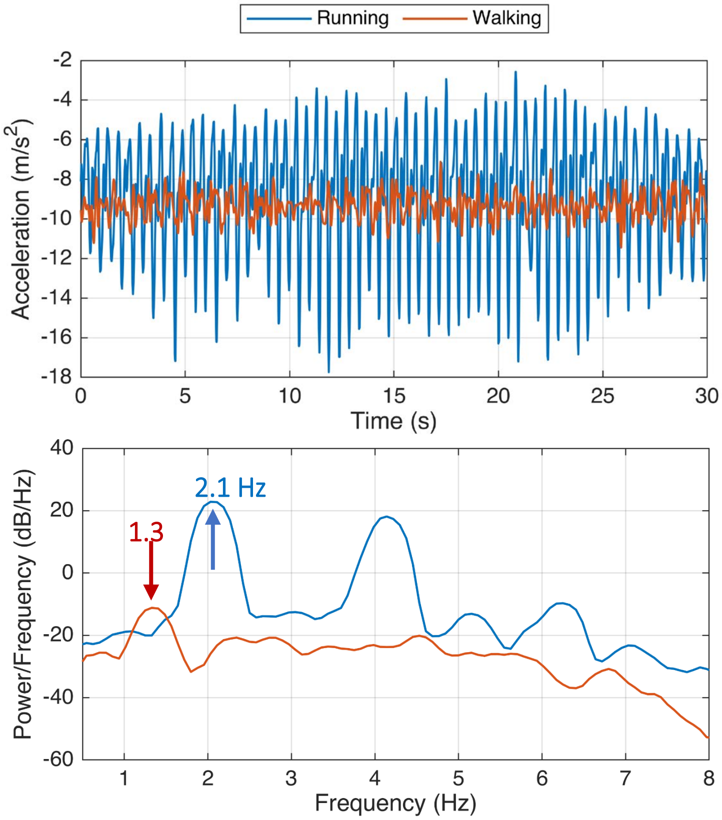

Figure 39. Comparison of the vertical acceleration of a subject in a 30-second run and walk (top). The power spectral density (PSD) revealed the dominant frequency of running (2.1 Hz) being higher than that of walking (1.3 Hz) (bottom). One way to differentiate between the two activities was using the PSD to compare dominate frequencies.

Overall, other characteristic features could be extracted from the power spectral density to identify the type of the physical activity, if needed.

Finally, the sensitivity of the IMU was sufficient to capture coughs, however, the amplitude was low and they may not be able to distinguish whether the subject was also performing other activities such as running.

3.5.4. Summary of PUF Design Iterations

Table 5 summarizes the important features associated with key designs.

Table 5. Summary of features of each PUF housing design.

Category Version	**Key features**	**Urine Channel Diameter (mm)**	**Key results**
V1	Foam patch with hydrogel adhesive with punched hole to pass through a housing	4	Foam patch deformed labia, impeded micturition
V6-V7	Modified funnel dimensions, Improved urine channel to funnel silicone attachment. Increased urine channel diameter	4-6	Improved connection from rigid body of the housing to the flexible funnel
V8	Hybrid stiffness, V1 geometry 3D printed in a single printing process (with Stratasys® J750)	6	Difficult wax cleaning process in the fabrication, weak soft-rigid interface at the funnel neck
V8.2	Uniform structure with Flexible SLA resin (Formlabs®) to use with wound dressing (Tegaderm®).	6	Small funnel could not provide a good attachment to the adhesive patch
V9.x	Uniform structure, larger elliptical funnel (3 different sizes) Flange added to provide a better support for the attachment	6-7	Base design was approved for the first instrumented test, minor leakage around the vaginal opening
V10.x	Added vaginal flap with different shapes (with and without flange)	7	Vaginal flap was not effective in sealing the bypass leakage close to the vaginal opening.
V11	Upgraded V9 by refining dimensions	7	The first successful benchtop instrumented test, minor back pressure in high flow rates
V11.2	Outlet buffer membrane uniformly was printed at the end of the outlet	7	Outlet membrane was too stiff to be opened by the fluid stream, not tested on subjects

V12	Used in the first instrumented PUF testing session	7.5	Lack of post sensor buffer membrane resulted in inaccuracies due to empty channel
V12.1-2	Added pre and post sensor mesh	7.5	Too much resistance against urine flow in benchtop test from the mesh
V12.3	Added guide veins in the “funnel”	7.5	Veins were close to the urethral meatus and could cause discomfort
V12.4-7	Added pre and post sensor hair like structure to condition the flow type	7.5	Features were ineffective and had high resistance against flow
V12.8	Dual part design to add a custom intermediate nylon membrane in between	7.5	Hard to control the fabrication quality and consistency, ineffective membrane function
V13.1	Used in the second instrumented PUF testing session, with different flexible membrane shapes inside and outside the urine channel,	7.5	Post sensor buffer membrane impeded the normal micturition process, housing detachment in 70% of the micturition episodes, 82% accuracy in quantifying leakage volumes in 3 subjects
V13.2	Used in the third testing session (the first 4-hour long test outside the facility), added external and internal silicone flexible post sensor membrane, rigid biocompatible housing material (Formlabs® Dental SG Resin), included sensor attack angle	9	Elliptical flange caused skin marks close to the clitoris of one subject, cable direction impeded the defecation process, temperature of the determining unit worn under the clothing increased and drifted the calibration.
V14.x (**V14.4** tested in subjects)	Used in the fourth testing session, Molded Nusil® MED2-4220 boat shape funnel over a rigid housing 3D-printd from biocompatible resin, increased urine channel diameter, flipped the cable direction to pass anteriorly around the clitoris to the determining unit worn on the lateral aspect of the iliac crest, determining units were calibrated in the elevated temperatures	9	Most comfortable funnel design. 2/3 subjects did not feel the existence of the housing. Could perform 4 hours of ADL. Incontinence pad blocked the housing outlet and trapped urine inside the housing, could measure leakage incidents but not accurate flow rate qualification. All new determining unit insensitive to the temperature change was required.
V15.1-8 V16.1-6	Trimmed vaginal flap to better fit patients with pelvic organ prolapse, flap edges fused to funnel flange with a single profile, added post sensor windows on the urine channel wall to bypass trapped urine, different softness and materials were tested to refine the final comfort and built quality, denture cream (Fixodent®) was applied, pressure sensitive adhesive (PSA) was used	9	The vaginal flap was uncomfortable, bypass leakage due to poor adhesion of the biocompatible silicone coating of the housing to the dressing sheet or the hydrocolloid patch, Fixodent® was not effective in sealing, PSA provided a good laminating layer between the adhesive patch, dressing and PUF housing

V17	**Incorporated successful features**: boat shape silicone funnel, post membrane flexible membrane, cable direction not impeding the defecation, mixed use of hydrocolloid, PSA and wound dressing, sensor with an attack angle, new micro fabricated flow rate sensor, enhanced determining unit insensitive to the temperature variations.	10	To be tested (future suggested design)

3.6. Discussion

In this chapter, three existing knowledge gaps were addressed. First, a wearable personal uroflowmeter (PUF) device was designed and fabricated so its sensor housing comfortably fit over the urethral meatus and between the labia. Second, the PUF flow rate sensor could measure flow rates from a single droplet to 40 ml/s with an acceptable 20 db signal-to-noise ratio. Third, PUF was able to measure the posture and activity of the wearer simultaneously with the flow rate measurements.

The major strength of this uroflowmeter compared to the standard clinical uroflowmeters was its capability of being worn while also measuring changes in body postures and movements associated with the leakage of the wearer. These are the first measurements of actual activities related to the leakages of patients not involving a leakage diary or wearing pads which are weighed afterwards. There are other instrumented pads to measure when urine leaks [108] and roughly estimate the leakage amount. The PUF is distinctly different from other wetness sensors in the way that it measures the instantaneous flow rate and total urine leakage volume.

The design of the PUF sensor housing evolved through several iterations designed to improve its comfort level, durability of attachment to the body and flowmetry accuracy. In the initial design, a hole was punched in an anti-incontinence foam Finesse^{TM} patch to secure the rigid housing over the urethral meatus. This foam patch was designed to block leakage in stress incontinent women by obstructing the urethral meatus but also deforming labial anatomy. The deformation in labial anatomy also added resistance to the urine flow during micturition. In addition, while subjects could not feel significant bypass leakage with this design, urine was in fact getting absorbed due to the open cell structure of the foam. So instead, the idea of using a funnel to guide the urine from the external urethral meatus in order to facilitate the full urine flow during micturition was developed.

The funnel attachment to the body was also improved over several design iterations. It was found that, unfortunately, the hydrogel adhesives were not strong enough to hold the entire weight of the sensor housing and the cable assembly against the body in the ADLs. Fabricated dry adhesives and over the counter denture creams were also found to be ineffective in adhering the housing on the mucosal interlabial surfaces. The combination of a hydrocolloid adhesive (as a base layer), along with an intermediate layer of pressure sensitive silicone adhesive (to attach the housing to the hydrocolloid base layer), provided the best adhesion level among other solutions. A third layer of a permeable wound dressing also secured the housing assembly while allowing skin moisture to pass through.

The diameter of the urine channel was initially designed to match the nominal urethral diameter i.e., 4 mm. Through iterations, though, it was increased to 8 mm and further to 1 cm when the post sensor buffer membrane was included. Resistance to the high flow rates during micturition was higher in the design versions with the flexible post-sensor buffer membrane, nevertheless, subjects reported no pain and discomfort in this regard. In addition, the increase in the diameter of the urine channel restored the reported comfort levels during urination. In later experiments (with V14), two out of the three subjects did not even notice the device between their labia.

Another modification was the 180° rotation of the cable connection to the determining unit so as to pass anteriorly around the clitoris instead of passing posteriorly across the vaginal introitus and anus. This allowed subjects to defecate if they needed to when wearing the PUF for extended periods of 3 - 4 hours. Similarly, a determining unit placed on the sacrum was reported as being uncomfortable when subjects leaned against a seat back, so it was moved to the lateral iliac crest. It was found to be important biomechanically to secure the determining unit properly over a relatively rigid boney location on the body, like the iliac crest, in order to correctly measure the overall body movements rather than soft tissue vibration, which caused measurement artefacts [109].

There were several other limitations associated with the PUF device. The most important perhaps was the adhesion of the PUF housing to the moist and sensitive mucosal surfaces between the labia. The average attachment duration could last up to 2.5 hours without bypass leakage, and could be improved to reach the 4 hours ideally. It was found, however, that the present attachment method was ineffective on a subject with pelvic organ prolapse.

Another limitation was that the wearer could not install the PUF by herself; otherwise, the urine channel may not be placed accurately over the meatus and that would create resistance against flow during micturition. In addition, the resulting backpressure would cause the PUF to detach the housing from the body.

Sensitivity, dynamic range and more importantly the sensor life were also marginally acceptable in the current setting. For a robust application, all those factors needs to be improved.

For example, with a better filament design and enhanced micro fabrication methodologies one could expect improvements in overall quality and reduction in the thermal artefacts.

Running the flow rate sensor using DC current reduces the life of the filaments because of the well known electromigration phenomena. This is because the resistance of the filaments changes after minutes of running under constant direct current, and therefore significantly affects the accuracy of the circuit. The life of the sensor filaments could be significantly improved by using alternating currents to reduce the effects of the electromigration phenomena [110].

By redesigning the flow rate die into a full bridge configuration, the sensitivity of the circuit doubles and the instrumentation circuitry would become simpler as the DC voltage offset would ideally become zero. Moreover, the output voltage drift caused by the electromigration phenomena would approach zero.

There is a hysteresis effect associated with any sensor and PUF flow rate sensor was not an exception. This can be minimized by using smaller area filaments and higher supply current, so that the temperature of the filament would rise faster in response to the increased flow rate. The minor slope change around mid-range calibration profile might be a result of this effect. Another possibility is the change in fluid flow regime from laminar to turbulent.

Information provided by the IMU data was used to extract different key features of various postures (standing, reclining, lying to the sides or back, bending, etc.) and physical activities (walking, running, walking up or down stairs, jumping, etc.). However, each individual subject had her own unique gait and posture and therefore the extracted features from the IMU signals associated with individual subjects varied to some degree. Therefore, if machine-learning classification methods are to be employed to automatically identify the correct activity type, a well-trained neural network containing data from many individuals is needed.

Finally, while the overall concept has proven feasible, more subjects are required to fully test all aspects of the latest PUF design and further evaluate its flowmetry performance in the different ADLs.

CHAPTER 4

Testing the PUF Device

Parts of this chapter has been published in US provisional patent app 62/925309 on October 24th 2019 and accepted for presentation at the *American Urogynecologic Society* (AUGS) virtual *Pelvic Floor Disorders* Week (2020).

4.1. Introduction

This chapter discusses experiments carried out on human subjects wearing the PUF device in order to test the fully instrumented PUF for its flowmetry and activity recognition capabilities in women.

Four testing sessions were carried out at one of the FemCare research facilities in a Procter & Gamble (Cincinnati, OH) research complex under an UM IRB exemption (HUM 00142989). In every testing session, 3-4 incontinent patients were recruited for testing PUF devices. In the last two studies, subjects were also asked to leave the facility wearing the device and return after 4 hours for PUF removal. The P&G safety committee for the P&G research facility also approved the device and the experiments that are described here.

4.2. Methods

4.2.1. PUF Testing Inside the Research Facility

After multiple design iterations (discussed in section 3.5.4) of the PUF sensor housing the desired comfort and fit levels for the selected panelists was achieved, so the fully instrumented version of the PUF device was now tested. In the first and second study sessions, each subject was asked to come to the facility with a full bladder. A registered nurse attached the PUF device, and then subjects were asked to sit on the commode setup (Figure 40) and urinate.

Figure 40. Commode setup above the precision balance (1) where the urine collection container (not shown in the figure) was placed. A thermometer (2) also recorded the temperature of the voided urine into the container with its probe (3) when placed in the collection container. A camera (4) was used to record bypass leakages occurred during the micturition.

A precision scale acted as the reference uroflowmeter to measure the weight of the urine collected in the container over time and hence provide the urine flow rate. The settings of the scale were adjusted such that it provided more accurate weight measurements of liquid filling in the container. The determining unit used in this phase had a Bluetooth low energy module (nRF52832, Nordic, Trondheim, Norway) and could transmit signals to a PC located in the next room in the real time at 30 Hz. An observer could monitor and record both signals transmitted from the determining unit and precision scale simultaneously.

Subjects were also asked to perform ADLs while also wearing an incontinence pad. They were to log the activity they were doing at every leakage incident. Finally, they were also asked to report sensation of leakage qualitatively if it occurred. The IMU signals were recorded and matched with the activity diary of the panelist. The weight of the pad before and after the study was accurately measured and the difference was used to validate the leakage volume reported by the PUF device.

4.2.2. PUF Testing Outside the Research Facility

In the third and fourth studies, panelists were recruited to test the device outside the CRT facility for up to 4-hour periods. The same procedures were used as in the first two testing session to attach the device. After receiving instructions, subjects were asked to leave the facility while doing normal ADLs that included going for a run. Subjects were instructed to complete a diary every 30 minutes of the ADLs they were doing, such as driving, walking, exercising, doing household chores, etc. They were also asked to manually enter the times that activities caused leakage. Finally, they also logged their bathroom visit times and times when they felt leakage. After returning to the facility, nurses carefully examined the device for any detachment or marking on the body – a sign of a poor housing fit or attachment method.

In these testing sessions, the determining unit recorded the data on a memory card inside the determining unit. Data from determining units were collected after subjects returned to the facility. Pad weighing was again used as a reference to verify the sensor results.

4.3. Results

4.3.1. First two testing sessions

Subjects reported little to no discomfort while wearing the PUF and felt minimal resistance during micturition in all sessions. In the first two studies inside the lab, five subjects had 10 voiding episodes while wearing the instrumented PUF. In five of the voiding episodes, video cameras recorded bypass leakage and the portion of the urine stream only passed though the urine channel. Therefore, the scale recorded a higher flowrate and those sessions were excluded from the results.

In the five remaining micturition sessions, the uroflowmetry profiles obtained from the PUF and uroflowmeter matched with a mean cross correlation factor of 0.96 and an average root mean square error (RMSE ± stdev) of 4.1 (± 2.3) ml/s. Figure 41 also shows sample uroflowmetry readings of the PUF device compared with the gold standard reference.

Table 6. Summary of the recordings of the PUF device compared with the reference uroflowmeter in the first (subject #1 and #2) and second testing sessions (subject #3).

Subject	Voiding #	Scale (ml)	PUF (ml)	Maximum Urine Velocity (m/s)	Error (%)	RMSE (ml/s)	Cross Correlation Coefficient
1	1	612.1	611.4	0.75	0.1	4.1	0.96
	2	892.2	877.3	1.27	3.3	7.6	0.96
2	3	222.7	231.5	0.43	3.9	3.4	0.98
	4	127.2	140	0.36	10	1.3	0.96
3	5	497	461.9	0.39	7.1	4.3	0.93
				Mean	**4.9**	**4.1**	**0.96**
				St. dev.	**3.8**	**2.3**	

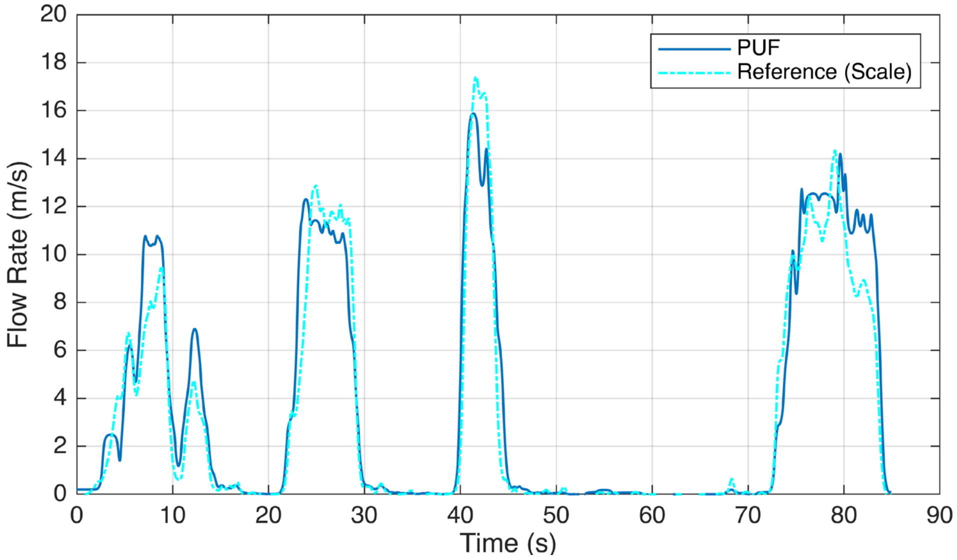

Figure 41. Sample urine flow rate recording of the instrumented wearable uroflowmeter worn by a woman trying to void, after which she paused voluntarily for five separate intervals.

The determining unit tested in these early studies proved the feasibility of the wearable uroflowmetry design in measuring leakage episodes of stress incontinent women (Table 7). The mean error between PUF and pad-weighing measurements in the second testing session was 8.4 ml (18 %).

Table 7. Results from instrumented PUF test on three subjects (second testing session). Total voided urine volume recorded with PUF device and compared the pad weight gain after the experiment.

Subject #	Urine volume captured by the pad (ml)	PUF readings (ml)	Error (ml)
1	103.8	97.4	6.4
2	38.7	53.3	14.6
3	36.3	40.6	4.3

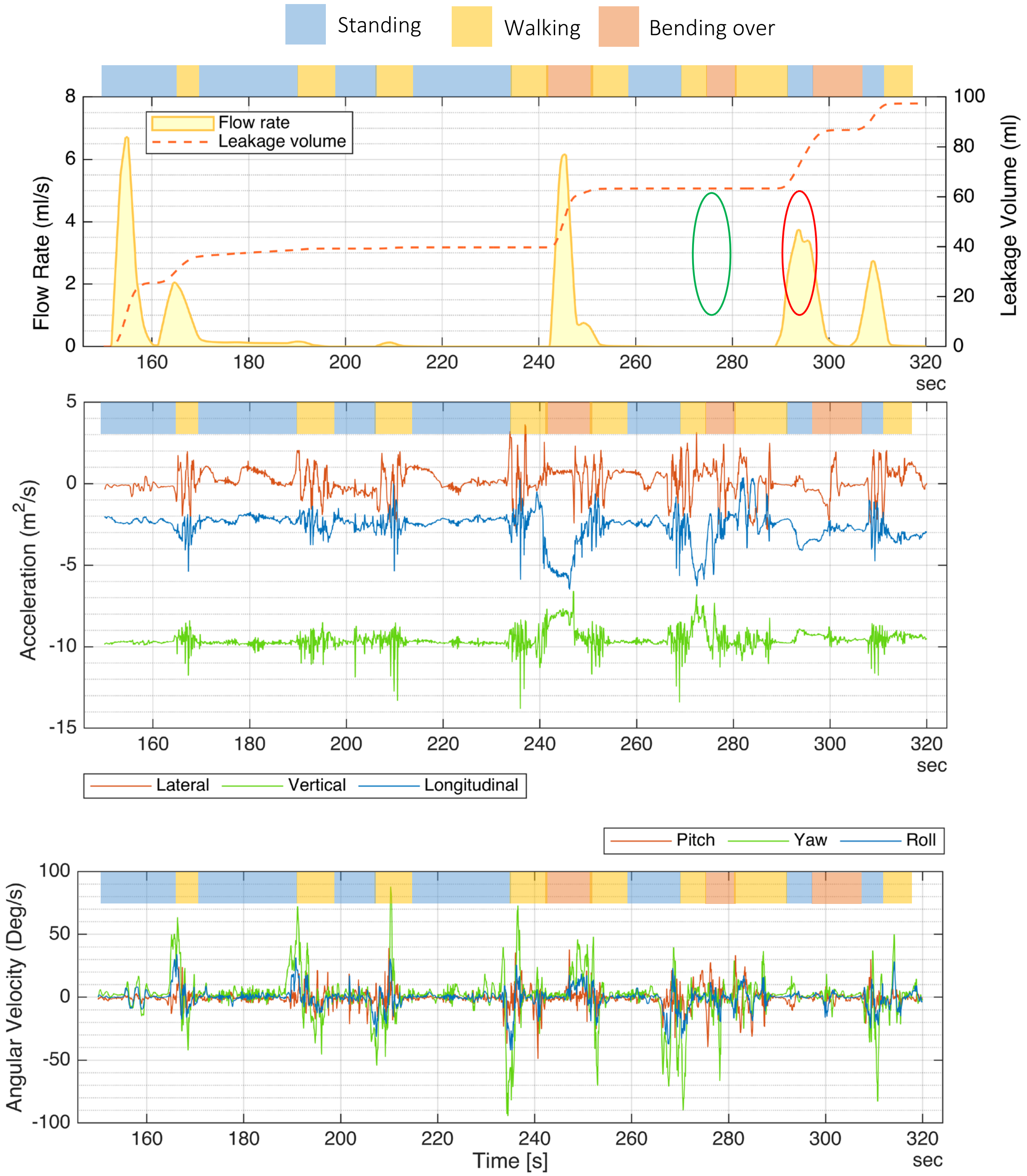

Figure 42. Sample flow rate, leakage volume and IMU signals recorded by the PUF unit during activities performed by one panelist in the P&G testing facility. Some of the performed activities are highlighted; “walking” in yellow, “standing” in blue, and “bending over” in red. The green circle shows bending posture which subject reported would cause leakage (similar to t=240 s). Although no leakage was measured until the following red circle showing the participant standing quietly but experiencing leakage presumably due to release of the labial reservoir upon standing. In the bottom plot, the rotational rate around the transverse (lateral) axis is shown in red. Similarly, rotational rate around vertical (yaw) and longitudinal (roll) axes are shown in green and blue. For example, the green spikes in the yaw signal represents times when the subject had turned on her feet.

Results from the second study also revealed that a more sensitive sensor was required for some panelists. An interesting phenomenon is exhibited in Figure 42. Between time points 270 s and 290 s a classic example of urine leaking occurs; yet it does not leave the labia and the housing until time points 290 s to 300 s when the person stood up from a bending pose. Our explanation for this delay is that the urine became trapped in the labial reservoir while she was bending and not released until the participant stood up (Appendix I). This is the first time that this "labial reservoir emptying behavior" has been ever been captured.

4.3.2. Second two testing sessions

Two other experiments (study 3 & 4) with six more subjects were carried out next. However, since they had worn the determining unit under warm winter clothing for long periods of time, the operating temperature of the determining units rose from a room temperature of 21 °C up to 41 °C - slightly higher than the body temperature. Because of the sensitivity of some electrical components to temperature change, the calibration settings of the sensor drifted within 20 minutes of operation, and the output signals were saturated.

In the fourth experiment since the entire determining unit was calibrated in the elevated temperatures known from the third experiment, timing of the leakage events could at least be captured and they happened mostly while the subject was running. However, the flowmetry signals were not still accurate. Therefore, a new circuit with less sensitivity to temperature change was required.

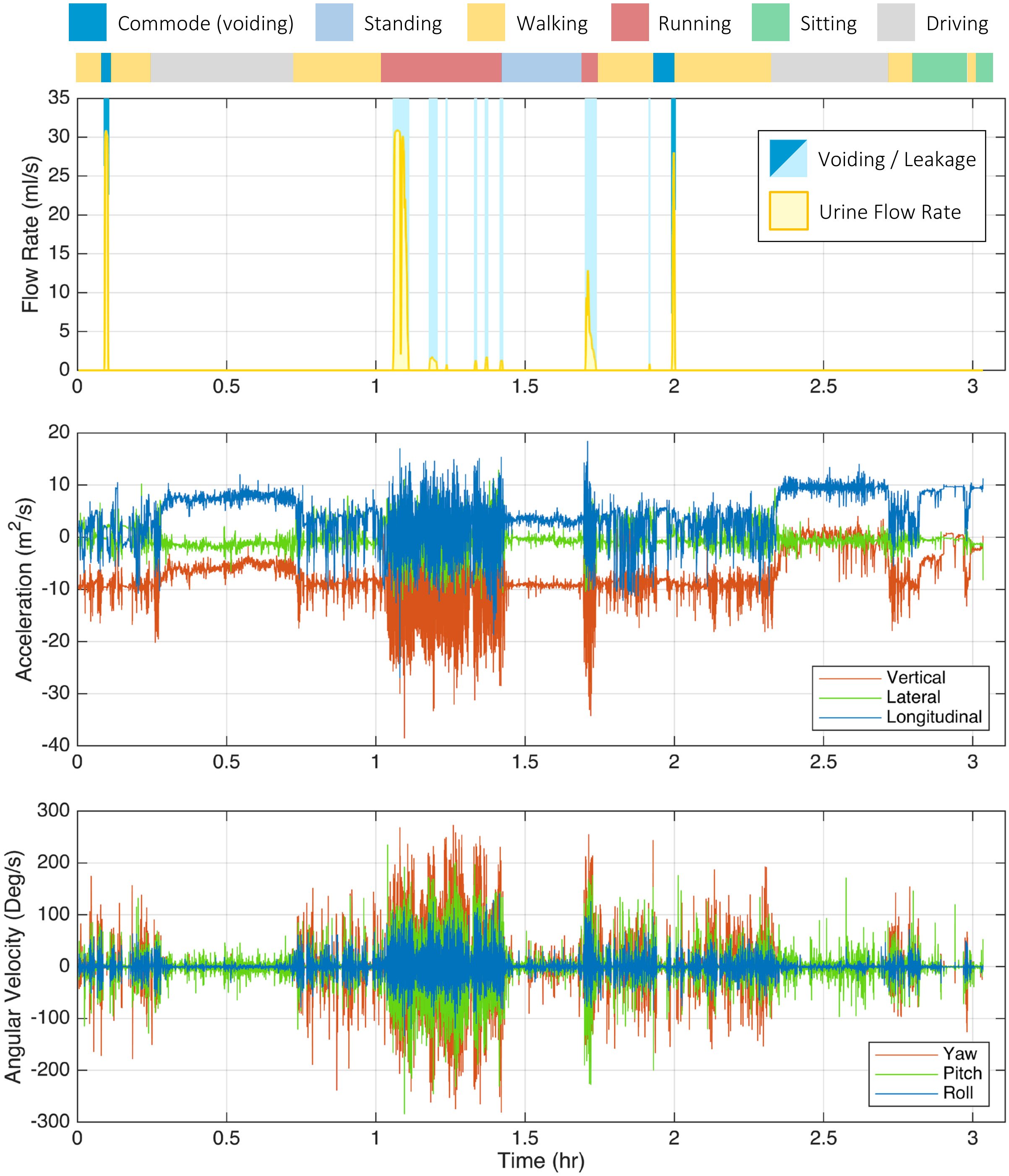

Figure 43. Leakage and voiding episodes (top plot) recorded simultaneously with IMU signals (middle and bottom) of one subject who had the device on for three hours outside the research facility. Top bar shows the activity of the subject. Dark blue blocks in the top plot and the activity bar shows the voiding time reported by the user and captured by the PUF. Leakage episodes (light blue) mostly happened during running (red) where the high acceleration existed.

4.4. Discussion

The experimental PUF flowmetry data from micturition was found to lie within 10% of that measured via the gold standard reference method. The accuracy in quantifying leakage was 82%. The error in the leakage quantification study mainly originated from the fact that in that study PUF design (V12) had no post sensor flexible membrane to buffer small amounts of leakage.

Although the addition of the flexible membrane to the PUF housing in the second study (with PUF V13.1) had improved the leakage measurements in the benchtop setup, it generally impeded the micturition of two subjects and therefore the diameter of the urine channel was increased to 9 mm for the third and fourth study.

In the third study, since that was a 4-hour long study conducted outside the research facility in winter and subjects had worn determining units under their clothing, the temperature of the electronic units was markedly increased due to the insulated clothing so the calibration settings unfortunately drifted.

In the fourth study, without changing the internal circuitry, the determining unit was calibrated at body temperature (37°C) before the study, and the minor temperature deviations were compensated with the help of an on-board temperature sensor. However, it was perceived that the membrane could also block the urine channel if it contacts the incontinence pad. Therefore, for the next phase of test (V15 and after), the length of the urine channel test was increased by 6 mm and bypass vents were added to its wall distal to the flexible membrane.

There was face validity in that the waist-mounted wearable activity sensor output correlated with the volunteer's subjectively recorded physical activity and therefore PUF, for the first time, could be able to record stress incontinency leakage episodes with the corresponding activity of the wearer. Therefore, the PUF-measured urine leakage significantly correlated with a given physical activity recorded by the waist-mounted wearable determining unit. More data are required in order to be able to use machine-learning classification methods.

4.4.1. Limitations

The major limitation of all these feasibility experiments was the small sample size. More subjects are required to test the performance of the device in extended durations. Since this was an evolving design process, both front- and back-end design approaches were adopted to minimize the number of trials and errors, and increase the efficiency of the procedure. Therefore, a maximum possible number of 3 - 5 subjects were recruited at each step. Moreover, some of the subjects were asked to come back again for a follow up study in order to check whether the design improvements were indeed effective.

There were certain errors associated with PUF measurements. A major source of error was associated with transient response of the sensor; although the sensor time constant was 200 ms, it turned out that it was not fast enough to correctly measure the peak flow rates of leakages. To resolve this issue, further design improvements are necessary. Another possible error source can be spotted when checking the calibration plot (Figure 35) in which there is a change in the slope of the curve around 15 ml/s which could be due to flow regime change from laminar to turbulent, the insufficient operating power of the sensor or hysteresis effect. All can be improved eventually with a better housing, sensor, instrumentation and filter design.

Another source for the error could be due to the non-uniform urine flow inside the sensor channel especially during transient flows; although the addition of the flexible membrane helped to capture low urine flow rate, it possibly could have disturbed the flow inside the channel.

ADLs with high accelerations levels such as running also might have caused perturbations in the urine flow.

Another category of errors was rooted in the temperature change in the housing and the determining unit. In the second two studies were subjects wore the determining unit under winter clothing for a few hours, so the determining unit temperature had increased and the calibration settings drifted. The housing temperature when it was worn by the subject could have been different from the case it was calibrated in the benchtop setup.

Finally, not all errors were associated with the PUF; the reference measurements were not error free. For example, the impact of the urine stream on the bottom of the beaker that was placed over the precision scale (reference uroflowmeter) might have caused errors. Although the scale signals were filtered to a certain degree and this error existed mainly at the beginning of the micturition when the beaker was empty, it could have been further eliminated by placing a large collecting funnel to buffer the urine into the beaker. However, one could argue that this large funnel over the scale might also would change the flow characteristics by delaying and buffering the flow rate. Similarly, the pad weight measurements were not error free. As one can speculate, the secreted moisture from labial skin during activities (specially running) can also be absorbed by the pad and therefore increase the reference leakage measurements.

While 5% error in measuring micturition flow rate values was acceptable for this early design, further improvements are necessary to reduce 18% leakage measurement error. The maximum flow rate of the 40 ml/s reported from urodynamic studies in the literature could be measured by the PUF, however it is speculated that the urine velocity during high acceleration activities such as running could be higher. Therefore, the dynamic range and sensitivity of the sensor needs to be further improved.

4.4.2. Future Improvements

Several aspects of the PUF device require further improvements. The most important issue that needs to be addressed is the temperature drift observed initially in the first 4-hour test outside the CRT facility in winter (third instrumented test). To solve that, components with lower temperature coefficient/sensitivity should be selected.

Another issue concerns the design of the sensor dies. A new ‘full bridge’ filament design along with new fabrication method should be used (Figure 44). Moreover, to increase the life of the sensors, alternating current source can be used; this markedly slows down the degradation caused by the electromigration phenomena, without affecting the sampling rate [110].

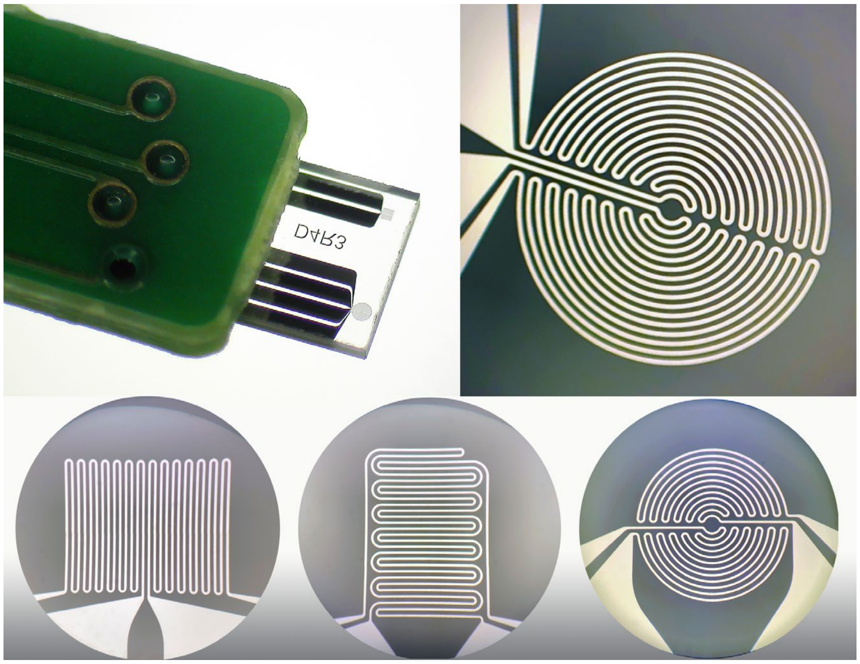

Figure 44. PUF flow rate sensor with four different filament design fabricated with improved micro-fabrication techniques (with filament width of 5 μm). Dual filament design to form a full-bridge configuration doubles the sensitivity of the sensor and simplifies the instrumentation circuitry. As a result, the determining unit would also have fewer components susceptible to thermal noise and drift. Initial assessment of the circular filament, for example, showed better geometric consistency and quality.

Minor improvements can also be implemented on the power management components to increase signal quality and reduce the noise and ripple in the analog signals originated from the digital circuit sections.

To summarize, this chapter describes the first successful uroflowmetry measurements in women made during normal ADLs, including jogging and driving, performed beyond the confines of a research facility.

CHAPTER 5

Design of the DM Device

Parts of this chapter have been submitted to the PLOS ONE (PONE-D-20-01826), *Digital Health Technology* special issue.

5.1. Introduction

As mentioned in Chapter 1, the HR-ARM requires a relatively expensive system, an additional visit for the patient, and experienced staff to operate and interpret the results. Hence HR-ARM has become limited to tertiary care medical centers with the result that many patients are deprived of the opportunity to be properly diagnosed and triaged to appropriate therapy [6], [111], [112].

It was hypothesized that a simpler and less costly system might be able to provide the most salient information provided by HR-ARM at the point of clinical service. Therefore, this chapter addresses the knowledge gap KG7 (section 1.3.7) whether it is possible to develop a disposable index finger-based system to assess anorectal function. This system is termed “digital manometry” (DM) [113]–[116] and not only it would measure the anorectal pressures but also muscle coordination.

5.2. Design of the DM Device

DM consisted of a disposable, instrumented glove and a reusable wrist-mounted determining unit (WDU) (Figure 45).

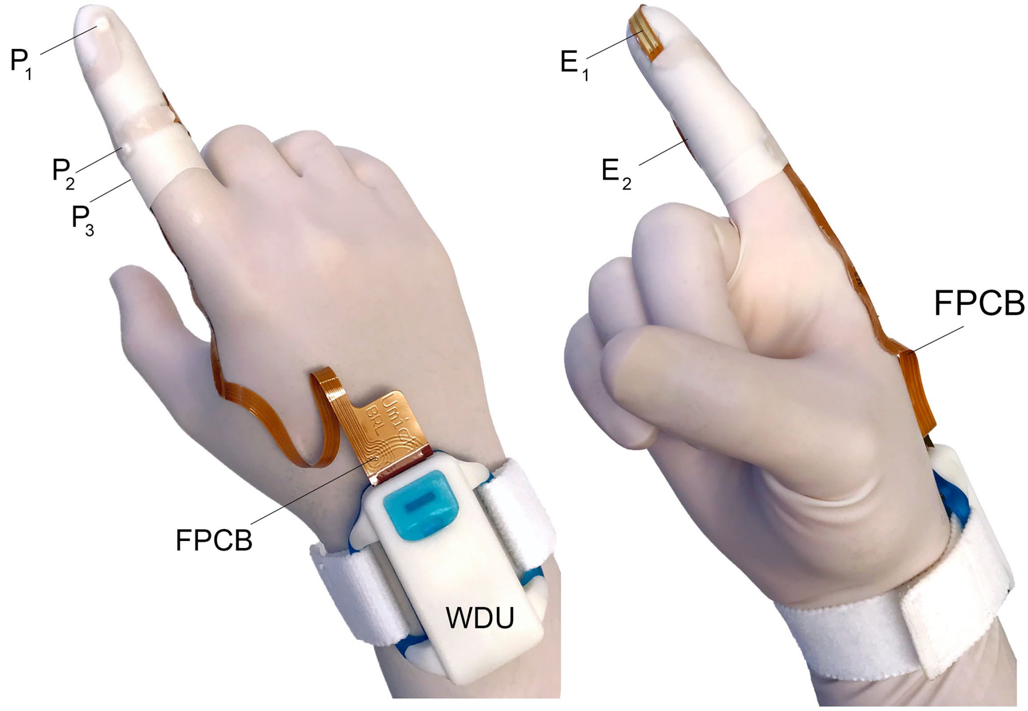

Figure 45. Wearable DM system. Two views of the DM disposable instrumented glove along with the reusable wrist-mounted determining unit (WDU). (Left) The three pressure sensors, $P_{1\text{-}3}$, are mounted on the flexible printed circuit board (FPCB) that wraps around the index finger under a finger cot. (Right) The two myoelectric electrodes, $E_{1\text{-}2}$, also connected to the FPCB, are shown adhered to the surface of the finger cot. WDU amplifies and transmit signals from the pressure sensors and myoelectric electrodes wirelessly to a nearby computer for display purposes. The patient myoelectric ground electrode and cable that connect to the WDU are not shown for simplicity.

The glove had three miniature (1 mm × 1 mm × 0.6 mm) piezo-resistive micro-electromechanical pressure sensors (P1602 NovaSensor [100 kPa], Amphenol, Wallingford, CT, USA) mounted on a 300 µm-thick custom flexible printed circuit board (FPCB) made from biocompatible polyimide substrate [117]. Each sensor was covered with a smooth uniform layer of biocompatible silicone elastomer (MED2-4220, Nusil, CA). Afterwards, in a clean environment, the FPCB was adhered to the outside of the index digit of a standard non-latex surgical glove using biocompatible silicone adhesive (MED-1011, Nusil, CA). The location of pressure sensors of the FPCB were on the tip of the distal phalange over where the operator's nail would be, the medial aspect of the middle phalanx, and the lateral interphalangeal joint, respectively. This arrangement enables measuring intrarectal and anal sphincter (AS) pressures during the detailed digital rectal examination (see Figure 46). The base sensors (P_2 and P_3 shown in Figure 45) of the DM device were designed to be kept within the AS maximum pressure zone. Additionally, the FPCB had two pairs of gold-plated myoelectric electrodes, each spaced 1 mm apart over the index fingertip pad and on the aspect of the middle segment of the index finger, to measure the myoelectric activity of puborectalis (PR) and anal sphincter muscles, respectively. The entire circuit board was covered by an extra protective layer provided by a silicone rubber finger cot with openings to expose only the myoelectric electrodes (Figure 45).

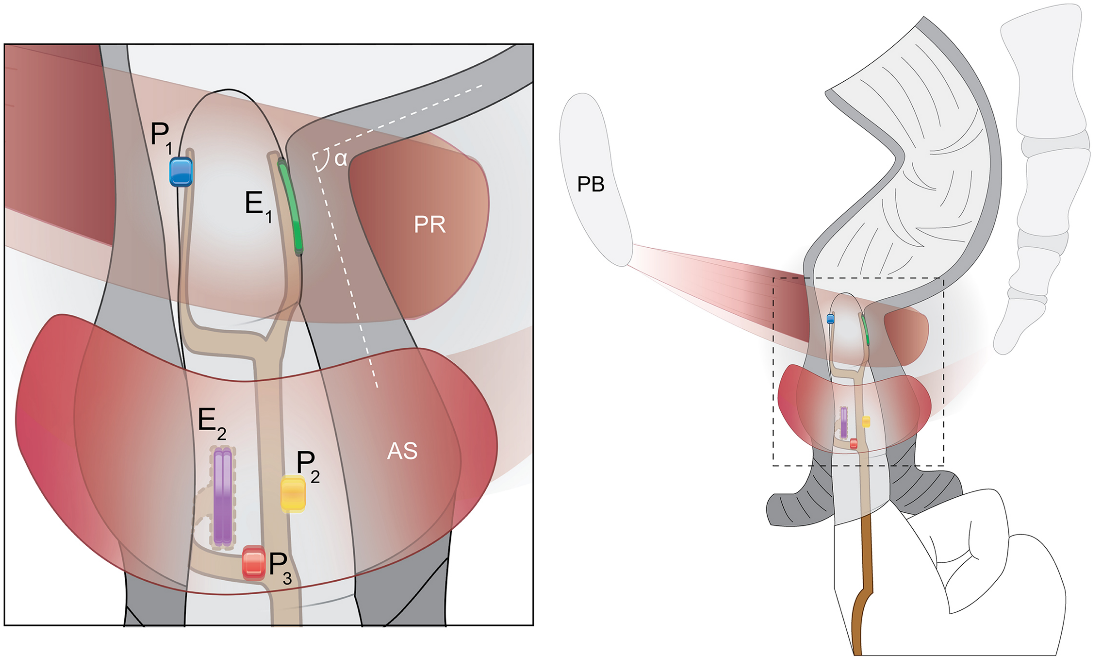

Figure 46. A schematic illustration showing a left lateral view of the DM disposable glove during an anorectal canal assessment. Single pressure sensors are located over the fingernail (P_1), middle phalanx (P_2), and the proximal interphalangeal joint (P_3), as well as two bipolar gold plated myoelectric activity electrodes (E_1 and E_2) for the puborectalis (PR) and anal sphincter (AS) muscles. The inset at left shows how the printed circuit board wraps around the index finger. α is the anorectal angle. Note that the ipsilateral PR muscle is shown as being transparent to permit a view of rectal canal.

A reusable wrist-mounted signal conditioning unit transmitted data from the index finger-based sensors to a computer for further analyses and display. This unit was comprised of a first order high-pass passive filter with a corner frequency of 186 Hz to attenuate any DC offset and dual instrumentation amplifiers (INA2128, Texas Instruments, Dallas, TX, USA) to amplify myoelectric signals with a gain of 10,000. The myoelectric signal was hardware rectified and filtered. Finally, an over-the-counter electrocardiogram electrode was used over the greater trochanter of the femur as the ground reference. Computers recorded pressures from the anorectal complex as well as the myoelectric activity of AS muscles at 60 Hz. The pressure and myoelectric signals were processed using a center point moving window to calculate the average of 20 data points.

5.3. Calibration of the DM Device

In order to calibrate instrumented gloves, they were placed inside a custom made air pressurized vessel individually (Figure 47). This vessel was connected to reservoir tank connected to a column of water. The pressure of the chamber was increased to 220 mmHg, and output signals form the pressure sensors were calibrated upon stabilization of the water level in the column. This process was repeated up to 5 times and the obtained calibration coefficients were averaged. Maximum non-linearity of NovaSensor P1602 sensors were 0.2% of full-scale output (FSO), therefore linear calibration procedure was suitable.

For the myoelectric measurement system, having an impedance matching circuit would be ideal to compensate for different tissue impedances. For example, amount of fat in a tissue or mucus covering surface of tissues could change the input impedance and respectively reduce the sensitivity of the amplifier circuit. However, to miniaturize and simplify the EMG amplifier circuit, a first order high-pass filter with 30 Hz cut-off frequency found to be appropriate for the application. It was observed that with this setting the amplifier circuit was most sensitive to the myoelectric signals generated from the lip or tongue muscles during the design phase.

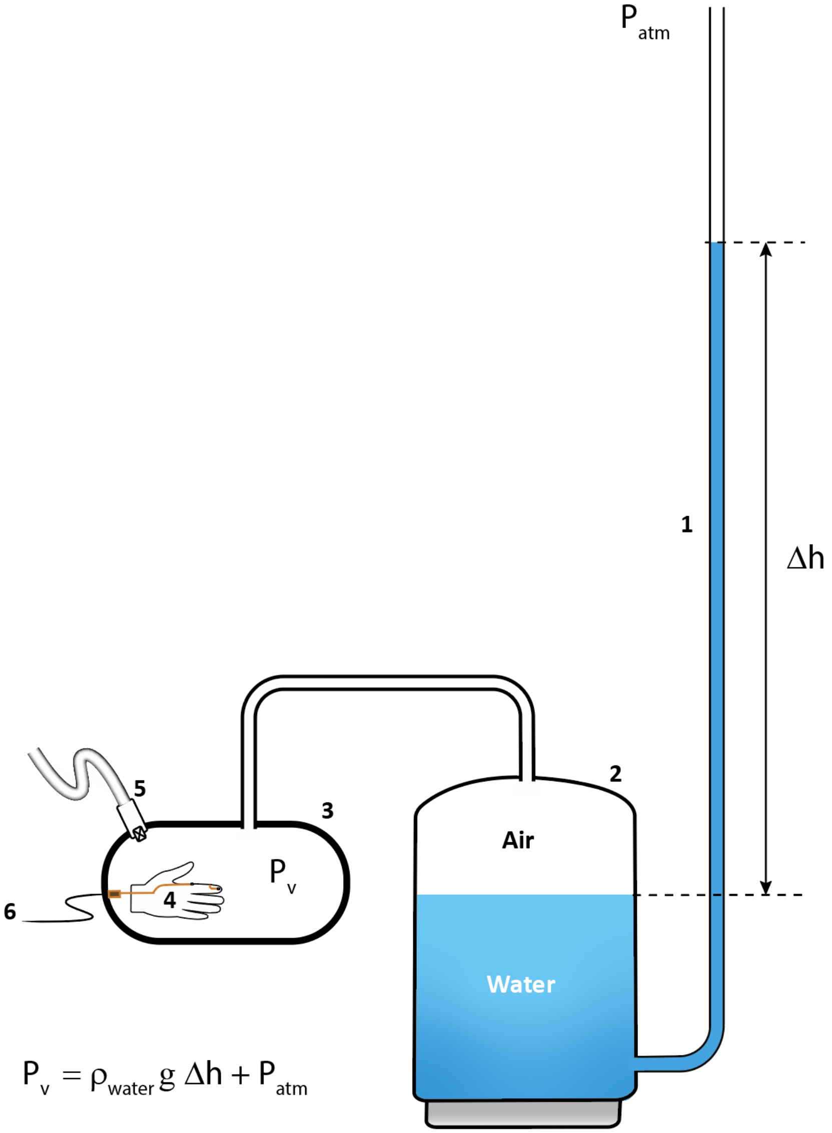

Figure 47. Setup for calibrating the pressure sensors mounted on the DM glove. 1) Column of water (3 m), 2) water reservoir, 3) pressurized vessel, 4) DM probe inside the pressurized vessel, 5) air pressure control valve connected to the compressed air piping and 6) connection to the data acquisition unit. The output of signals of the pressure sensors mounted on the glove were calibrated at least at two pressure values of $P_v = P_{atm}$ and $P_v = 220$ mmHg + P_{atm}. The pressure of the vessel kept constant at these two specific pressures. A column of water was used to measure the pressure inside the pressurized chamber. The nonlinearity of the sensors was less than 0.2% FSO. ρ in the equation shown in the figure is the water density, g is the magnitude of gravity and Δh is the height of water in the right column with respect to the water level in the reservoir.

CHAPTER 6

Testing the DM Device

Parts of this chapter have been submitted to the PLOS ONE (PONE-D-20-01826), *Digital Health Technology* special issue.

6.1. Introduction

In this chapter, three hypotheses are tested:

1) In three different activities, rest, squeeze, and simulated defecation, DM pressure readings are equivalent to those measured with a HR-ARM in a sample of healthy subjects, and patients with chronic constipation and fecal incontinence.

2) Using DM only, the change in the myoelectric activities of the puborectalis muscle (PR) is proportional to change in anal sphincter (AS) maximum pressure recorded by the DM device

3) There is no difference in comfort reported by individuals undergoing DM and HR-ARM.

6.2. Methods

6.2.1. Experimental Design

This was a single center, cross-sectional, observational cohort study of AS pressures in three different physical activities: at rest, during maximum squeeze, and during simulated defecation measured with both the DM system and a commercially available HR-ARM system.

This study was approved by the institutional review board (HUM00046068) and all subjects signed a written consent form prior to the experiment.

6.2.2. Participants

A total of 16 participants of both sexes were recruited under an experimental protocol (HUM00046068) approved by the institutional review board. Participants were either healthy (2 males, 2 females), or had diagnosed with chronic constipation (2 males, 2 females) or fecal incontinence (1 male, 7 females). The median age was 61 years (range: 31 – 85 years), and the mean BMI was 29.4 (SD: 5.9) kg/m2. The healthy volunteers were recruited by public advertisement, free of gastrointestinal symptoms, and not taking medications affecting gastrointestinal or colonic function. The chronic constipated patients fulfilled the Rome IV criteria [118] for chronic functional constipation and were referred for HR-ARM to evaluate persistent constipation symptoms despite laxative therapies. Finally, FI subjects had at least one episode of accidental bowel leakage in the previous month [46], [119]. All subjects were free of structural anorectal diseases or previous anorectal or colonic surgery.

All participants underwent the same procedures with the DM and HR-ARM systems. A board-certified gastroenterologist used the DM, and a medical technician performed the HR-ARM procedure. The operators were blinded as to the other’s results. The order of performing the assessment with two measurement methods was randomized for each subject to minimize possible learning effects.

6.2.3. HR-ARM Apparatus; Gold Standard Device

A Sandhill Scientific® HR-ARM system (Denver, CO, USA) was used with a 4 mm diameter catheter (UNI-ANO-M0138) (Figure 48) having five sets of 4 radially- and orthogonally-arranged pressure sensors spaced 1 cm apart. A single sensor on the catheter was located away from the array and exposed to the atmospheric pressure outside the rectum as a calibration for the other sensors. The catheter had two single sensors at the distal end, one of them being inside an inflatable balloon (Figure 49).

Figure 48. HR-ARM probe Sandhill Scientific® HR-ARM system (Denver, CO, USA) comprised of an array of pressure sensors on a 4 mm diameter catheter with internal air tubing to inflate the balloon (not installed in this picture) on the tip of the catheter.

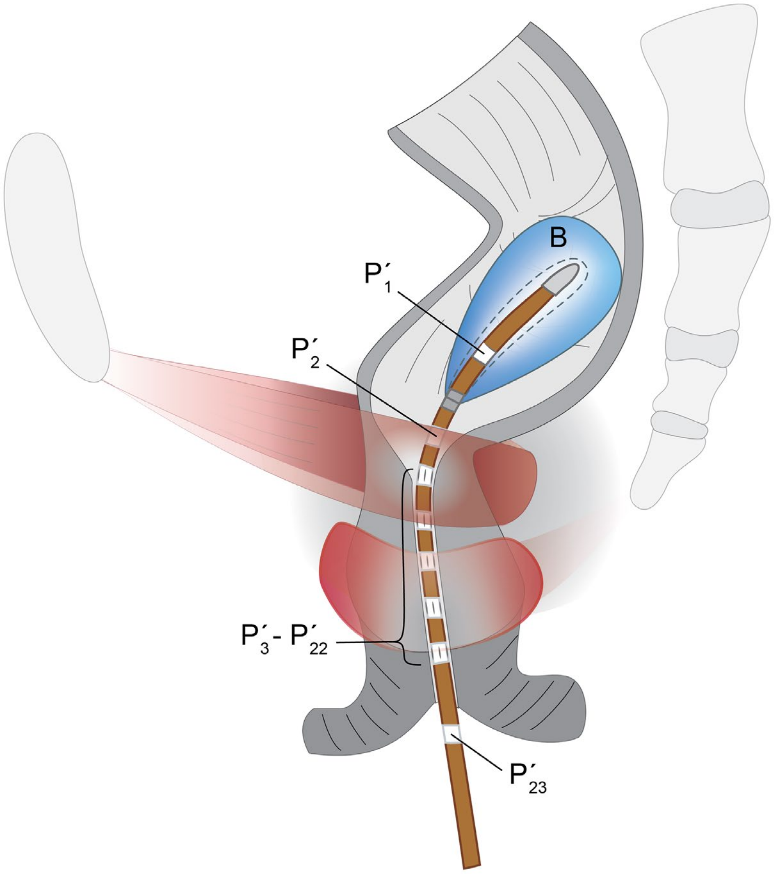

Figure 49. Illustration of the HR-ARM 4 mm–diameter catheter inside the anal canal during the anorectal manometry procedure. Also shown are, relative to the patient, the proximal 60 (cm^3) inflated balloon (B) with its single pressure sensor inside (P'_1), a single pressure sensor outside the balloon (P'_2), five sets of four radially and orthogonally arranged pressure sensors ($P'_3 - P'_{22}$), and the external pressure reference pressure sensor (P'_{23}) distally.

6.2.4. Study Procedures

During the clinical visit, the examiner first checked the anal canal to ensure it was free from scars and evidence of bleeding. Each participant was asked to lie in the left lateral decubitus position with both legs flexed. The reusable HR-ARM catheter was sterilized and recalibrated prior to each study. Upon insertion of either the lubricated DM probe or HR-ARM catheter, the examiners asked each subject to relax their anorectal muscles for at least one minute to measure the average resting pressures. Afterwards, participants were asked to maximally squeeze the AS muscle for 5 seconds as if they were trying to prevent accidental bowel leakage. Once the subject's AS pressure returned to the baseline, they repeated the same maneuver with a subsequent rest period at least twice. Finally, participants were asked to simulate defecation by expelling the digit of the examiner wearing the DM instrumented glove or the HR-ARM catheter.

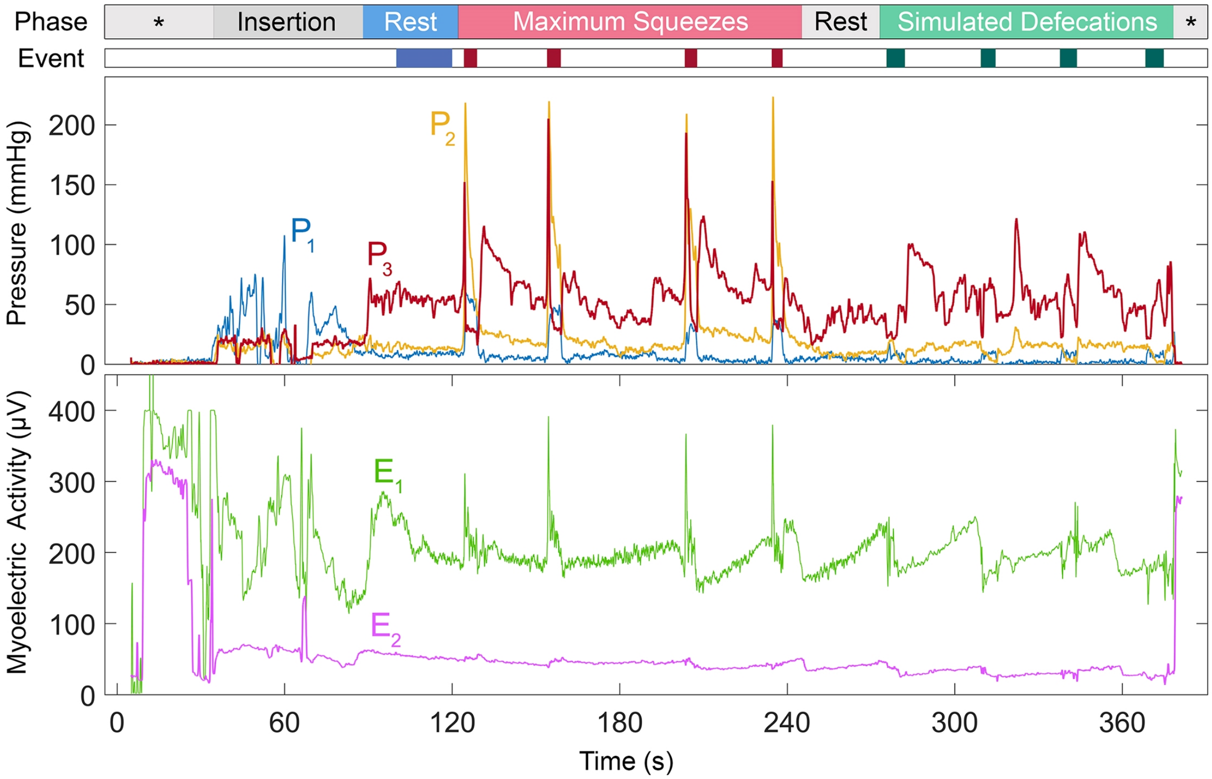

Figure 50. Sample simultaneous AS and rectal pressures (P1-P3) with myoelectric activities (E1 and E2) of the anorectal muscles recorded from a healthy male (subject #3). The first bar ("Phase") along the top of the illustration shows the exam phases. The first asterisk denotes the period before the sensors are inserted into the body. Baseline activity was recorded with the patient resting ("Rest"). The patient was then asked to maximally contract their AS muscles four times interspersed by rest periods. After another rest ("Rest"), the patient was asked to simulate defecation four times ("Simulated Defecations"). The last asterisk denotes the device being removed from the body and outside the body. The second color-coded ("Event") bar shows the intervals when the patient pressed the hand-held event marker during which measurements were made. (Note that the floating myoelectric activity signal prior to insertion of the probe at t = 35 s).

Pressure signals were recorded continuously throughout the entire session and available to the clinician as real time visual feedback. In the case of DM, myoelectric activities were recorded simultaneously (Figure 50). Subjects were asked to press an event marker button at the beginning and end of each trial of each activity that they were asked to perform.

Once both procedures were completed, subjects were asked to complete a survey on the comfort level of each system. A 10-point visual analog discomfort scale was used with ‘1’ labeled ‘unbearable’, ‘5’ being ‘bearable’, and ‘10’ representing ‘very acceptable’ on three factors: smoothness, shape, and size of the probes. The ‘overall comfort level’ as well as the ‘duration’ of each method were also rated on the same scale. Finally, in the survey, subjects were asked to describe their opinion or experience during studies and whether DM could be improved in any way.

6.2.5. Statistical Analyses

To test the primary hypothesis the Bland-Altman [120] limits of agreement (LoA) method was used to compare pressure readings for the rest, squeeze, and simulated defecation procedures (paired differences = DM - HR-ARM). In the field of gastroenterology, pressures are either measured in mmHg or cmH_2O; and the former is chosen in reporting results. For the rest values, mean (SD) were calculated from at least 10 seconds of DM data and mean values taken from HR-ARM output. The maximum pressure during squeeze was calculated by taking the peak value in the interval between the event markers. For each subject, the simulated defecation episode was selected with the maximum pressure decrease from the rest value just prior to the effort to the minimum pressure measured during the maneuver. For the HR-ARM, since it had more sensors than DM, the mean pressure value from each set of four radially-arranged sensors was first calculated for each 5-second interval. Then, the maximum value was found along the catheter to represent the high-pressure zone in the AS.

The absolute and relative intraobserver errors [121], [122] were calculated for three consecutive maximum squeeze pressures by each subject for only DM since the reproducibility of measurements made with the HR-ARM device have already been documented [123].

To test the secondary hypothesis, least squares regression was used to find the correlation between the changes in the relative EMG activity of the PR muscle and AS pressure change in maximum squeeze maneuver.

Finally, to compare the comfort level of both systems a two-sided Mann-Whitney U-test was used with a p level of 0.05 to compare the DM and HD-ARM ratings for comfort, smoothness, size, shape, and duration.

6.3. Results

The data support the primary hypothesis in that the LoA showed acceptable DM performance for measuring AS pressure at rest (Figure 51A) and during simulated defecation (Figure 51B). For the rectal pressure measurement, a greater variance was noted (Figure 51). The largest difference between the two methods was found in the measurement of AS pressure during a maximum squeeze (Figure 51D). If two outliers from the results of the maximum squeeze episodes were excluded (see Discussion), mean ± SD LoA decreased from -20 ± 172.6 to 7.2 ± 93.6 mmHg. The mean of the standard deviations of maximum pressures in all squeeze episodes across all subjects for DM and HR-ARM were 14.9 mmHg and 9.5 mmHg, respectively (Table 8).

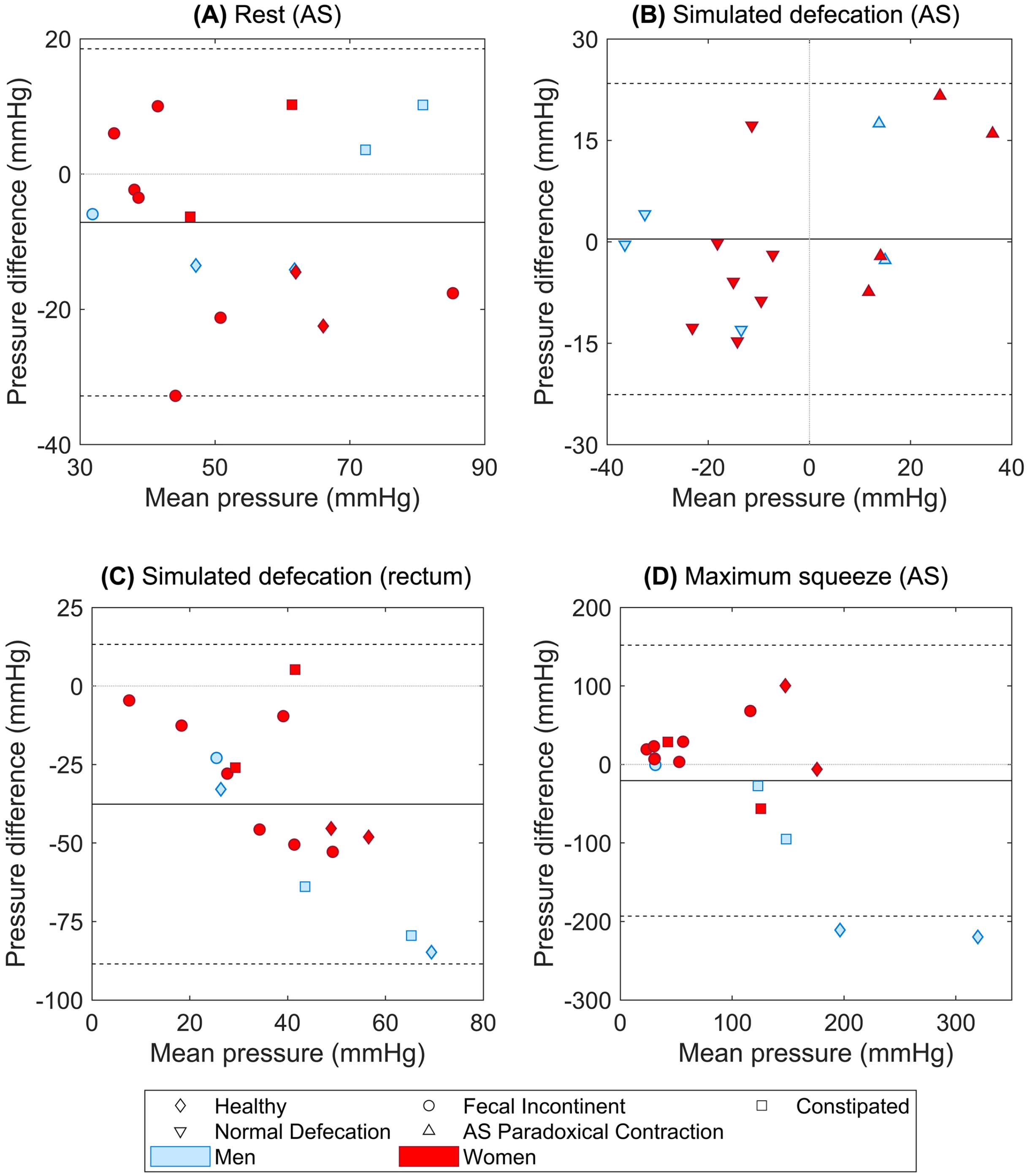

Figure 51. Bland & Altman comparisons between DM and HR-ARM (direction of difference DM - HR-ARM) in measuring anorectal pressures. (A) AS resting pressure, (B) AS pressure change during simulated defecation, (C) rectal pressure change during simulated defecation, and (D) AS pressure change during maximum squeeze.

Table 8. Results from Bland & Altman test comparing DM and HR-Arm on the AS and rectum pressure recordings

Maneuver	**Mean Paired Difference** [a] **(DM − HR-ARM)**	**LOA** [b] **(CI: 95%)**
AS pressure at rest	-7.1	±25.7
AS pressure change in simulated defecation	0.4	±23
Rectal pressure change in simulated defecation	-37.6	±50.9
AS pressure increment in maximum squeeze	-20.6	±172.6

[a, b] units are in mmHg

During simulated defecation, 37.5% of the subjects paradoxically contracted their AS by the predicate HR-ARM. There was complete agreement between DM and HR-ARM in distinguishing paradoxical AS contraction during simulated (Figure 51B). The samples on the left side of the plot, show examples of subjects with normal AS relaxation during simulated defecation (i.e., negative AS pressure change), whereas the points on the right side of the plot represent subjects who paradoxically contracted their AS (i.e., positive AS pressure change).

The mean (SD) absolute and relative intraobserver variability of DM were 12 (21.2) and 14% (21%) with ICC of 0.94.

For the DM device, the slope and intercept of the regression line (Figure 52) between the percent change in the PR myoelectric activity and increment in AS squeeze pressure was found to be 0.6 µV/(µV.mmHg) and 25.5 µV/µV, respectively ($R^2 = 0.4$), so the change in RMS myoelectric activity of the PR muscle was proportional to the change in AS maximum squeeze pressure, supporting the secondary hypothesis.

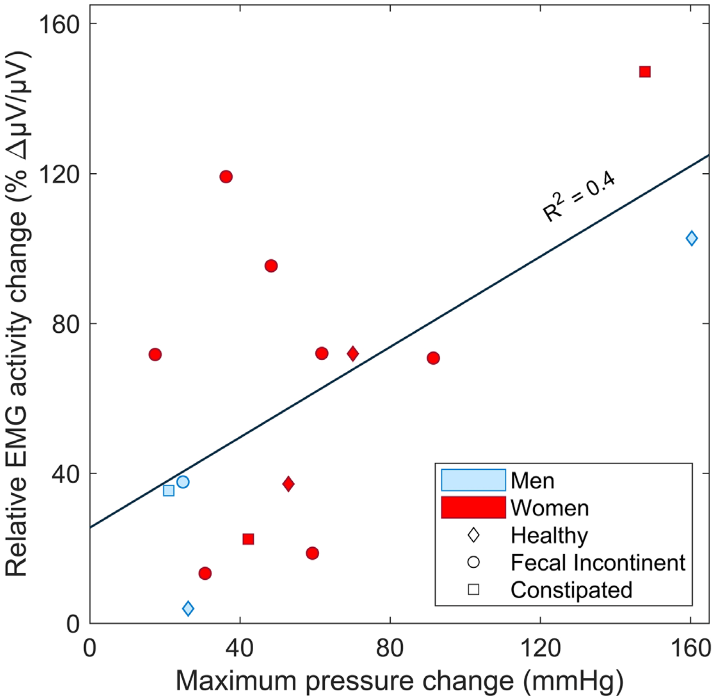

Figure 52. Maximum change in PR myoelectric activity vs AS pressure change in simulated defecation across all patients. Trials were selected which showed the largest change in peak PR myoelectric activity compared with the maximum decrease in the AS pressure during that defecation maneuver in 15 of 16 subjects (no myoelectric activity was recorded in the first subject due to equipment malfunction). Note that the patients with dyssynergic defecation could not decrease AS pressure.

Finally, the results from survey (Table 9) showed that the difference between comfort levels of both systems were not significant (Table 10).

Table 9. Examples of the participants' responses to the survey question on DM system comfort.

"Great study… not too long"
"It was much more preferable once it was in."
"The device was as comfortable as it could be."
"Went very well. I would rather do DM if it gives the same results."
"Everything went well. It wasn't too uncomfortable and very thorough."
"Not knowing what to expect, there is no comparison between the two tests. The new device is so much easier."

Table 10. Comparison of DM and HR-ARM subjective post-hoc test assessment levels on a visual analog scale from 1 to 10, with '1' labeled 'unbearable' and '10' representing 'very acceptable'. 'Min' denotes minimum and 'max' denotes maximum.

	DM			**HR-ARM**			
Factor	Mean (SD)	Min	Max	Mean (SD)	Min	Max	**P-Value**
Comfort	9.3 (1.0)	7	10	9.1 (1.5)	5	10	1
Smoothness	9.6 (0.8)	8	10	9.2 (1.6)	4	10	0.56
Shape	9.6 (1.0)	7	10	9.3 (1.6)	5	10	0.67
Size	9.3 (1.1)	7	10	9.3 (1.8)	4	10	0.68
Duration	9.9 (0.5)	8	10	9.3 (1.7)	4	10	0.35

6.4. Discussion

Although physicians have worn wearables in the form of stethoscopes and loupes to augment their sensory acuity for over a century, the miniaturization of sensors and electronics is providing new opportunities for developing wearables for clinicians to use to evaluate patients quickly and easily. This chapter describes testing the novel DM wearable which allows providers to better understand the etiology of chronic constipation and fecal incontinence at the point of service. If validated by others, digital manometry could, for the first time, offer providers in low-resource settings the ability to gain information that would otherwise require referral to a tertiary center for comprehensive anorectal function testing. Further, this was an early phase prototype. It is certainly conceivable that the instrumented glove and wrist-mounted determining unit can be linked to a smart phone via Bluetooth.

The primary hypothesis was supported in that the DM provided accurate pressure readings compared to the gold standard HR-ARM system. It did so at a hardware cost that is an order of magnitude less than HR-ARM (Table 11). More specifically, DM was equivalent to the gold standard HR-ARM system in measuring the AS pressure during rest and simulated defecation episodes.

Table 11. Estimated cost comparison between DM and HR-ARM methods.

	DM	**HR-ARM**
Overall system cost	$10,000	$122,000
Hardware cost	$1,500	$116,000
Probe cost	$10	$6,000 [a]
Sterilization cost [b]	$0 [c]	$20
Hardware cost per exam	$10	$50

[a] 200 usages per catheter, [b] per session, [c] disposable instrumented glove

There are, of course, indirect costs associated with the use of any new instrumentation. One of these costs is training the operator. DM does not necessarily require a physician to operate it. Rather, anyone who has been trained to perform a rectal exam, including advanced practice providers or nurses, would be able to use it after demonstrating the ability to record reliable measurements on a few patients. The lower hardware costs of DM places it within the primary care office budget, so compared to HR-ARM in tertiary care, an earlier patient assessment should help reduce overall care costs.

In the maximum squeeze maneuver, DM recorded systematically lower average AS pressures compared to HR-ARM. Most of that difference was caused by the results from two men (Figure 51D - blue outliers). Interestingly, the literature reports higher pressure readings of HR-ARM compared to the standard conventional manometry [124]–[128], especially in men compared to women [129]. Indeed, recent papers on HR-ARM have suggested that new standards and limits are needed for HR-ARM based on the catheter type and size to address systematic differences in pressure measurements [128], [130].

Three main reasons possibly resulted in the difference between recorded AS pressures using DM and HR-ARM. The first is the hypersensitivity of HR-ARM in squeeze test [127], [128], [130], which could be due to the relatively high bending stiffness of its probe. Any bending of the probe due to posterior movement of the anterior rectal wall would cause the HR-

ARM probe to measure high tissue contact stress (force per unit area) in the vicinity of its tip, where the shaft is bent over the anorectal angle, as well as at the anal sphincter, rather than just measuring fluid pressure within the AS or rectum [131]. On the other hand, although the sensors in the DM probe are supported by index finger tissues, the finger can be purposely relaxed to adopt the shape of the anorectal angle thereby reducing tissue contact stress. Therefore, the reason that DM measured smaller pressure change than HR-ARM in three activities (Table 8) was because the pressure sensitivity of the sensors were detuned by thickening the silicone layer over the sensor dies in order to improve their sensitivity to lower pressures. Whereas, the Bland-Altman analysis treats the HR-ARM as the gold standard measurement, it can be concluded that these results corroborate the literature suggesting HR-ARM has its own measurement biases caused by its having a catheter that is stiffer than the anorectum in bending.

The test of the secondary hypothesis showed that the change in the relative myoelectric activity of the PR muscle measured by the electrode at the distal end of the examining finger was proportional to the pressure change in the AS pressure during maximum squeeze maneuver (Figure 52). Unfortunately, the examining finger tended to often be partially expelled during attempted defecation making the PR muscle myoelectric measurements unreliable.

The combined pressure and myoelectric activity data provided by DM enables the identification of dyssynergic defecation caused by poor coordination of the abdominal wall and anorectal muscles. More specifically, dyssynergic defecation is identified by paradoxical contraction of anal sphincter muscles when simulating defecation. Simulated defecation is the attempt to expel either the inserted DM or the HR-ARM probe. In a normal defecation, the intra-rectal pressure (P_1 in the DM) rises and the sphincter pressures (P_2 or P_3) decreases. If the patient paradoxically contracts his/her anal sphincter, the anal sphincter pressure would increase instead. Therefore, a positive pressure change in the anal sphincter during simulated defecation suggests that the patient has dyssynergic defecation. Moreover, in contrast to the normal defecation, the myoelectric activity of the puborectalis muscle measured by DM does not reduce. To make sure this was a real finding, he/she was asked to repeat the simulated defecation maneuver at least three times in case the patient mistakenly had performed the maneuver incorrectly. A primer of DM and HR-ARM results indicative of dyssynergic defecation can be found in Table 12.

Table 12. AS pressure change from rest to activity measured with DM and HR-ARM; positive changes represent dyssynergic defecation.

	AS pressure change [a]		
Subject	**DM**	**HR-ARM**	Defecation Type
1	8.0	15.4	Dyssynergic
2	-30.5	-34.6	Normal
3	-36.7	-36.3	Normal
4	-8.2	-6.3	Normal
5	-13.9	-5.2	Normal
6	-18.0	-12.1	Normal
7	-21.6	-6.9	Normal
8	13.0	15.1	Dyssynergic
9	-2.8	-20	Normal
10	44.2	28.2	Dyssynergic
11	-20.0	-7.0	Normal
12	22.5	5.0	Dyssynergic
13	-18.3	-18.1	Normal
14	-29.5	-16.8	Normal
15	36.6	15.0	Dyssynergic
16	13.6	16.3	Dyssynergic

[a] units are in (mmHg)

The comfort surveys from the participants suggest that DM provides comparable levels of comfort and usability even though the HR-ARM probe was a quarter of the diameter of the DM covered index finger (Table 10). The lowest score received by DM on any of the five variables was 7 out of 10, whereas HR-ARM was a 4 out of 10. The slightly higher average score of DM on the smoothness could be due to the silicone cover layer over the instrumentations of the glove.

6.4.1. Limitations

Sample size

A major limitation of this feasibility study was the small sample size in each group. Since this was a feasibility study, healthy subjects were studied as controls along with two common patient types. The data showed that it is feasible to mount pressure sensors on the index finger, obtain meaningful measurement of anorectal pressures, and observe paradoxical contraction of AS muscles during simulated defecation. More subjects in prospective DM studies are needed to corroborate and extend the present results and define normal pressure ranges [126], [132], [133].

Probe size

A second limitation was the use of one DM and one HR-ARM observer; although the intraobserver error were calculated, the interobserver error was not obtained for either modality. The use of the single observer also meant that the effect of different index finger diameters and lengths on the DM measured pressure recordings could not be examined. Although the breadth of the PIP joint of this examiner was 19 mm, pressure recordings of AS muscle using a rigid 20 mm diameter probe can average 37 mmHg and 50 mmHg higher than with a rigid 4 mm probe [134] during rest and maximum squeeze. The fact that on average the DM readings were 7.1 mmHg less relative to HR-ARM suggests that the compliance and shape change of the finger in the glove can compensate for the effect of the finger having a larger diameter than the 4 mm probe. There is also the possibility of measurement artefact in the ARM data causing increased pressures if the rectal tissues tend to bend the probe tip over the anorectal angle, which would increase ARM-recorded pressures at the anorectal angle and anal sphincter. In terms of DM, one can anticipate a range of clinician index finger mean diameters ranging from 1.8 cm to 2.3 cm [135], so future studies should examine the effect of examiner digit finger diameter and anthropometry on measured anorectal pressures. It may be possible to create a look up table or nomogram to interpret the measured pressures. Clearly, additional studies are needed on the effect of probe diameter on measured pressures.

Movement of probes

A third limitation was the axial movement of either probe away from the AS high-pressure zone during the maximum squeeze and simulated defecation maneuverers. In HR-ARM, the recordings show that the region of high pressure moves about 1 cm proximally on the catheter during the maximum squeeze. Similarly, in DM, although the examiner tried to minimize the probe displacement from the high AS pressure zone, some sensor movements relative to high-pressure zone was inevitable because the examiner can never exactly match the movement of the patient's anorectal complex. This is reflected in the finding that 1 cm displacement from high pressure zone in the AS can result in a 30% reduction in pressure reading [134]. Therefore, both systems were susceptible to movement artifact, but the advantage of the HD-ARM is that it provides redundancy by multiple measurements over a longer length of the probe. Such redundancy in the number and arrangement of sensors can be incorporated in future DM systems. Similarly, there were errors due to the flexion and extension of the DM probe, especially on the tip pressure sensor (P_1). Although the middle pressure sensor of the DM (P_2) was faced medially and it was less affected by the flexion of the digit, other sensors were prone to such error.

Effect of Straining

A fourth limitation of this study revolves around using the measured intrarectal pressure to control for straining during maximum squeeze efforts. This is possible for both DM and HR-ARM systems. However, the correlations between the DM and HR-ARM was actually lower after subtracting the intrarectal pressure than when it was not subtracted. This reduction in correlation was mainly due to measurement artefact on the intrarectal pressures recorded by the HR-ARM probe being bent over the anorectal angle, especially during the maximum squeeze attempts. It is also possible that too much fingernail counter pressure against the rectal wall could inflate the DM measurement of intrarectal pressure. However, the operator can be trained to flex their finger in the anorectum to avoid this artefact.

Since DM probes are disposable, they eliminate the risk of patient-to-patient transmission of infection compared with HR-ARM. Even though the HR-ARM system provides detailed spatial pressure recordings throughout the AS complex, it can be cost prohibitive for many patients and health care providers. Therefore, if validated by others, DM could provide an inexpensive anorectal screening modality for a provider to determine next best steps for a patient with dyssynergic defecation or fecal incontinence. For example, if DM is abnormal, a provider might decide to refer the patient to a tertiary medical center or perhaps directly to biofeedback and pelvic floor physical therapy. Clearly, further studies will also be needed to determine how best to use the information provided by DM.

6.5. Conclusions

DM provided comparable recordings of resting AS pressure, as well as the important changes in anorectal pressures during prescribed activities, as HR-ARM. Further validation requires larger sample sizes, and interobserver differences should be examined. Also, DM myoelectric data could help identify paradoxical contraction of the AS and PR muscles suggestive of dyssynergic defecation. Finally, the two systems had similar comfort levels despite different probe diameters.

CHAPTER 7

General Discussion

It is clear from the foregoing chapters that there is more complexity to the structure-function relationships of the urethra than is often appreciated. While the general structure is known, there are still many finer structural details that remain obscure, such as the attachment locations of the longitudinal smooth muscle, as does the overall control of the different substructures of the urethral sphincter only hinted at by the systems diagram in Chapter 1. Therefore, the first subject-specific urethra model of the urethra (Chapter 2) with its individual muscles capable of contracting along their fiber directions or lines-of-actions necessarily had to contain many simplifications. Although the contribution of the periurethral muscles and fascia to the continence mechanism is explored in other studies, the role of individual muscle layers to continence had not even been calculated theoretically. As discussed in Chapter 2, it was found that the striated muscle was 3 to 4 times more effective in contributing to the closure pressure than the smooth muscle. A contrasting finding was the role of longitudinal muscle that counteracted the effect of circular muscles in constricting the urethra. In fact, in the single subject-specific urethra model that was studied in this dissertation, the longitudinal muscle not only reduced the closure pressure, but also shortened the urethral length. These results suggested that longitudinal smooth muscle has a role in initiating the micturition process.

The simplified sub-model of a portion of the length of the proximal vascular plexus urethral layer in Chapter 2 represents a first attempt to understand how the plexus provides a hermetic seal and affects continence, based on the interactions between the vesical and effective arteriovenous plexus pressures and the elasticity of the plexus layer. But unfortunately there was not time to integrate this model into the larger subject-specific multiphysics model of the urethra. However, the tissue mechanics simulation did hint at how functional urethral length may be a function of those pressures. Nevertheless, it did not fully explore the effects of age and disease on this function, which may be important. For example, to model the effect of aging on the striated muscle, a better method was to construct a new geometry from an old woman rather than considering the posterior portion as a connective tissue. Aging also affects the number of fibers [66], [97] in all layers and therefore material properties would also change. Perhaps a more detailed method to simulate the effect of aging, disease and injury would be to use the Holzapfel-Gasser-Ogden model [136].

Future models will also need better data on vascular pressure and flow rate scenarios, perhaps made via Doppler ultrasound, in order to understand this structure's function better. Certainly, a major limitation associated with the vascular plexus model and the associated system diagram may be the over-simplification in modeling the remarkable vascular plexus layer. According to Huisman [61], the tortuosity of the pressurized veins of the arteriovenous anastomoses (AVA) plexus may play a significant role in sealing the urethral lumen by both acting as viscoelastic springs in the longitudinal and radial directions. This most interesting feature of the vascular plexus could unfortunately not be addressed in the simple vascular plexus model that was developed with its uniform blood filled layer. The current MR scan used to create this 3D model was selected from a series of MR scans from different women. After checking those scans, it was noted that there were dimensional variations between urethras. So one should study different urethral scans, classify them, and build more 3D models to see if the same results would be obtained.

Another simplification of the urethral model in Chapter 2 was that it did not include the bladder or the compressor urethrae muscles. The inclusion of the bladder would obviously be important in better understanding urge and mixed incontinence. Finally, the role of urethral support, which has figured so prominently for the past decades was not addressed. This was because we believe the function of the urethra is at least, if not more important, than urethral support in providing continence, as discussed in Chapter 1.

The urethral system diagram (Chapter 1) only hints at the complexity of the neural control of continence and completely omits all that is known about the sympathetic and parasympathetic control of continence. Thus, one might consider combining other physics and domains with the present urine-tissue (fluid-solid) interaction model of the urethra to create a holistic model of LUT, which can then be used to better understand LUT dysfunctions and pathologies.

The latter also highlights and combines with the second limitation, which is the lack of relationship between the recruitment intensity of muscle, its material stiffness and its stretch ratio, which is also due to the lack of material property data of the live urethral tissues. These may be able to be measured via ultrasound shear wave elastography, for example, and could help reveal, for example, whether a particular smooth muscle layer only contract to a certain strain limit, rather than simply assuming they can maximally contract up to 60% of resting length.

Finally, the detailed contribution of urethral support structures was simply represented by a constant elastic foundation instead of active elements. The focus of the presented model was on the urethra and UCP only; however, although UCP is an important factor in SUI, the lower urinary tract is a complex system and isolated tissues cannot accurately be studied in isolation.

To validate the output of the system diagram model, i.e., quantifying the timing and amount of urine leakage, a wearable PUF was presented in Chapters 3 and 4. The PUF is a new tool which was invented, developed, and tested and should help take uroflowmetry to the next level by providing activity-related information. It does so by simultaneously providing data for two overall blocks in the presented system diagram: 1) the inertial movements of body, and 2) urine leakage or micturition volume, the final output of the urethral system diagram without a catheter. In future studies, the PUF can be used together with an intravaginal pressure sensing device [137] to better understand pressure-flow relationships. With an additional IMU mounted on (or even intravaginally in) the abdomen, the entire system would present new opportunities for investigators to further study the coordination of the pelvic floor complex.

If we consider the studies performed on the Knack maneuver [138] and the fact that PUF can provide real-time feedback to the SUI patients may allow researchers to design and carry out an intervention study to test the capability of the PUF in reducing leakage frequency and severity. How? With the real-time audible or haptic feedback information of leakage incidents provided by PUF, patients would gradually become aware of activities and postures which result in leakage through knowledge of results. Consequently, they can learn to alleviate or even prevent the leakage by performing the Knack maneuver or at least limiting movements causing the leakage episodes.

Moreover, although the UI prevalence in male population is one third of female one, PUF can be modified to be used by men by adhering it to the penis or fitting it on the end of a condom, therefore male UI patients can also benefit from PUF.

As mentioned in the patent application, different sensors can be implemented in the same funnel housing to measure salinity of the urine, the existence of specific proteins, or bacteria, for example. This potentially makes the PUF a wearable urinalysis device that could be useful for monitoring fluid status in critically-ill, cognitively impaired, or hospitalized patients via continuous monitoring and even warning of bladder infections. However, to do this would require it to be improved to adhere for at least a 12-hour nursing shift in the hospital to be practical and economically viable.

An overall weakness regarding the Chapters 2 through 4 was the use of PUF device to validate the urethra model developed in the Chapter 2. Although PUF was tested on few incontinent patients, unfortunately, it was not tested on the subject on whom the urethra model was based.

Finally, in adult incontinence (AI) products industry, quantification of both urine leakage flow rates and leakage volumes is important. This is because large urine flow rates can exceed the ability of certain AI products to absorb them. If absorbent pads cannot absorb the fluid fast enough, it caused the urine to flow beyond the pad to the lower limbs and onto clothing, sometimes with absolutely humiliating results for the patient. Considering the business model of such companies being a marginal profit on large number of inexpensive products, the design needs to have just enough absorbent material without causing bypass leakages to the clothing. Therefore, results provided by the PUF device would be useful for those industries.

Although the PUF has shown potential, it still needs improvements in certain aspects. The major challenge is the attachment of the sensor housing to the mucosal tissue lining the inner surface of the labia majora. With the latest sensor housing design, the housing can stay adhered for up to two hours on the body without any detachment. The desired four-hour attachment could not always be achieved without partial minor detachment and the risk of bypass leakage. Besides, in some patients, sudden discharge of the urine during micturition can also cause bypass leakage and eventual detachment. The early investigations on replicating ‘dry adhesives’ [101], [139], inspired by octopus tentacle suckers. for this application suggested that there is still a need for a better dry adhesive, mucoadhesives or bioadhesives [140] to help secure the attachment during ADLs. A backup idea would be to partially adhere to the skin on the outside of the labia instead of, or in addition to, the mucosa on the inside.

Although the shape of the collection funnel of the PUF has been improved iteratively over about 40 iterations, the challenge of quite different labial anatomies means that one shape and size does not necessary fit all anatomies. Usually there is a trade-off between the comfort and performance aspects of a design which cannot be brought together into one universal form. For example, a design that fits well in a high BMI patient may not necessarily be suitable for a low BMI patient. Or it may serve a sedentary individual well but not stay adhered to a woman training in high acceleration activities such as running.

Another limitation was the difficulty of attaching the device to women with prolapse. Recent testing on the attachment of the passive housing demonstrated that prolapse moves the position of the sensor housing downward away from the vestibule to the labia majora upon assuming the standing posture. In fact, often, the labia majora tissues provide additional support in patients without prolapse. Considering the significant overlap of the UI women with women who have prolapse, this attachment challenge must be addressed so that the PUF can be used by the entire UI population.

The survey results showed significant improvement in the comfort levels of the device, however, while most panelists have reported no discomfort, there were still some patients who could not tolerate having the unit attached over their urethral meatus.

Finally, with the current attachment method, while a registered nurse or clinician can install the unit, a patient cannot attach the device by herself. This likely limits the use of the device to labs, clinics, hospitals, and elderly care facilities. It is not yet a device that any woman can wear and use at home. For men, it may be easier to create a PUF that would work for most individuals in a self-use situation.

This modeling technique and system diagram presented in Chapter 2 can be extended to other nearby sphincters, muscles and tissues in the pelvic floor. As an example, the anorectal complex can also be modeled in a similar fashion, providing opportunities to further explore the mechanisms underlying fecal continence and related defecatory dysfunctions in silico. In the ultimate version, one can imagine studying the dual incontinent patients i.e., both UI and FI, who represent about 6% of the total female population [141]. In addition, for additional validation the DM wearable can be used (Chapters 4 and 5).

The DM device provided comparable pressure measurements of the anal sphincter at rest and simulated defecation with a gold standard device at an order of magnitude lower cost, and superiority of providing myoelectric data from anorectal muscles. Every physician knows how to conduct a detailed rectal examination (DRE) but the results of DRE are considered subjective. This office-based wearable device provides additional objective information on anorectal coordination.

DM can also be used by other researchers and clinicians in physical exams when detailed objective information is needed through palpation, for example, in pelvic floor examination by obstetricians and gynecologist. DM also helps provide detailed objective data via the myoelectric probes and pressure transducers, increasing the positive predictive values in assessing the extent of spine injuries [72]. Overall, DM proved the feasibility of physicians using instrumented wearables to provide point-of-care information at a lower cost.

Most of the DM limitations are described in detail in the Chapter 5. To summarize, so far, the limited number of subjects in testing the performance of the DM device was the key limitation. A larger number of subjects could either make the limits of agreement smaller or may reveal a systematic difference from the gold standard HR-ARM. Our study clearly revealed the effect of the diameter difference between the two probes on the results. A nomogram or conversion table could be provided to interpret the DM results in terms of a standard scale, thereby ensuring different index finger anthropometries of examiners would not affect the accuracy of the measurements. Lack of impedance matching circuitry would reduce the sensitivity of the amplifier circuitry especially when the anal canal was not fully prepped before the study. That translates into results which are not necessarily normalized across subjects. This point should be addressed when DM is used on a large scale.

Overall, the urethral model and the two proposed devices (PUF and DM) provide new capabilities for investigators to obtain better insights into pelvic floor function and dysfunction. The feasibility of the proposed solutions has only been examined so far, and further testing and improvements are needed for them to become reliable for clinical use. They may eventually provide the means to quantify certain failure mechanisms in the sphincters that cause incontinence or lower urinary tract symptoms.

CHAPTER 8

Conclusions

- The system diagram approach was used to test the overarching hypothesis and address the knowledge gaps.
- Better tools for measuring and understanding pelvic floor sphincter function and dysfunction than are available today were presented.

Chapter 2

- STM contributed the most to the UCP and three times more than the CSM.
- LSM made no contribution to the UCP and only shortened the urethra.
    - The simulation results still need validation via results from experimental tests.
- The posterior connective tissue of the STM resulted in reduction in maximum urethral pressure especially on the posterior wall side.
- The effective vascular pressure between the arterial and venous pressures in vascular plexus layer, relative to intravesical pressure, contributes to functional urethral length.

Chapters 3 and 4

- It was feasible to design a personal uroflowmeter (PUF) that comfortably fits between the labia to measure urine flow rate and leakage or voided urine volume (from 1 droplet to 40 ml/s).

- The experimental PUF flowmetry error in measuring micturition and leakage episodes was 5% and 18% with respect to the gold standard reference (i.e., scale and the AI pads weight difference respectively).
- It was possible to record and identify the physical activity of the wearer and correlate the leakage with that activity during daily living. There was face validity in that a waist-mounted wearable activity sensor output correlates with the volunteer's subjectively recorded physical activity.

Chapters 5 & 6

- It was possible to design and build a disposable wearable point-of-service device to measure pressures of the anorectal sphincter an order of magnitude cheaper than the gold standard high-resolution anorectal manometry.
- There was a correlation between myoelectric activity of puborectal and the external anal sphincter muscles.
- There was no difference in comfort reported by individuals undergoing DM and HR-ARM.

CHAPTER 9

Suggestions for Future Research

Following points are suggested for the future work:

Chapter 2

- To further validate results, urethral sensorimotor assessment tools should be used. To measure the urethral closure pressure either a T-DOC with inflatable sleeves (Laborie, Ontario, Canada) or micro flexible fiber optic FISO (Quebec, Canada) micro-catheter can be used.
- With the help of an intravaginal Doppler ultrasound probe, it may be possible to measure changes in muscle layer thickness, and especially the thickness of the vascular-mucosal core, as well as the relative timing of these events in micturition or cough, say. Finally, it may be possible to tetanically stimulate either the striated or the smooth muscle of the urethra via transvaginal electrical stimulation.
- To better model the fibers in the distal ends of the LSM
- Improved methods to simulate striated muscle contraction considering the tissue stiffness, stretch ratio and material properties relationships.
- Consideration of the velocity dependence in muscle contraction (i.e., viscoelasticity).
- Inclusion of the detailed remarkable vascular plexus layer in the model.
- Inclusion of luminal tissue coaptation
- Validation needed of each muscle layer's contribution via electrical stimulation.

Chapters 3 and 4

- Development of a better dry, muco- and bio-adhesives for the PUF attachment
- Improving adhesion times to 12-hour nursing shifts.
- Adapting the design of the PUF device for males.
- Using PUF device in a Knack intervention study test the efficacy of the PUF in providing real-time feedback and reducing the leakage incidents in SUI patients.
- Developing a better determining unit circuitry insensitive to the temperature changes.
- Incorporating new micro-fabricated flow sensors with higher dynamic range accuracy.
- Use of alternative current excitation to increase the life of the sensor filaments.
- Incorporating new flowmetry methods such as optical sensing
- Developing a more energy efficient instrumentation and sensor technology to wirelessly power the flow sensor.
- Better signal processing to increase the accuracy of transient responses and reduce the errors in quantifying the leakage volumes.
- Testing the PUF device with more patients to confirm its performance.

Chapters 5 and 6

- Testing the DM device with larger cohort to verify the performance of DM against the gold standard HR-ARM.
- Testing the DM device with multiple examiners with different hand anthropometries to find the effect of the index finger size on the results. This will provide and standardization protocol to normalize DM results, which can also be helpful comparing results with the results of the gold standard HR-ARM.

- Testing the DM device in other clinical exams involving palpation, such as in pelvic floor examination.

APPENDICES

Appendix I

Labial Reservoir

1. Introduction

This appendix describes mainly the modeling of the volume between the labia majora - called the vestibule - which can be filled upon leakage of urine from the urethra (Figure 53).

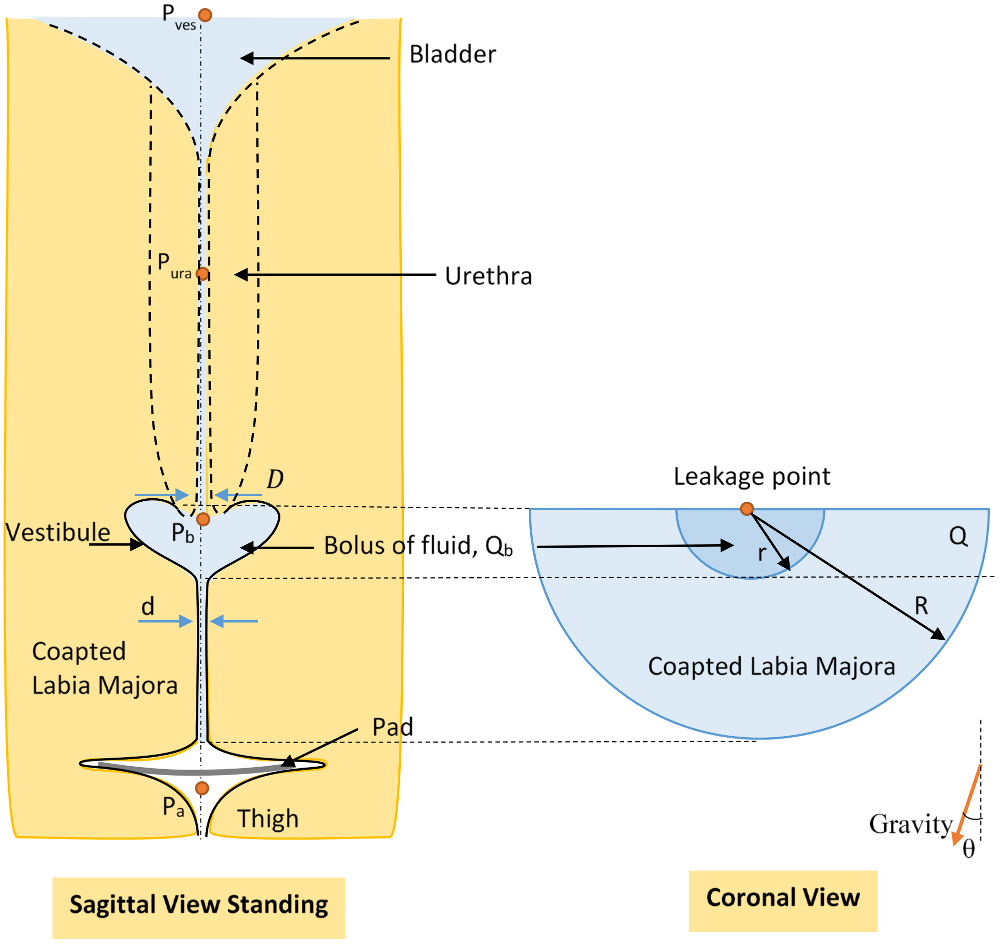

Figure 53. Sagittal view of a frontal plane section through a model of the urethra and labia majora in standing posture (left) and a lateral view of a mid-sagittal section through the model showing the reservoir (dark blue) and leakage path (arrow) through the initially coapted labia (right).

Examples are during a sneeze or lifting a heavy object while sitting, and emptying to atmosphere at a later time during an activity of daily living (ADL), such as getting up from a chair. In analyzing the results of the ambulatory uroflowmeter (PUF) designed and tested in Chapters 3 and 4, this phenomenon could explain the delay between the activity causing the passage of urine through the urethra and the (later) time of the evident urine leakage from the labia. Also, knowing where urine would end-up after leakage is crucial for the manufacturers of adult incontinence products (AI) to improve the efficacy of their product designs.

2. Method of Modeling the Labial Vestibule

The volume of this vestibule can be modelled using a similar technique used in Chapter 2 for modeling the pelvic floor tissues. MR scans of a pelvic floor of a supine woman in coronal (Figure 54) reveal the boundaries of thighs, external genitalia as well as inner mucosal tissues. Using the same segmentation technique (Figure 55), and stitching them together, the 3D volume of the vestibule between labia can be visualized (Figure 56). Moreover, other main skin clefts and folds such as intergluteal cleft and labiocrural fold (Figure 57) can also be segmented and modelled. These folds and clefts can also play a role in determining the leakage path and change in the direction of the path of the leaked urine with changes in posture (i.e., supine vs standing). Finally, a simplified surface model for FE analyses was created (Figure 58).

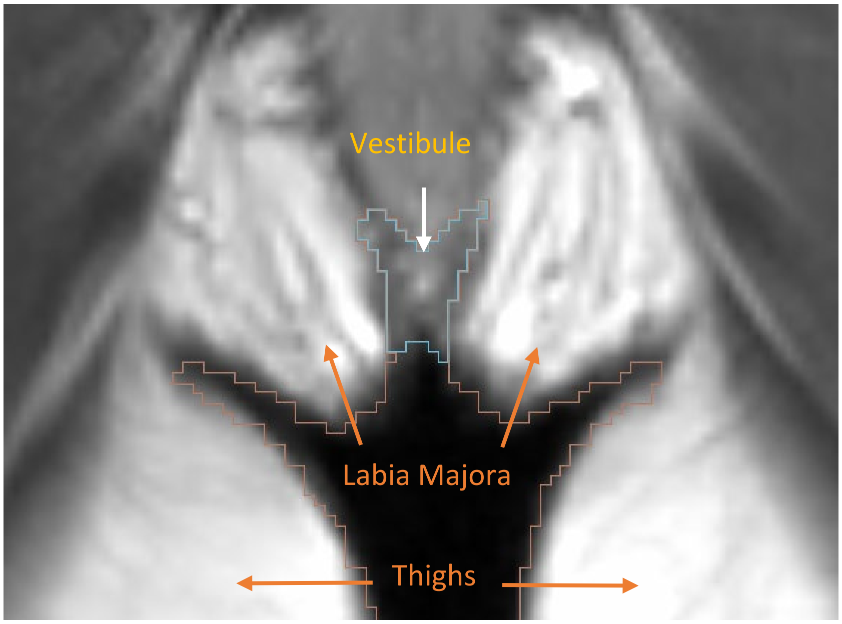

Figure 54. Coronal view of an MR scan of an adult woman showing the labia, thighs, and overlaid segmentation of vestibule volume (blue outline) and skin surface (pink outline).

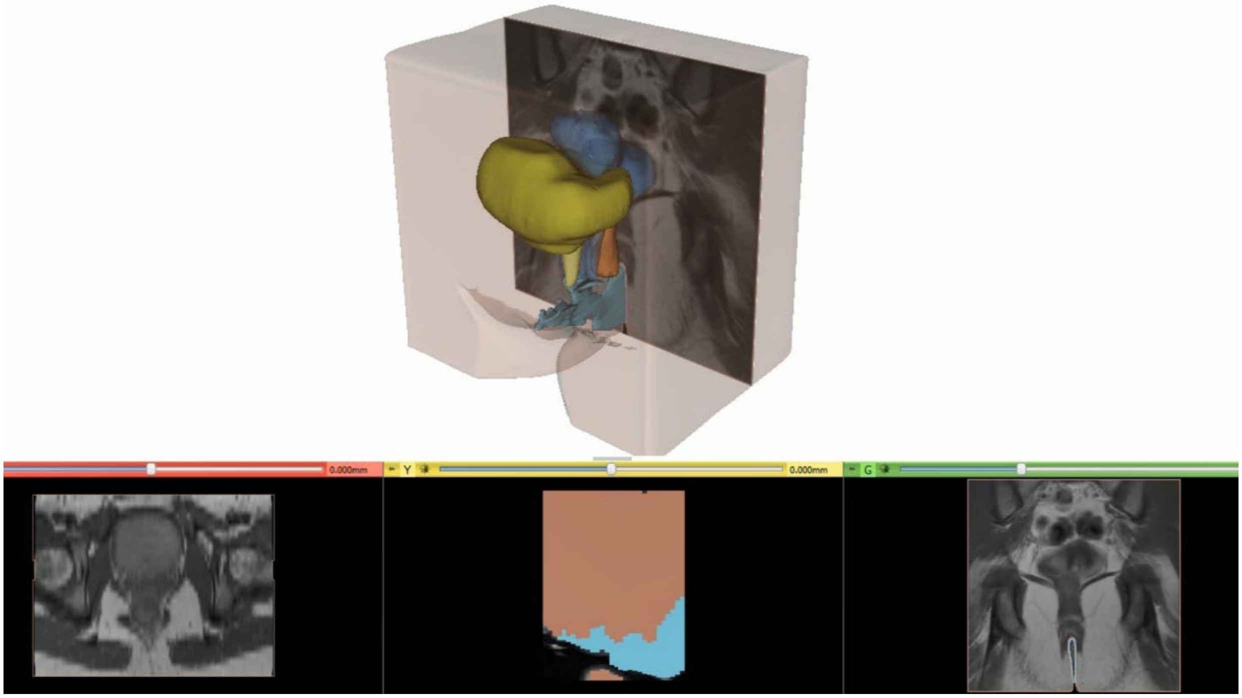

Figure 55. Snapshot of the 3D Slicer® application used to construct vestibule volume using MR scans from an adult woman. 3D views (top) along with axial, sagittal, and coronal views (bottom left to right) were used to create 3D volumes.

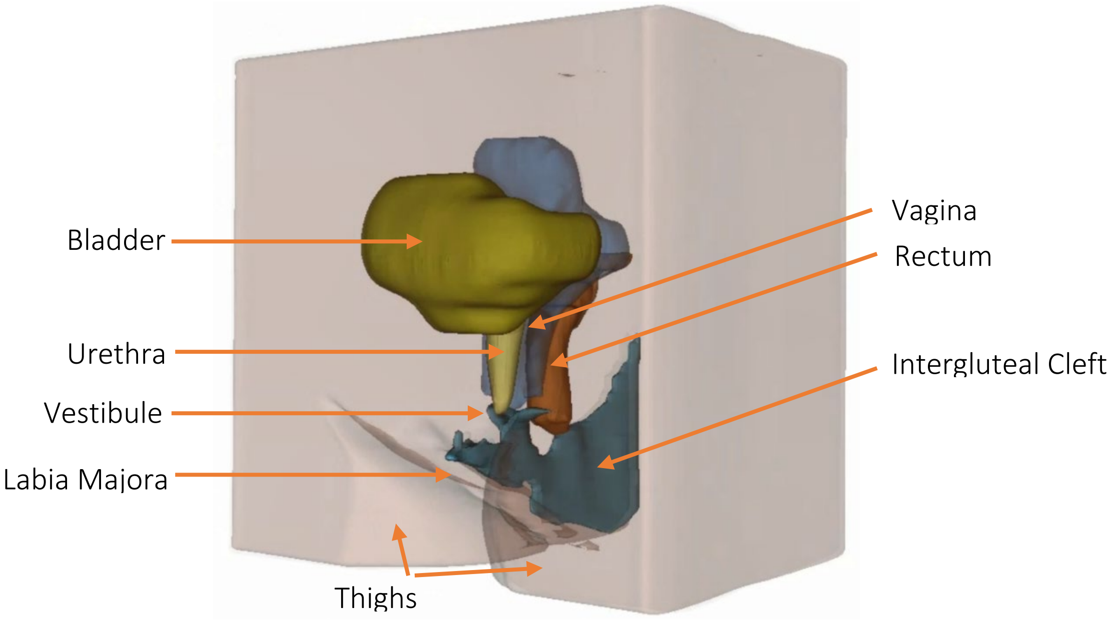

Figure 56. An example of the constructed 3D model (bounded by a box in 3 directions) that includes the vestibule volume and intergluteal cleft (teal), bladder and urethra (yellow), vagina (blue), rectum (orange), and skin surface (labia and thighs).

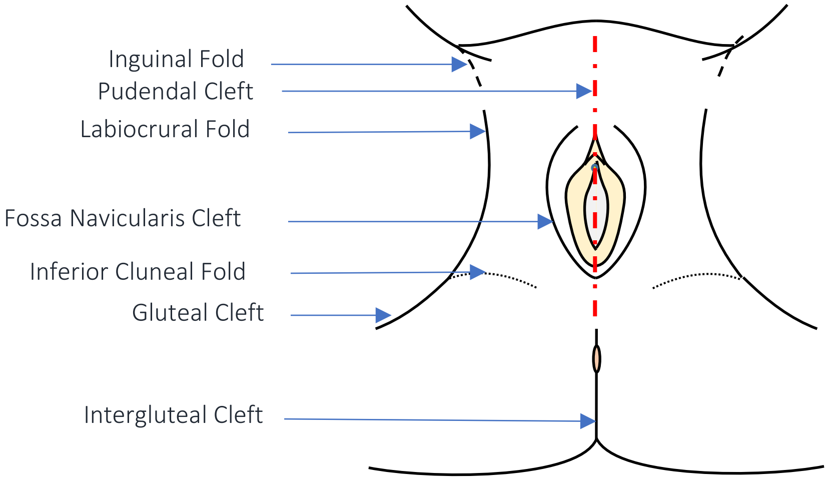

Figure 57. Schematic drawing showing the main clefts and folds around the female external genitalia shown in lithotomy position. Depending on the posture, these folds can change the direction of the urine leakage on the body.

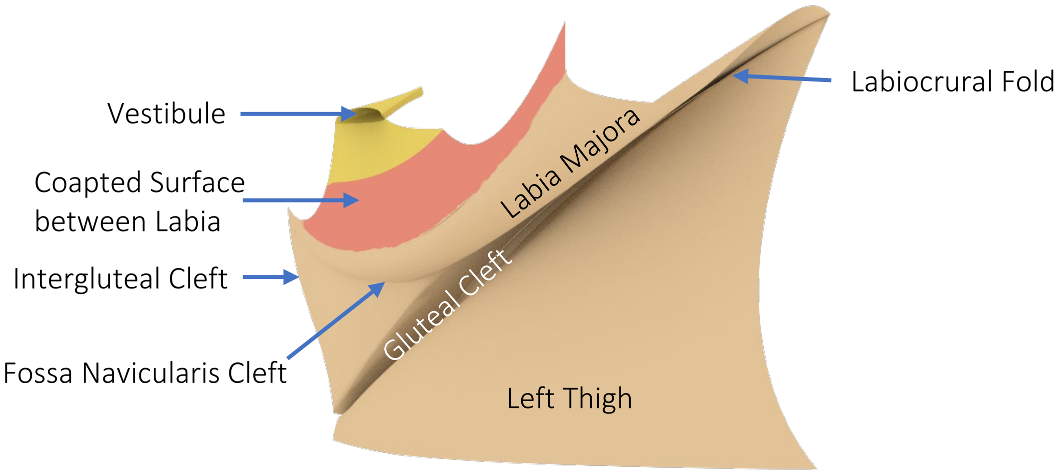

Figure 58. A simplified non-uniform rational B-spline (NURB) surface model of the external genitalia and thighs are created from the 3D meshed volumes, which is useful for the further FEM analyses of the effect of posture on fluid leakage paths. The clefts and folds that are modeled will likely modulate the urine leakage dynamics by transferring the leaked urine droplets posteriorly along the intergluteal cleft or anteriorly toward the clitoris depending on whether the woman is lying on her back or front.

3. Discussion

Due to coaptable mucosal inner surfaces of the labia majora and how specific postures (e.g., sitting) result in coaptation of those labial surfaces, an alternative path of leakage forms either posteriorly toward anus, or anteriorly towards clitoris due to the hydrostatic pressure differential. Moreover, clefts and folds around the external genitalia are expected to play a significant role in modulating the leakage dynamics and paths. Other possible flow channels, caused by the folds and clefts, are depicted in the Figure 59. Identifying these leakage paths is beneficial in optimizing the design of adult incontinence products.

This analysis begins to explain why urine that is leaked from the urethral meatus does not necessarily always pass immediately beyond the labia to an incontinence pad, clothing or the rest of the body until a later change in posture. Changes in the pose of the torso relative to gravity (supine, prone, sitting), changes in the distance between the thighs that can change how much the labia are compressed together, or changes in the orientation of one or both thighs relative to the torso can affect whether or not the labia remain coapted sufficiently to block a urine leakage path along one or more of the fold lines.

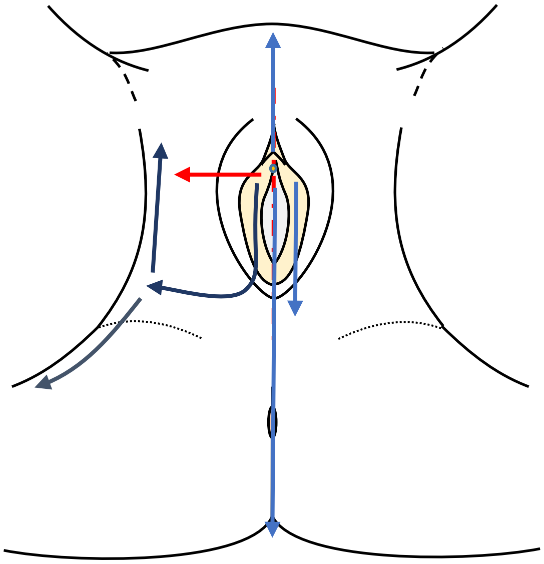

Figure 59. Possible leakage path along major clefts and folds; dripping downward directly (red), following intergluteal cleft posteriorly toward anus or anteriorly (light blue), or following clefts and folds around thigh (dark blue).

Appendix II

Personal Uroflowmeter (PUF) Determining Unit Circuit

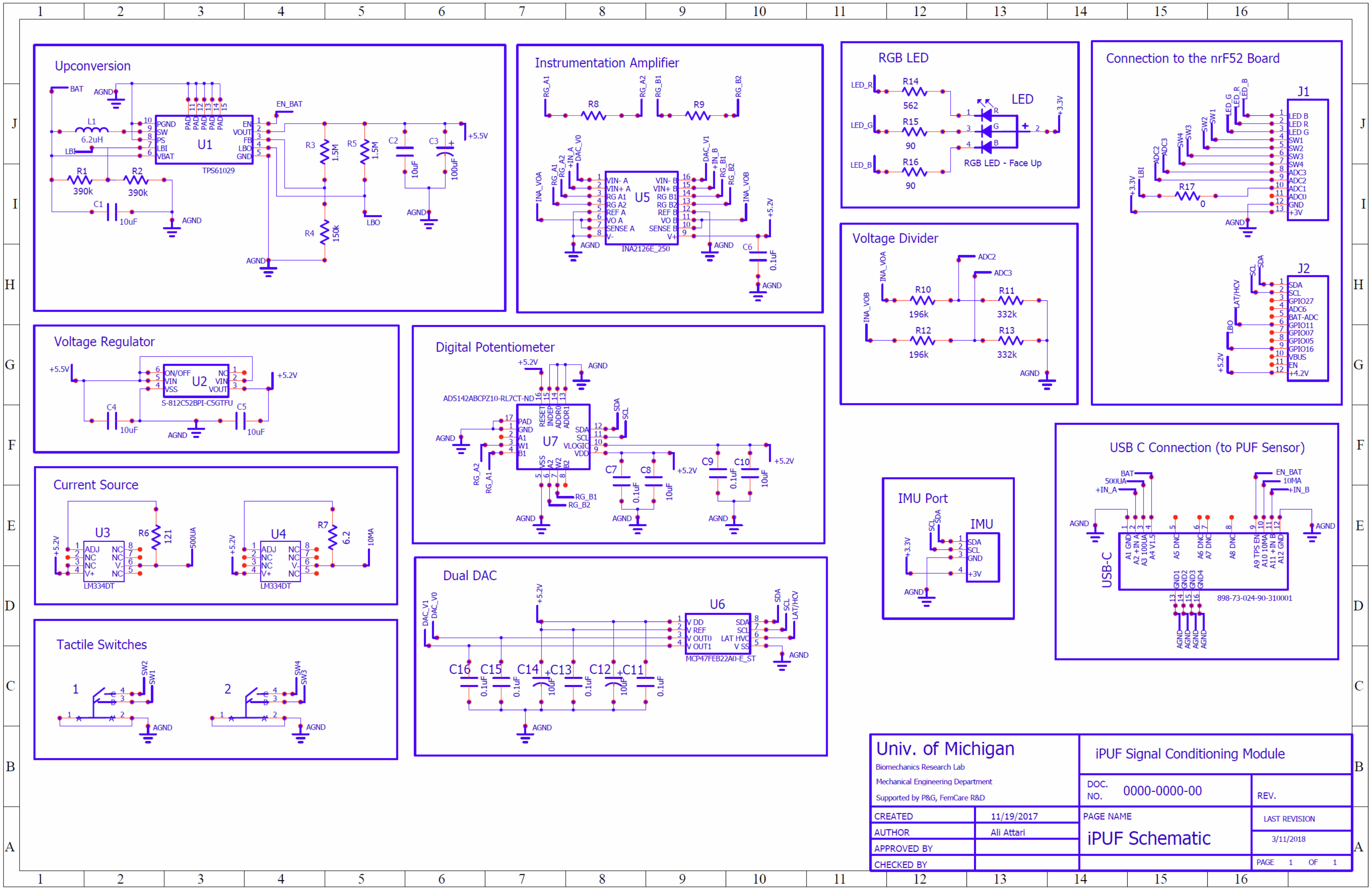

Figure 60. Schematic of the main board of the determining unit of the PUF used with Feather NRF52832 and NXP Precision 9DoF IMU (both from Adafruit®, New York, NY, US).

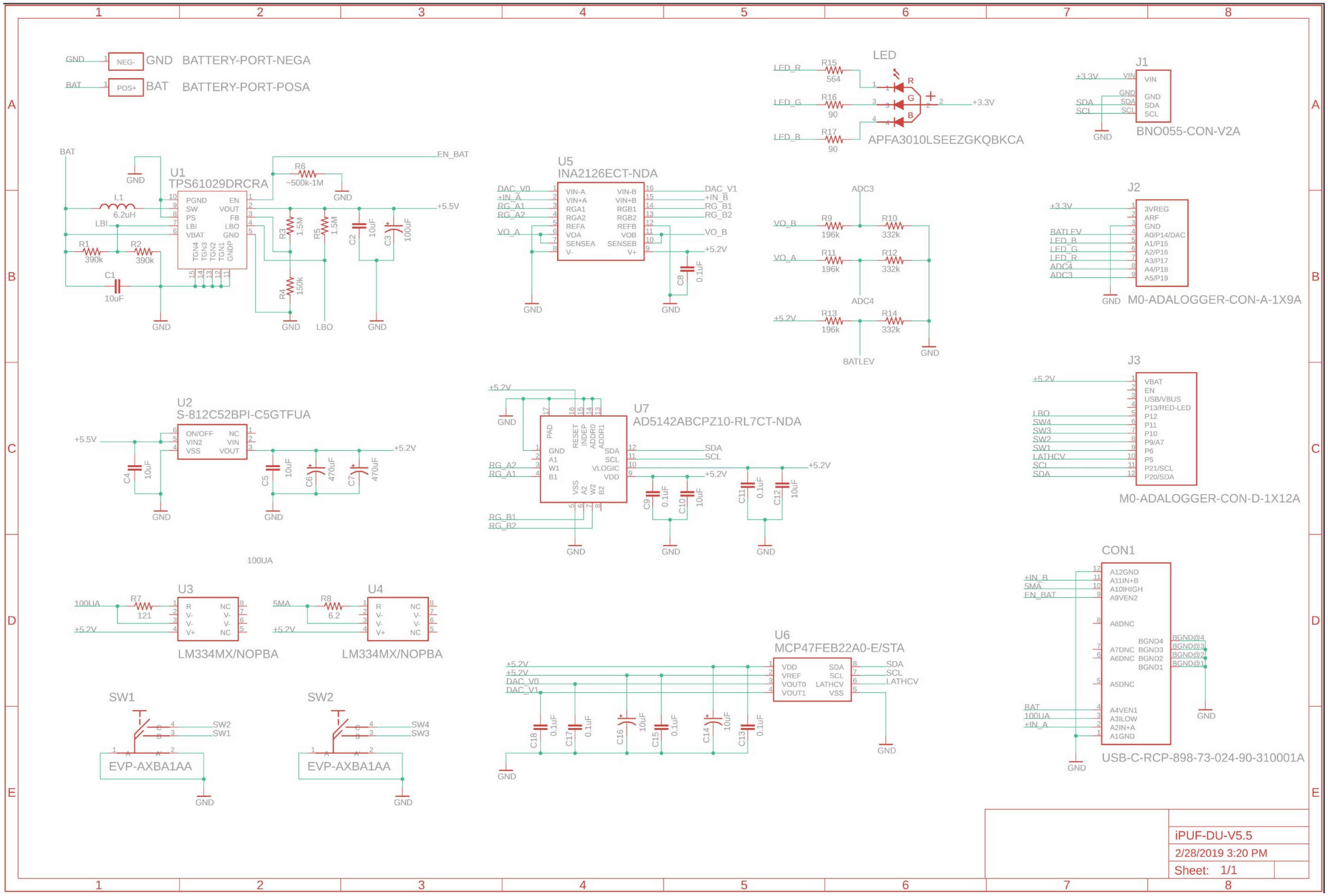

Figure 61. Schematic of the main board of the determining unit of the PUF used with Feather M0 Adalogger and BNO055 Absolute Orientation Sensor (Adafruit®, New York, NY, US). This board was used in the third and fourth study sessions where subjects left the facility.

Appendix III: Digital Manometry (DM) Determining Unit Circuit

Schematics of the portions of the wrist-mounted determining unit hardware that involved the pressure and myoelectric signal processing are show in the Figure 62.

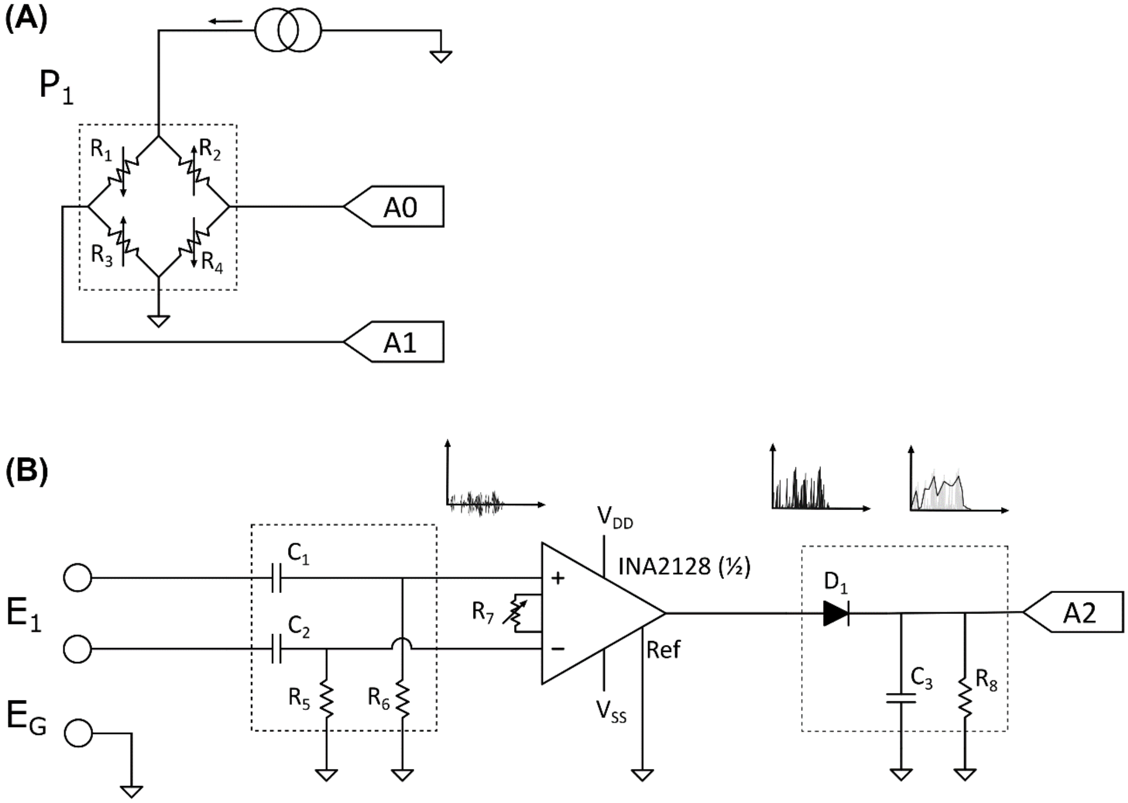

Figure 62. A) Schematic of the pressure sensing circuitry for each of the pressure sensors (i.e., $P_{1\text{-}3}$). A 5 mA constant current source powers the piezo-resistive (P1602) pressure sensor. The following values were used for components: R_1, R_2, R_3 and R_4 = 5 kΩ. A0 and A1 were connected to a 12 bit analog to digital converter. The difference of A0 and A1 signals changes linearly with the pressure. The difference voltage was large enough to be measured directly using the analog to digital converter. B) Simple schematic of the myoelectric signal amplifier for the myoelectric electrodes (i.e., E1-2). EG represents the body ground electrode. Signals were passed through the first order high pass filter (fc = 186 Hz), amplified (INA2128), rectified (D1), and finally modulated using a simple RC envelope detector (C3 and R8). A2 is another 12 bit analog to digital converter. The following values were used for components: C1 and 2 = 22 nF, R5 and 6 = 39 kΩ, R7 = 20 Ω, C3 = 4.7 µF and R8 = 10 kΩ. The input pins of the INA2128 are automatically protected from electrostatic discharges via the hardware design.

REFERENCES

[1] E. C. Chong, A. A. Khan, and J. T. Anger, “The financial burden of stress urinary incontinence among women in the United States,” *Curr. Urol. Rep.*, vol. 12, no. 5, pp. 358–362, 2011.

[2] K. S. Coyne, A. Wein, S. Nicholson, M. Kvasz, C. I. Chen, and I. Milsom, “Economic burden of urgency urinary incontinence in the United States: A systematic review,” *J. Manag. Care Pharm.*, vol. 20, no. 2, pp. 130–140, 2014.

[3] T. C. Chai *et al.*, “Future Directions of Research and Care for Urinary Incontinence: Findings from the National Institute of Diabetes and Digestive and Kidney Diseases Summit on Urinary Incontinence Clinical Research in Women,” *J. Urol.*, vol. 198, no. 1, pp. 22–29, 2017.

[4] M. E. Albo, H. J. Litman, H. E. Richter, and G. E. Lemack, “TOMUS 2 Year: Treatment Success of Retropubic and Transobturator Midurethral Sling at 24 Months,” *Curr. Drug Targets*, vol. 16, no. 7, pp. 700–710, 2015.

[5] G. Basilisco and A. E. Bharucha, “High-resolution anorectal manometry: An expensive hobby or worth every penny?,” *Neurogastroenterol. Motil.*, vol. 29, no. 8, pp. 1–6, 2017.

[6] M. Portalatin and N. Winstead, “Medical Management of Constipation,” *Clin. Colon Rectal Surg.*, vol. 25, no. 01, pp. 012–019, Mar. 2012.

[7] R. C. RITTER, N. R. ZINNER, and J. PAQUINA, “Clinical Urodynamics. Ii. Analysis of Pressure-Flow Relations in the Normal Female Urethra,” *J. Urol.*, vol. 91, no. 2, pp. 161–165, 1964.

[8] D. J. GRIFFITHS, “The Mechanics of the Urethra and of Micturition,” *Br. J. Urol.*, vol. 45, no. 5, pp. 497–507, 1973.

[9] K.-A. Backman, “URODYNAMICS-THE HYDRODYNAMICS OF MICTURITION IN

NORMAL FEMALE SUBJECTS," *Acta Neurol. Scand.*, vol. 42, no. 20, pp. 79–85, 1996.

[10] D. Griffiths, "The pressure within a collapsed tube, with special reference to urethral pressure.," *Phys. Med. Biol.*, vol. 30, no. 9, pp. 951–963, 1985.

[11] A. Chanda, V. Unnikrishnan, S. Roy, and H. E. Richter, "Computational Modeling of the Female Pelvic Support Structures and Organs to Understand the Mechanism of Pelvic Organ Prolapse: A Review," *Appl. Mech. Rev.*, vol. 67, no. 4, pp. 1–14, 2015.

[12] K.-J. Kim, "BIOMECHANICAL ANALYSES OF FEMALE STRESS URINARY INCONTINENCE," Univevrsity of Michigan, 1994.

[13] H. Yamada and F. G. Evans, *Strength of biological materials.* 1970.

[14] K. F. Noakes, A. J. Pullan, I. P. Bissett, and L. K. Cheng, "Subject specific finite elasticity simulations of the pelvic floor," *J. Biomech.*, vol. 41, no. 14, pp. 3060–3065, 2008.

[15] A. Bhattarai, R. Frotscher, M. C. Sora, and M. Staat, "A 3D finite element model of the female pelvic floor for the reconstruction of urinary incontinence," *11th World Congr. Comput. Mech. WCCM 2014, 5th Eur. Conf. Comput. Mech. ECCM 2014 6th Eur. Conf. Comput. Fluid Dyn. ECFD 2014*, no. Wccm Xi, pp. 923–934, 2014.

[16] F. S. Q. da S. Brandão, M. P. L. Parente, P. A. G. G. Rocha, M. T. da Q. e. C. de M. Saraiva, I. M. A. P. Ramos, and R. M. Natal Jorge, "Modeling the contraction of the pelvic floor muscles," *Comput. Methods Biomech. Biomed. Engin.*, vol. 19, no. 4, pp. 347–356, 2016.

[17] Y. Peng, R. Khavari, N. A. Nakib, T. B. Boone, and Y. Zhang, "Assessment of urethral support using MRI-derived computational modeling of the female pelvis," *Int. Urogynecol. J.*, vol. 27, no. 2, pp. 205–212, 2016.

[18] D. D'Aulignac, J. A. C. Martins, E. B. Pires, T. Mascarenhas, and R. M. N. Jorge, "A shell finite element model of the pelvic floor muscles," *Comput. Methods Biomech. Biomed. Engin.*, vol. 8, no. 5, pp. 339–347, 2005.

[19] Y. Zhang, S. Kim, A. G. Erdman, K. P. Roberts, and G. W. Timm, "Feasibility of using a computer modeling approach to study sui induced by landing a jump," *Ann. Biomed. Eng.*,

vol. 37, no. 7, pp. 1425–1433, 2009.

[20] T. A. Spirka and M. S. Damaser, “Modeling physiology of the urinary tract,” *J. Endourol.*, vol. 21, no. 3, pp. 294–299, 2007.

[21] T. A. Spirka, “Finite element modeling of stress urinary incontinence mechanics,” 2010.

[22] T. Spirka, K. Kenton, L. Brubaker, and M. Damaser, “PATHWAY TO FINITE ELEMENT ANALYSIS OF STRESS URINARY INCONTINENCE MECHANICS,” 2011, pp. 1–2.

[23] T. Spirka, K. Kenton, L. Brubaker, and M. S. Damaser, “Effect of material properties on predicted vesical pressure during a cough in a simplified computational model of the bladder and urethra,” *Ann. Biomed. Eng.*, vol. 41, no. 1, pp. 185–194, 2013.

[24] K. Chun, S. J. Kim, and S. T. Cho, “Noninvasive medical tools for evaluating voiding pattern in real life,” *Int. Neurourol. J.*, vol. 21, pp. 10–16, 2017.

[25] K. W. Coates, R. L. Harris, G. W. Cundiff, and R. C. Bump, “Uroflowmetry in women with urinary incontinence and pelvic organ prolapse,” *Br. J. Urol.*, vol. 80, no. 2, pp. 217–221, 1997.

[26] E. S. Lukacz, Y. Santiago-Lastra, M. E. Albo, and L. Brubaker, “Urinary incontinence in women a review,” *JAMA - J. Am. Med. Assoc.*, vol. 318, no. 16, pp. 1592–1604, 2017.

[27] I. Nygaard and R. Holcomb, “Reproducibility of the seven-day voiding diary in women with stress urinary incontinence,” *Int. Urogynecol. J.*, vol. 11, no. 1, pp. 15–17, 2000.

[28] D. G. Tincello, K. S. Williams, M. Joshi, R. P. Assassa, and K. R. Abrams, “Urinary Diaries,” *Obstet. Gynecol.*, vol. 109, no. 2, Part 1, pp. 277–280, Feb. 2007.

[29] J. M. Rabin, J. McNett, and G. H. Badlani, “A computerized voiding diary,” *J. Reprod. Med. Obstet. Gynecol.*, vol. 41, no. 11, pp. 801–806, 1996.

[30] J. M. Miller, J. A. Ashton-Miller, and J. O. L. Delancey, “Quantification of Cough-Related Urine Loss Using the Paper Towel Test,” *Obstet. Gynecol.*, vol. 91, no. 5 Part 1, p. 705, 1998.

[31] S. Thoen, “SENSOR, AN INCONTINENCE GARMENT, AND A METHOD FOR

ACTIVATING AN INCONTINENCE GARMENT," USOO9724247B2, 2017.

[32] E. Li, "INTELLIGENT INCONTINENCE MONITOR," USOO9649230B1, 2017.

[33] P. Curran *et al.*, "CAPACITIVE WETNESS SENSOR AND METHOD FOR MANUFACTURING THE SAME," US009314381 B2, 2016.

[34] P. M. Lewis, K. M. Carey, A. M. Cottenden, D. A. Barda, P. Curran, and D. Black, "INCONTINENCE MONITORING AND ASSESSMENT," USOO9283123B2, 2016.

[35] F. Ramirez, "INCONTINENCE DETECTION SYSTEM," US008772568B1, 2014.

[36] W. R. Addington, S. Miller, and R. E. Stephens, "TECHNIQUES FOR EVALUATING URINARY STRESS INCONTINENCE," USOO8690790B2, 2014.

[37] L. M. Ang *et al.*, "Wireless intelligent incontinence management system using smart diapers," in *2008 5th International Conference on Electrical Engineering/Electronics, Computer, Telecommunications and Information Technology*, 2008, vol. 1, pp. 69–72.

[38] B. R. Dick, R. T. Duke, E. E. Osborne, S. P. Sable, T. E. Scott, and C. Taverner, "INCONTINENCE DETECTION DEVICE," US005537095A, 1996.

[39] Frederick Colin Flack and E. D. James, "Incontinence measurement sensor," 3759246, 1973.

[40] E. J. Cha, K. A. Kim, S. B. Lee, and S. S. Choi, "UROFLOWMETER ATTACHABLE TO TOILET," US2011/0265576A1, 2011.

[41] R. S. Van Buskirk and R. R. Clappier, "URNE COLLECTION MONITOR WITH TEMPERATURE SENSING," 5062304, 1991.

[42] A. A. DiMino, M. E. Drummer, J. M. Campbell, A. Malik, and L. Curameng, "APPARATUS AND METHOD FOR UROFLOWMETRY," US9775556B2, 2017.

[43] M. Whitaker, M. Drinnan, A. Bray, C. Griffiths, and R. Beckwith, "URINE FLOW MEASURING APPARATUS," US2014/0296746A1, 2014.

[44] F. Ams, M. Baier, and R. Schafer, "APPARATUS FOR MEASURING THE THROUGHFLOW OF A BODY LIQUID," 5046510, 1991.

[45] E. V. Carrington *et al.*, “Advances in the evaluation of anorectal function,” *Nat. Rev. Gastroenterol. Hepatol.*, vol. 15, no. 5, pp. 309–323, May 2018.

[46] W. E. Whitehead *et al.*, “Fecal Incontinence in US Adults: Epidemiology and Risk Factors,” *Gastroenterology*, vol. 137, no. 2, pp. 512-517.e2, Aug. 2009.

[47] J. F. Johanson and J. Lafferty, “Epidemiology of fecal incontinence: the silent affliction.,” *Am. J. Gastroenterol.*, vol. 91, no. 1, pp. 33–6, Jan. 1996.

[48] P. D. R. Higgins and J. F. Johanson, “Epidemiology of Constipation in North America: A Systematic Review,” *Am. J. Gastroenterol.*, vol. 99, no. 4, pp. 750–759, Apr. 2004.

[49] T. Rud, K. E. Andersson, M. Asmussen, A. Hunting, and U. Ulmsten, “Factors maintaining the intraurethral pressure in women.,” *Invest. Urol.*, vol. 17, no. 4, pp. 343–7, Jan. 1980.

[50] D. Perucchini, J. O. L. DeLancey, J. A. Ashton-Miller, A. Galecki, and G. N. Schaer, “Age effects on urethral striated muscle: II. Anatomic location of muscle loss,” *Am. J. Obstet. Gynecol.*, vol. 186, no. 3, pp. 356–360, 2002.

[51] J. O. L. Delancey, “Structural aspects of urethrovesical function in the female,” *Neurourol. Urodyn.*, vol. 7, no. 6, pp. 509–519, 1988.

[52] A. N. Natali *et al.*, “Mechanics of the urethral duct: tissue constitutive formulation and structural modeling for the investigation of lumen occlusion,” *Biomech. Model. Mechanobiol.*, vol. 16, no. 2, pp. 439–447, 2017.

[53] A. N. Natali, C. G. Fontanella, and E. L. Carniel, “Biomechanical analysis of the interaction phenomena between artificial urinary sphincter and urethral duct,” *Int. j. numer. method. biomed. eng.*, vol. 36, no. 3, pp. 1–10, 2020.

[54] A. N. Natali, E. L. Carniel, and C. G. Fontanella, “Investigation of interaction phenomena between lower urinary tract and artificial urinary sphincter in consideration of urethral tissues degeneration,” *Biomech. Model. Mechanobiol.*, no. 0123456789, 2020.

[55] C. Masri, G. Chagnon, D. Favier, H. Sartelet, and E. Girard, “Experimental characterization and constitutive modeling of the biomechanical behavior of male human

urethral tissues validated by histological observations,” *Biomech. Model. Mechanobiol.*, vol. 17, no. 4, pp. 939–950, 2018.

[56] R. Rudyk, M. Malinowski, A. Mackiewicz, R. Bedzinski, J. Skonieczna, and J. P. Madej, “NUMERICAL ANALYSIS OF DEFORMATION AND FLOW IN THE PROXIMAL AREA OF THE URETHRA,” vol. 25, no. 2, pp. 130–141, 2020.

[57] A. N. Natali *et al.*, “Urethral lumen occlusion by artificial sphincteric devices: a computational biomechanics approach,” *Biomech. Model. Mechanobiol.*, vol. 16, no. 4, pp. 1439–1446, 2017.

[58] M. Malinowski, A. Mackiewicz, R. Rudyk, J. Madej, and J. Skonieczna, “NUMERICAL MODELS OF THE URETHRAL LOWER DUCT,” in *41st Solid Mechanics Conference*, 2018, no. Solmech, pp. 40–41.

[59] M. A. Mistry, N. Klarskov, J. O. DeLancey, and G. Lose, “A structured review on the female urethral anatomy and innervation with an emphasis on the role of the urethral longitudinal smooth muscle,” *Int. Urogynecol. J.*, vol. 31, no. 1, pp. 63–71, 2020.

[60] W. Schäfer, “Some biomechanical aspects of continence function.,” *Scand. J. Urol. Nephrol. Suppl.*, vol. 5599, no. 207, pp. 44–60; discussion 106-25, 2001.

[61] A. B. Huisman, “Aspects on the anatomy of the female urethra with special relation to urinary continence.,” *Contrib. Gynecol. Obstet.*, vol. 10, pp. 1–31, 1983.

[62] T. M. Oelrich, “The striated urogenital sphincter muscle in the female,” *Anat. Rec.*, vol. 205, no. 2, pp. 223–232, 1983.

[63] J. O. L. DeLancey *et al.*, “Stress urinary incontinence: relative importance of urethral support and urethral closure pressure.,” *J. Urol.*, vol. 179, no. 6, pp. 2286–90; discussion 2290, Jun. 2008.

[64] P. HILTON and S. L. STANTON, “Urethral pressure measurement by microtransducer: the results in symptom-free women and in those with genuine stress incontinence.,” *Br. J. Obstet. Gynaecol.*, vol. 90, no. 10, pp. 919–33, Oct. 1983.

[65] D. Perucchini, J. O. L. DeLancey, J. A. Ashton-Miller, U. Peschers, and T. Kataria, “Age

effects on urethral striated muscle: I. Changes in number and diameter of striated muscle fibers in the ventral urethra," *Am. J. Obstet. Gynecol.*, vol. 186, no. 3, pp. 351–355, 2002.

[66] A. Clobes, J. O. L. DeLancey, and D. M. Morgan, "Urethral circular smooth muscle in young and old women," *Am. J. Obstet. Gynecol.*, vol. 198, no. 5, pp. 1–5, 2008.

[67] E. R. Trowbridge, J. T. Wei, D. E. Fenner, J. A. Ashton-Miller, and J. O. L. DeLancey, "Effects of aging on lower urinary tract and pelvic floor function in nulliparous women," *Obstet. Gynecol.*, vol. 109, no. 3, pp. 715–720, 2007.

[68] B. T. Haylen *et al.*, "An international urogynecological association (IUGA)/international continence society (ICS) joint report on the terminology for female pelvic floor dysfunction," *Neurourol. Urodyn.*, vol. 30, no. Jan 2011, p. n/a-n/a, 2009.

[69] K. Bø and R. D. Herbert, "There is not yet strong evidence that exercise regimens other than pelvic floor muscle training can reduce stress urinary incontinence in women: A systematic review," *J. Physiother.*, vol. 59, no. 3, pp. 159–168, 2013.

[70] K. J. Kim, J. a. Ashton-Miller, K. Strohbehn, J. O. L. DeLancey, and A. B. Schultz, "The vesico-urethral pressuregram analysis of urethral function under stress," *J. Biomech.*, vol. 30, no. 1, pp. 19–25, 1997.

[71] R. Kikinis, S. D. Pieper, and K. G. Vosburgh, "3D Slicer: A Platform for Subject-Specific Image Analysis, Visualization, and Clinical Support," in *Intraoperative Imaging and Image-Guided Therapy*, New York, NY: Springer New York, 2014, pp. 277–289.

[72] "COMSOL Multiphysics®." COMSOL AB, Stockholm, Sweden, 2018.

[73] H. L. Sweeney and D. W. Hammers, "Muscle Contraction," *Cold Spring Harb. Perspect. Biol.*, vol. 10, no. 2, p. a023200, Feb. 2018.

[74] N. J. Campbell and C. V. Maani, *Histology, Muscle*. 2019.

[75] G. S. Lynch, R. T. Hinkle, J. S. Chamberlain, S. V. Brooks, and J. A. Faulkner, "Force and power output of fast and slow skeletal muscles from mdx mice 6-28 months old," *J. Physiol.*, vol. 535, no. 2, pp. 591–600, 2001.

[76] S. V. Brooks and J. A. Faulkner, "Forces and powers of slow and fast skeletal muscles in

mice during repeated contractions.," *J. Physiol.*, vol. 436, no. 1, pp. 701–710, 1991.

[77] M. H. Stromer, "The cytoskeleton in skeletal, cardiac and smooth muscle cells," *Histol. Histopathol.*, vol. 13, no. 1, pp. 283–291, 1998.

[78] R. A. Murphy, J. T. Herlihy, and J. Megerman, "Force-generating capacity and contractile protein content of arterial smooth muscle," *J. Gen. Physiol.*, vol. 64, no. 6, pp. 691–705, 1974.

[79] H. Abé, K. Hayashi, and M. Sato, *Data Book on Mechanical Properties of Living Cells, Tissues, and Organs*, vol. 66. Tokyo: Springer Japan, 1996.

[80] J. R. Sellers, "Contractile proteins," 2006.

[81] J. A. Shaw, K. Dasharathi, A. S. Wineman, and M. S. Si, "A simple model for myocardial changes in a failing heart," *Int. J. Non. Linear. Mech.*, vol. 68, pp. 132–145, 2015.

[82] P. A. L. S. Martins *et al.*, "Uniaxial mechanical behavior of the human female bladder," *Int. Urogynecol. J.*, vol. 22, no. 8, pp. 991–995, 2011.

[83] M. Aagaard, N. Klarskov, J. Sønksen, P. Bagi, H. Colstrup, and G. Lose, "Urethral pressure reflectometry; A novel technique for simultaneous recording of pressure and cross-sectional area: A study of feasibility in the prostatic urethra," *BJU Int.*, vol. 110, no. 8, pp. 1178–1183, 2012.

[84] P. J. Prendergast, "Analysis of Prolapse in Cardiovascular Stents: A Constitutive Equation for Vascular Tissue and Finite-Element Modelling," *J. Biomech. Eng.*, vol. 125, no. 5, p. 692, 2003.

[85] O. Schenk, K. Gärtner, and W. Fichtner, "Scalable parallel sparse factorization with left-right looking strategy on shared memory multiprocessors," *Lect. Notes Comput. Sci. (including Subser. Lect. Notes Artif. Intell. Lect. Notes Bioinformatics)*, vol. 1593, no. 1, pp. 221–230, 1999.

[86] D. R. Gustafson, *Physics: Health and the human body.* Wadsworth Publishing Company, 1980.

[87] D. Putnam, "Composition and Concentrative Administration," *Security*, no. July, 1971.

[88] K. W. Kim, Y. H. Choi, S. B. Lee, Y. Baba, H. H. Kim, and S. H. Suh, “Analysis of Urine Flow in Three Different Ureter Models,” *Comput. Math. Methods Med.*, vol. 2017, no. Figure 1, 2017.

[89] R. A. Oppliger, S. A. Magnes, L. R. A. Popowski, and C. V. Gisolfi, “Accuracy of urine specific gravity and osmolality as indicators of hydration status,” *Int. J. Sport Nutr. Exerc. Metab.*, vol. 15, no. 3, pp. 236–251, 2005.

[90] J. M. Yang, S. H. Yang, and W. C. Huang, “Functional correlates of Doppler flow study of the female urethral vasculature,” *Ultrasound Obstet. Gynecol.*, vol. 28, no. 1, pp. 96–102, 2006.

[91] C. A. Brincat, J. O. L. DeLancey, and J. M. Miller, “Urethral closure pressures among primiparous women with and without levator ani muscle defects,” *Int. Urogynecol. J.*, vol. 22, no. 12, pp. 1491–1495, Dec. 2011.

[92] J. O. L. DeLancey, D. E. Fenner, K. Guire, D. A. Patel, D. Howard, and J. M. Miller, “Differences in continence system between community-dwelling black and white women with and without urinary incontinence in the EPI study,” *Am. J. Obstet. Gynecol.*, vol. 202, no. 6, pp. 584.e1-584.e12, Jun. 2010.

[93] D. J. Griffiths, C. E. Constantinou, and R. van Mastrigt, “Urinary bladder function and its control in healthy females.,” *Am. J. Physiol.*, vol. 251, no. 2 Pt 2, pp. R225-30, 1986.

[94] J. Morley Kotchen, H. E. McKean, and T. A. Kotchen, “Blood pressure trends with aging,” *Hypertension*, vol. 4, no. 5, pp. 128–134, 1982.

[95] R. E. Harvey, J. N. Barnes, E. C. J. Hart, W. T. Nicholson, M. J. Joyner, and D. P. Casey, “Influence of sympathetic nerve activity on aortic hemodynamics and pulse wave velocity in women,” *Am. J. Physiol. - Hear. Circ. Physiol.*, vol. 312, no. 2, pp. H340–H346, 2017.

[96] S. E. Baker, J. K. Limberg, G. A. Dillon, T. B. Curry, M. J. Joyner, and W. T. Nicholson, “Aging alters the relative contributions of the sympathetic and parasympathetic nervous system to blood pressure control in women,” *Hypertension*, vol. 72, no. 5, pp. 1236–1242, 2018.

[97] A. Carlile, I. Davies, A. Rigby, and J. C. Brocklehurst, “Age changes in the human female

urethra: A morphometric study," *J. Urol.*, vol. 139, no. 3, pp. 532–535, 1988.

[98] O. Gassmann and M. Zeschky, "Opening up the solution space: The role of analogical thinking for breakthrough product innovation," *Creat. Innov. Manag.*, vol. 17, no. 2, pp. 97–106, 2008.

[99] F. (Fritz) Zwicky 1898-1974., *Discovery, invention, research through the morphological approach*, [1st Ameri., no. New York]. New York]: Macmillan, 1969.

[100] W. M. Kier, "The Structure and Adhesive Mechanism of Octopus Suckers," *Integr. Comp. Biol.*, vol. 42, no. 6, pp. 1146–1153, 2002.

[101] S. Baik, D. W. Kim, Y. Park, T. J. Lee, S. Ho Bhang, and C. Pang, "A wet-tolerant adhesive patch inspired by protuberances in suction cups of octopi," *Nature*, vol. 546, no. 7658, pp. 396–400, 2017.

[102] W.-C. Lin and M. A. Burns, "Low-power micro-fabricated liquid flow-rate sensor," *R. Soc. Chem.*, vol. 7, no. 9, pp. 3981–3987, 2015.

[103] S. C. Roh, Y. M. Choi, and S. Y. Kim, "Sensitivity enhancement of a silicon micro-machined thermal flow sensor," *Sensors Actuators, A Phys.*, vol. 128, no. 1, pp. 1–6, 2006.

[104] W. Lin, "Multifunctional Micro-Scale Sensors for Water Safety Monitoring with Only Bare Platinum Electrodes," 2017.

[105] M. Sadeghi, R. Peterson, and K. Najafi, "Air flow sensing using micro-wire-bonded hair-like hot-wire anemometry," *J. Micromech. Microeng*, vol. 23, pp. 85017–11, 2013.

[106] D. Bestion, J. P. GaviglioJ Bonnet, J. Gaviglio, and J. P. Bonnet, "Comparison between constant-current and constant-temperature hot-wire anemometers in high-speed flows," *Cit. Rev. Sci. Instruments*, vol. 54, no. 10, 1983.

[107] M. B. Del Rosario, N. H. Lovell, and S. J. Redmond, "Learning the orientation of a loosely-fixed wearable IMU relative to the body improves the recognition rate of human postures and activities," *Sensors (Switzerland)*, vol. 19, no. 13, 2019.

[108] A. Lazaro, M. Boada, R. Villarino, and D. Girbau, "Battery-Less Smart Diaper Based on

NFC Technology," *IEEE Sens. J.*, vol. 19, no. 22, pp. 10848–10858, 2019.

[109] S. T. Boerema, L. van Velsen, L. Schaake, T. M. Tönis, and H. J. Hermens, "Optimal sensor placement for measuring physical activity with a 3D accelerometer," *Sensors (Switzerland)*, vol. 14, no. 2, pp. 3188–3206, 2014.

[110] O. Elíasson, G. Vasile, S. Ægir Jónsson, G. I. Gudjonsson, M. Arikan, and S. Ingvarsson, "Power regulation and electromigration in platinum microwires," *Rev. Sci. Instrum.*, vol. 85, no. 11, p. 114709, Nov. 2014.

[111] C. Norton *et al.*, "Habit training versus habit training with direct visual biofeedback in adults with chronic constipation: study protocol for a randomised controlled trial," *Trials*, vol. 18, no. 1, p. 139, Dec. 2017.

[112] G. R. Locke, J. H. Pemberton, and S. F. Phillips, "American Gastroenterological Association medical position statement: Guidelines on constipation," *Gastroenterology*, vol. 119, no. 6, pp. 1761–1766, Dec. 2000.

[113] W. D. Chey, J. A. Ashton-Miller, and B. M. R. Spiegel, "Digital manometry finger-mountable sensor device," WO2013090681 A3, 20-Jun-2012.

[114] W. D. Chey, J. Baker, A. Attari, B. M. Spiegel, and J. A. Ashton-Miller, "Mo2022 A Glove-Based, Disposable, Point-of-Service Device Which Allows Detailed Physiological Assessment of the Anorectum: A Proof of Concept Study in Healthy Volunteers," *Gastroenterology*, vol. 146, no. 5, p. S-720, May 2014.

[115] W. D. Chey, J. Baker, A. Attari, and J. A. Ashton-Miller, "931 A Glove-Based, Disposable, Point-of-Service Device Which Allows Physiological Assessment of the Anorectum: Concordance With Anorectal Manometry in Chronic Constipation Patients," *Gastroenterology*, vol. 148, no. 4, p. S-178, Apr. 2015.

[116] A. Attari, W. D. Chey, J. Baker, and J. A. Ashton-Miller, "Development of a Disposable Point-of-Service Digital Manometry Device to Assess Anorectal Function," in *American Society of Biomechanics*, 2017, pp. 645–646.

[117] R. R. Richardson, J. A. Miller, and W. M. Reichert, "Polyimides as biomaterials: preliminary biocompatibility testing," *Biomaterials*, vol. 14, no. 8, pp. 627–635, Jan.

1993.

[118] O. S. Palsson *et al.*, “Development and validation of the Rome IV diagnostic questionnaire for adults,” *Gastroenterology*, vol. 150, no. 6, pp. 1481–1491, 2016.

[119] J. M. Jorge and S. D. Wexner, “Etiology and management of fecal incontinence.,” *Dis. Colon Rectum*, vol. 36, no. 1, pp. 77–97, Jan. 1993.

[120] J. M. Bland and D. G. Altman, “Statistical methods for assessing agreement between two methods of clinical measurement.,” *Lancet (London, England)*, vol. 1, no. 8476, pp. 307–10, Feb. 1986.

[121] Z. B. Popović and J. D. Thomas, “Assessing observer variability: a user’s guide,” *Cardiovasc. Diagn. Ther.*, vol. 7, no. 3, pp. 317–324, Jun. 2017.

[122] K. O. McGraw and S. P. Wong, “Forming inferences about some intraclass correlation coefficients.,” *Psychol. Methods*, vol. 1, no. 1, pp. 30–46, Mar. 1996.

[123] S. Chakraborty, K. J. Feuerhak, A. R. Zinsmeister, and A. E. Bharucha, “Reproducibility of high-definition (3D) manometry and its agreement with high-resolution (2D) manometry in women with fecal incontinence,” *Neurogastroenterol. Motil.*, vol. 29, no. 3, p. e12950, Mar. 2017.

[124] V. Vitton, W. Ben Hadj Amor, K. Baumstarck, J. C. Grimaud, and M. Bouvier, “Water-perfused manometry vs three-dimensional high-resolution manometry: a comparative study on a large patient population with anorectal disorders,” *Color. Dis.*, vol. 15, no. 12, pp. e726–e731, Dec. 2013.

[125] H. J. Lee *et al.*, “Normal values for high-resolution anorectal manometry/topography in a healthy Korean population and the effects of gender and body mass index,” *Neurogastroenterol. Motil.*, vol. 26, no. 4, pp. 529–537, Apr. 2014.

[126] E. V. Carrington *et al.*, “Traditional measures of normal anal sphincter function using high-resolution anorectal manometry (HRAM) in 115 healthy volunteers,” *Neurogastroenterol. Motil.*, vol. 26, no. 5, pp. 625–635, May 2014.

[127] E. V. Carrington, C. H. Knowles, U. Grossi, and S. M. Scott, “High-resolution Anorectal

Manometry Measures Are More Accurate Than Conventional Measures in Detecting Anal Hypocontractility in Women With Fecal Incontinence," *Clin. Gastroenterol. Hepatol.*, vol. 17, no. 3, pp. 477-485.e9, Feb. 2019.

[128] J. Gosling, A. Plumb, S. A. Taylor, R. Cohen, and A. V. Emmanuel, "High-resolution anal manometry: Repeatability, validation, and comparison with conventional manometry," *Neurogastroenterol. Motil.*, vol. 31, no. 6, p. e13591, Jun. 2019.

[129] K. Feuerhak, S. Chakraborty, P. Tirumanisetty, and A. E. Bharucha, "Sex Differences in Anorectal Pressures and Mechanisms of Defecation in Healthy People," *Gastroenterology*, vol. 152, no. 5, pp. S318–S319, Apr. 2017.

[130] A. M. P. Rasijeff, M. Withers, J. M. Burke, W. Jackson, and S. M. Scott, "High-resolution anorectal manometry: A comparison of solid-state and water-perfused catheters," *Neurogastroenterol. Motil.*, vol. 29, no. 11, p. e13124, Nov. 2017.

[131] R. R. Simpson, M. L. Kennedy, M. H. Nguyen, P. G. Dinning, and D. Z. Lubowski, "Anal Manometry: A Comparison of Techniques," *Dis. Colon Rectum*, vol. 49, no. 7, pp. 1033–1038, Jul. 2006.

[132] J. Noelting, S. K. Ratuapli, A. E. Bharucha, D. M. Harvey, K. Ravi, and A. R. Zinsmeister, "Normal Values for High-Resolution Anorectal Manometry in Healthy Women: Effects of Age and Significance of Rectoanal Gradient," *Am. J. Gastroenterol.*, vol. 107, no. 10, pp. 1530–1536, Oct. 2012.

[133] S. K. Ratuapli, A. E. Bharucha, J. Noelting, D. M. Harvey, and A. R. Zinsmeister, "Phenotypic Identification and Classification of Functional Defecatory Disorders Using High-Resolution Anorectal Manometry," *Gastroenterology*, vol. 144, no. 2, pp. 314-322.e2, Feb. 2013.

[134] C. P. Gibbons, J. J. Bannister, E. A. Trowbridge, and N. W. Read, "An analysis of anal sphincter pressure and anal compliance in normal subjects.," *Int. J. Colorectal Dis.*, vol. 1, no. 4, pp. 231–7, Oct. 1986.

[135] T. M. Greiner, "Hand Anthropometry of U.S. Army Personnel," pp. 66–73, Dec. 1991.

[136] G. A. Holzapfel, T. C. Gasser, and R. W. Ogden, "A new constitutive framework for

arterial wall mechanics and a comparative study of material models," *J. Elast.*, vol. 61, no. 1–3, pp. 1–48, 2000.

[137] S. Niederauer, J. de Gennaro, I. Nygaard, T. Petelenz, and R. Hitchcock, "Development of a novel intra-abdominal pressure transducer for large scale clinical studies," *Biomed. Microdevices*, vol. 19, no. 4, 2017.

[138] J. M. Miller, C. Sampselle, J. Ashton-Miller, G. R. S. Hong, and J. O. L. DeLancey, "Clarification and confirmation of the Knack maneuver: The effect of volitional pelvic floor muscle contraction to preempt expected stress incontinence," *Int. Urogynecol. J.*, vol. 19, no. 6, pp. 773–782, 2008.

[139] M. K. Kwak, H. E. Jeong, and K. Y. Suh, "Rational design and enhanced biocompatibility of a dry adhesive medical skin patch," *Adv. Mater.*, vol. 23, no. 34, pp. 3949–3953, 2011.

[140] J.-D. Mathias, M. Grédiac, and P. Michaud, "Bio-based adhesives," in *Biopolymers and Biotech Admixtures for Eco-Efficient Construction Materials*, vol. 2012, Elsevier, 2016, pp. 369–385.

[141] J. M. Wu, C. A. Matthews, C. P. Vaughan, and A. D. Markland, "Urinary, fecal, and dual incontinence in older U.S. adults," *J. Am. Geriatr. Soc.*, vol. 63, no. 5, pp. 947–953, 2015.